Pharmacological and Fluorometric Assessment of Neuronal KCNQ Channels, and Implications for Understanding Neurological Disease

by

Jingru Li

A thesis submitted in partial fulfillment of the requirements for the degree of

Master of Science

Department of Pharmacology

University of Alberta

ABSTRACT

Epilepsy affects 60 million people worldwide, and encompasses the most common forms of neurological disorders. Epilepsy manifests in diverse ways in patients, ranging from mild cognitive effects, to seizures, to the more severe epileptic encephalopathy. While many pharmacological approaches exist for the treatment of epilepsy, 30% of the epileptic population do not respond to such treatments. The resistance to treatment is perhaps due to the diverse neurological mechanisms underlying epilepsy, but also the limited molecular mechanisms by which conventional therapies target. Recent studies have made significant progress in unveiling the mechanisms of a novel class of anti-epileptic drugs, the Kv7/KCNQ activators, which targets a class of voltage-gated potassium channels involved in M-channel formation, and are implicated in neonatal seizures and epileptic encephalopathy. Retigabine (RTG) is the first-in-class clinically approved Kv7/KCNQ channel opener for the management of pharmacoresistant epilepsies. Despite its success in treating many patients, RTG was eventually removed from the market due to lack of target specificity and abundant side effects, which created concern for patient safety. Recently, another experimental compound was developed - ICA-069673 (ICA-73). ICA-73 has been shown through recent studies to exhibit greater specificity, selectivity, and state-dependence on limited members of the Kv7/KCNQ subclass. Currently, there remains a limited understanding of the function and regulation of KCNQ channels, particularly with regards to mechanisms behind subtype-selective tetrameric assembly and stability of the selectivity filter. In addition, there is little understanding of the relationship between KCNQ mutations and neurological disease. My thesis uses the improved understanding of ICA-73 to develop a pharmacological assay, which was used together with two electrode voltage clamp electrophysiology to study the relationship between genetic mutations in KCNQ channels and clinical cases of neurological disorders. Through our approach, we improved the current understanding of M-channels and determined that the calmodulin binding helices are likely involved in tetrameric channel assembly. We also determined that the selectivity filter of KCNQ channels are likely stabilized by a similar hydrogen bond previously identified in *Drosophila Shaker* channels, and disruption of this interaction can cause neonatal epilepsy.

Finally, we made significant improvements to an optical technique, voltage clamp fluorometry, by dramatically increasing the amplitudes and consistency of signals obtainable from KCNQ3, using an approach that can be expanded to other members of the KCNQ family, and can be potentially applied to study other poorly understood KCNQ-targeted drugs.

PREFACE

This thesis is an original work by Jingru Li. Other than Figure 5.1 (Kim et al., 2017) used to illustrate voltage clamp fluorometry, no part of this thesis has been previously published. All chapters relied on the contributions and technical assistance provided by Yubin Hao and Runying Yang, particularly with cloning and mutagenesis. Harley Kurata was the primary author who conceptualized and designed the research projects for all chapters. Frog surgeries, oocyte handling, and mRNA injections were done under the approval of University of Alberta Animal Care Protocol AUP00001752.

Chapter 3 of this thesis is submitted for publication at the Journal of Molecular Pharmacology as a manuscript titled "Heteromeric assembly of truncated neuronal Kv7 channels: implications for neurological disease and pharmacotherapy". The work in this chapter was conducted as part of a research collaboration, led by Elysa Marco (Cortica) and Harley Kurata (University of Alberta). Jingru Li designed experiments with Harley Kurata, performed all the experiments, and analyzed all the data. Manuscript was written by Jingru Li and Harley Kurata, along with the guidance and input from Jasmine Maghera, Shawn Lamothe, and Elysa Marco. Elysa Marco collected all clinical features of the proband, and obtained informed consent from the patient in this study.

Chapter 4 of this thesis is submitted for publication at Epilepsia Open as a manuscript titled "Benign familial neonatal epilepsy caused by the Kv7.3 selectivity filter mutation T313I". The work in this chapter was conducted as part of a research collaboration, led by Billie Au (University of Calgary) and Harley Kurata (University of Alberta). Jingru Li designed experiments with Jasmine Maghera and Harley Kurata, contributed to the experiments, and contributed to data analysis. Jingru Li also contributed to writing of the manuscript, along with Jasmine Maghera, Shawn Lamothe, Marvin Braun, Juan Appendino, Billie Au, and Harley Kurata. Billie Au, Marvin Braun, and Juan Appendino collected all clinical features of the proband, and obtained informed consent from the patient in this study.

Chapter 5 of this thesis is not currently being prepared for publication, since we wish to perform additional experiments to extend our experimental approach to other ion channels. Jingru Li designed experiments with Harley Kurata, performed all the experiments, and analyzed all the data.

Two manuscripts not included in this thesis have been submitted for publication. The first manuscript was submitted to Epilepsia and is titled "Functional and behavioural signatures of Kv7 activator drug subtypes" by Richard Kanyo, Caroline Wang, Laszlo Locskai, Jingru Li, Ted Allison, and Harley Kurata. The second manuscript was submitted to the Journal of General Physiology and is titled "Glycosylation tunes the sensitivity of Kv1.2 modulation by regulatory proteins" by Daniel Fajonyomi, Victoria Baronas, Damayantee Das, Jingru Li, Shawn Lamothe, and Harley Kurata.

One paper not included in this thesis has been published in the Journal of General Physiology, titled "One drug-sensitive subunit is sufficient for a near-maximal retigabine effect in KCNQ channels" by Michael Yau, Robin Kim, Caroline Wang, Jingru Li, Tarek Ammar, Runying Yang, Stephan Pless, and Harley Kurata.

ACKNOWLEDGEMENTS

I am immensely grateful to have met the people I worked with throughout my degree. First, I would like to express my gratitude to my supervisor, Harley Kurata, for his invaluable mentorship, patience, encouragement. I feel lucky for the opportunities you gave me, and enjoyed the stories you shared throughout the years. I would like to thank my committee members, Xing-Zhen Chen and Frances Plane, for their guidance, encouragement, and support in both research and career. In addition, I am grateful for the opportunity to conduct undergraduate summer research with Xing-Zhen Chen, where I truly became interested in electrophysiology and ion channel research, and became motivated to pursue graduate training. I would also like to thank the friends I have made in this lab, with whom I shared many unforgettable memories – Tarek Ammar, Victoria Baronas, Damayantee Das, Daniel Fajonyomi, Yubin Hao, Richard Kanyo, Robin Kim, Shawn Lamothe, Camilla Lund, Jasmine Maghera, Nazlee Sharmin, Grace Silver, Caroline Wang, Runying Yang, and Jihee Yoo. You have all made my graduate school experience fun, positive, and fulfilling.

The people in my personal life were also invaluable through my endeavours. First and foremost, I would like to thank my parents for their incredible perseverance to enable a better life for us in Canada, and their continuous support and understanding for my decisions along my journey. My personal friends, despite their own busy lives, also provided me the encouragement and support I needed throughout the years. Finally, I would like to thank Julie for her incredible patience, understanding, companionship, and unwavering support in these last few years, and for always being there when I needed her.

TABLE OF CONTENTS

LIST OF TABLES

LIST OF FIGURES

LIST OF ABBREVIATIONS

Kv – voltage-gated potassium
Kir – inwardly rectifying potassium
K2P – tandem pore domain potassium
Nav – voltage-gated sodium
CaM – calmodulin
N – amino
C – carboxy
Ach – acetylcholine
GPCR – G-protein coupled receptors
PIP_2 – phosphatidylinositol-4,5-bisophosphate
DAG – diacylglycerol
IP_3 – inositol-1,4,5-trisphosphate
PI – phosphatidylinositol
PI_4P – phosphatidylinositol-4-phosphate
PLC – phospholipase C
VSP – voltage sensitive phosphatase
VSD – voltage sensing domain
PD – pore domain
sid – subunit interaction domain
ER – endoplasmic reticulum
SR – sarcoplasmic reticulum
DSG – disuccinimidyl glutarate
BFNE – benign familial neonatal epilepsy
EE – epileptic encephalopathy
LQTS – long QT syndrome
JLNS – Jervell and Lang-Nielsen syndrome
WT – wild type
cDNA – complementary DNA
mRNA – messenger RNA
PCR – polymerase chain reaction
AED – antiepileptic drug
RTG – retigabine
ICA-73 – ICA-069673
K^+ – potassium ion
Na^+ – sodium ion
Ca^{2+} - calcium ion
Å – angstroms (10^{-10} m)
TEVC – two electrode voltage-clamp
VCF – voltage-clamp fluorometry
Cryo-EM – cryo-electron microscopy
FDA – Food and Drug Administration

AMINO ACID	3 LETTER CODE	1 LETTER CODE
Alanine	Ala	A
Arginine	Arg	R
Asparagine	Asn	N
Aspartate	Asp	D
Cysteine	Cys	C
Glutamine	Gln	Q
Glutamate	Glu	E
Glycine	Gly	G
Histidine	His	H
Isoleucine	Ile	I
Lysine	Lys	K
Methionine	Met	M
Phenylalanine	Phe	F
Proline	Pro	P
Serine	Ser	S
Threonine	Thr	T
Tryptophan	Trp	W
Tyrosine	Tyr	Y
Valine	Val	V

CHAPTER 1: INTRODUCTION

OVERVIEW OF VOLTAGE SENSITIVE POTASSIUM CHANNELS

Potassium channels are expressed in almost every known living organism (Miller, 2000). These channels are localized in the cell membrane and facilitate efflux of potassium ions along the direction of the electrochemical gradient. Regulating the passage of potassium ions across the membrane is critical for cellular electrical signaling (Miller, 2000; Kuang et al., 2015), and controls a vast array of physiological processes, including cognition, motor function, interpretation of sensory information, secretion of endocrine hormones, and contractions of the heart (Kuang et al., 2015). There are three major categories of potassium channels: the six transmembrane-domain (Kv) channels, the two transmembrane-domain inward rectifier (Kir) channels, and the four transmembrane-domain tandem pore domain (K2P) channels (Kuang et al., 2015). This thesis focuses on the Kv7 or KCNQ family of channels, which are members of the six transmembrane-domain Kv family of channels.

General Kv channel structure

All Kv channels are believed to follow a similar structural organization within the lipid bilayer, outlined in Figure 1.1 (Kuang et al., 2015), though significant variation exists in the voltage-sensing domain, pore domain, and N- and C-terminal domains between channel subtypes. Such variation produces functionally diverse Kv channels with distinct characteristics in gating, voltage-sensing, regulation, localization, and pharmacology (Bähring et al., 2012; Barros et al., 2012; Islas, 2016; Kim and Nimigean, 2016).

The structure of KCNQ1 (Kv7.1) in complex with calmodulin (CaM) was resolved by the MacKinnon group in 2017 through cryo-electron microscopy (Sun and MacKinnon, 2017). At the writing of this thesis, KCNQ1 is the only KCNQ channel with an atomically resolved structure. Since then, the KCNQ1 structure has been used to guide the study and modeling of other KCNQ subtypes, including the model of KCNQ3 used in this thesis. KCNQ1 is the cardiac isoform of Kv7 channels, and tetramerizes with

a C_4 configuration (Sun and MacKinnon, 2017). KCNQ1 possesses a classical Kv channel transmembrane architecture, also believed to be adopted by the neuronal KCNQ subtypes (Figure 1.1): each subunit contains six transmembrane helices (S1-S6) and intracellular N and C terminal domains (Doyle et al., 1998; Sun and MacKinnon, 2017). Helices S1-S4 form the voltage-sensing domain, which renders channel sensitivity to changing membrane voltages (Doyle et al., 1998; Islas, 2016). Helices S5-S6 and the pore loop together form the pore, allowing for conduction and specificity to potassium ions (Doyle et al., 1998). Four intracellular C-terminal helices (A-D) underlie interactions with PIP_2, CaM, regulatory proteins, and other KCNQ channels, providing the basis for KCNQ channel regulation and tetramerization (Doyle et al., 1998; Schwake et al., 2003; Kim et al., 2017). Finally, in neuronal KCNQ2 and KCNQ3 channels, an ankyrin G interacting region exists in the distal C-terminus and facilitates retention of channels to the axon initial segment and nodes of Ranvier of neurons (Pan et al., 2006).

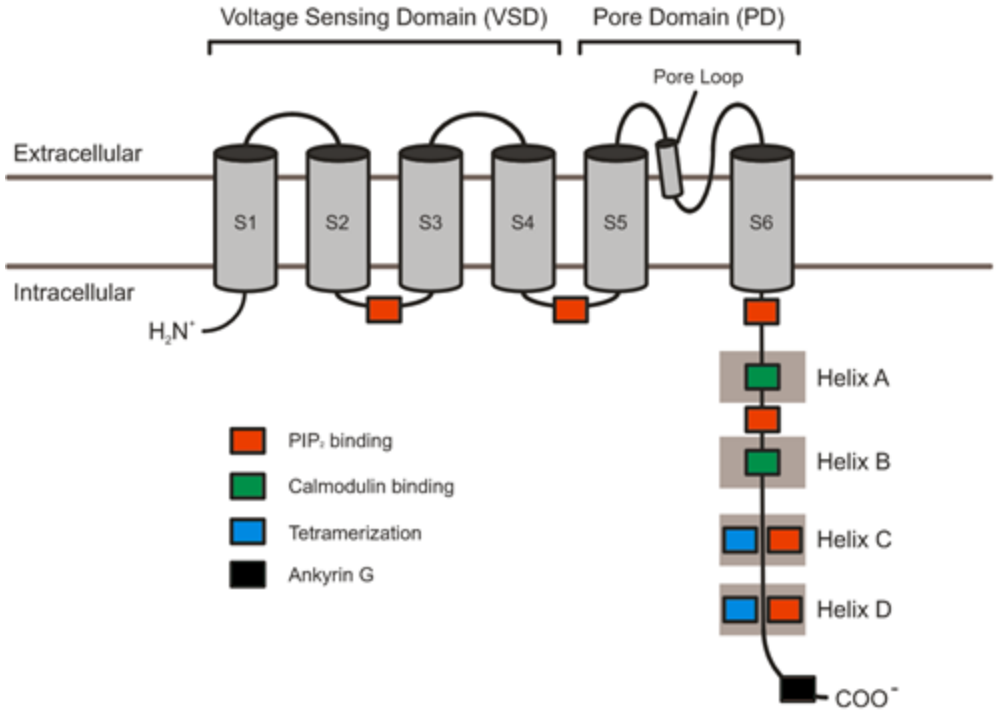

Figure 1.1: KCNQ structure schematic. KCNQ channels have intracellular N and C-terminal domains with six transmembrane helices (S1-S6). S1-S4 form the voltage-sensing domain, allowing channels to respond to changing membrane potentials. The S5-Pore Loop-S6 form the pore domain, allowing for the passage of and imparting specificity to potassium ions. Regulatory regions are clustered in the C-terminus of KCNQ channels for tetramerization with other KCNQ subunits and regulation by PIP_2, CaM, and ankyrin G. In addition to C-terminal regions, PIP_2 binding is also proposed to occur with the intracellular loops between transmembrane helices.

Ion selectivity and permeation

The ion conducting pore of Kv channels comprises distinct regions for mediating ionic selectivity and channel gating. The pore domains of four KCNQ subunits assemble to form the ion conducting pore (Doyle et al., 1998). Three distinct regions can be identified in the ion conducting pore, which are arranged in an inverted teepee formation (Doyle et al., 1998). The regions are, listed in order from the intracellular to the extracellular direction: the pore gate, the central cavity, and the selectivity filter (Doyle et al., 1998; Kim and Nimigean, 2016). The pore gate and central cavity regions have relatively larger diameters and contain a significant number of hydrophobic amino acid residues oriented towards the ion conducting region (Doyle et al., 1998). On the contrary, the selectivity filter is largely composed of hydrophilic residues, and contains the narrowest point (~ 3 Å) by which K^+ ions (~ 1.4 Å) must pass through (Doyle et al., 1998; Heginbotham et al., 1994). Specifically, the pore loop confers K^+ specificity through a Gly-Tyr-Gly-Asp motif conserved across Kv channels, and mutations to this motif have been shown to eliminate channel selectivity for K^+ ions (Heginbotham and MacKinnon, 1993; Heginbotham et al., 1994).

At sufficiently depolarizing voltages, Kv channels enter the open conformation to facilitate the efflux of K^+ ions (Yellen, 2002). K^+ conduction begins as hydrated ions enter through an open pore gate. The gate hinge responds to voltage sensor conformational changes to control the diameter of the pore gate, and is controlled by conserved Gly and Pro residues in the inner S6 helix of Kv channels: a Pro-X-Pro motif bends the S6 helix to tightly couple conformational changes between the S4-S5 linker and the S6 helix, and a Gly acts as the gate hinge by creating flexibility in the helices that control the pore gate diameter (MacKinnon, 2003; Labro and Snyders, 2012). Upon entry across the pore gate, K^+ ions proceed to the central cavity. Due to the cavity's position in the centre of the membrane bilayer, and the hydrophobicity of local amino acid side chains, ions in this region are at the highest energetic state in the conduction process (Doyle et al., 1998). Entry into the narrowest region, the selectivity filter, requires K^+ dehydration. Since dehydration is a destabilizing process and requires energy, K^+ must be energetically re-stabilized during conduction, and this is accomplished by forming coordination bonds with backbone carbonyl moieties in

the selectivity filter (Doyle et al., 1998). Na^+, due to its smaller Van der Waals radius (~ 1.0 Å), cannot form the coordination bonds sufficient for overcoming dehydration, and hence is selected against in ionic conduction through Kv channels (Doyle et al., 1998). Entry of subsequent K^+ ions into the selectivity filter disrupts the coordination bonds of the former ion, rapidly ejecting it into the extracellular space (Doyle et al., 1998). As the narrowest and the rate-determining region of transport, stabilization of the selectivity filter is critical for facilitating ion permeation and preventing inactivation via pore collapse (Doyle et al., 1998; Pless et al., 2013).

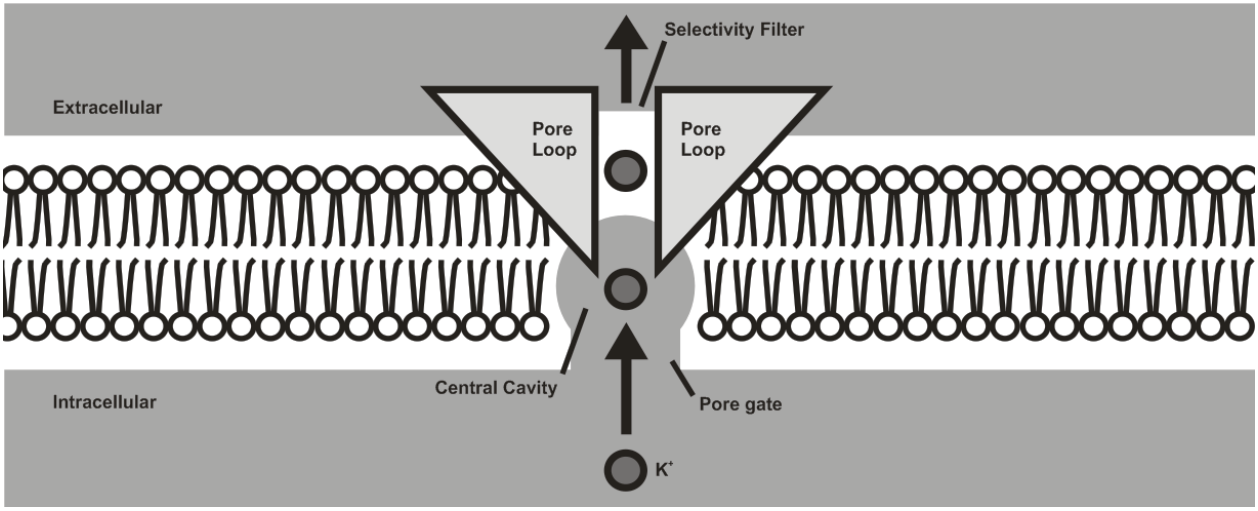

Figure 1.2: K^+ channel pore and ion permeation. The central cavity is an aqueous environment that is continuous with the cytosol. Hydrated K^+ (grey circles) enters the central cavity when the pore gate is in the open conformation. Due to the hydrophobic residues from Kv channels and positioning in the center of the membrane bilayer, ions in the central cavity are at their highest energetic state. Ions proceed into the selectivity filter and are stabilized by coordination bonds from hydrophilic backbone carbonyl groups. Ions stabilized via coordination are rapidly expelled as subsequent ions enter from the central cavity.

Voltage sensitivity and gating

Control of ion conductance across voltage-dependent channels requires the coupling of electric work to changes in protein conformation through gating charges (Bezanilla, 2008). Gating charges are the charged amino acids that mechanically shift in response to changes in the electric field. Initially characterized in the *Shaker* K^+ channel from *Drosophila melanogaster*, and later determined to be similar in human Kv channels, basic Arg and Lys residues are clustered in the S4 helix of the voltage sensing

domain and act as Kv channel gating charges (Bezanilla, 2000; Yellen, 2002; Cui, 2016). Despite the abundance of basic charged residues in the S4 helix that influence voltage sensitivity, only the first four Arg residues move significantly in response to voltage - with respect to *Shaker* numbering, these residues are R362, R365, R368, R371 (Aggarwal and MacKinnon, 1996). The voltage-driven movement of these gating charges produces transient gating currents which can be observed in electrophysiology records (Bezanilla and Stefani, 1998). Mutations eliminating these gating Arg in *Shaker* K^+ channels have been shown to reduce transient gating currents and K^+ conductance, reflecting the importance of these gating residues in the voltage sensitivity of Kv channels (Perozo et al., 1994; Aggarwal and MacKinnon, 1996). Finally, mutations in S4 that eliminate charged residues in KCNQ1 and KCNQ4 produced channels that are constitutively active, difficult to activate, and/or difficult to deactivate, again reflecting the importance of S4 in voltage-sensitivity (Panaghie and Abbott, 2007).

Movement of the S4 helix in Kv channels is coupled to channel gate conformational changes (Liu et al., 1997). Coupling between the voltage sensor and the pore requires the S4-S5 linker and membrane lipid PIP_2, the latter will be discussed in a later section (Lu et al., 2001, 2002; Zaydman and Cui, 2014). The voltage-dependent activation of the S4 helix applies a force on the S4-S5 linker, which induces a conformational change in the gate hinge to widen the channel gate for ion entry (Cui, 2016). Membrane repolarization causes the S4 helix to shift back to its deactivated position, relieving the force applied to the S4-S5 linker and causing the gating hinges to close, which stops ion flow (Cui, 2016). Problems with the voltage-sensitivity and/or gating of Kv channels can result in disease states caused by constitutively open or closed channels (Cui, 2016).

OVERVIEW OF KCNQ (Kv7) CHANNELS

There are five members of KCNQ, or Kv7, channels - KCNQ1-5 - expressed in humans (Barrese et al., 2018). KCNQ1 is the cardiac subtype important for generating the slow, delayed rectifier current (I_{Ks}) to repolarize cardiac myocytes, and KCNQ2-5 are neuronal subtypes with diverse neuronal functions both centrally and peripherally (Robbins, 2001). Two copies of each KCNQ gene are found in the human genome, one copy contributed by each of the maternal and paternal sets of chromosomes (Barrese et al., 2018). KCNQ genes are translated into monomeric protein subunits, and four subunits subsequently assemble to form functional tetrameric channels before trafficking to the cell surface (Soldovieri et al., 2011). KCNQ subunits can assemble into homotetramers *or* heterotetramers, and their expression and assembly vary across cell types (Soldovieri et al., 2011). Finally, Kv7 channels can assemble with auxiliary subunits, including KCNE1 and CaM, which can have effects on membrane expression, channel assembly, current behaviour, and inactivation properties (Ghosh et al., 2006; Shamgar et al., 2006; Strutz-Seebohm et al., 2011). Differential assembly and lipid/protein mediated regulation of KCNQ channels produce functional diversity in a channel class limited to only five members.

The differential expression and assembly of KCNQ subunits contribute to the diverse and often critical physiological roles of KCNQ channels (Soldovieri et al., 2011). KCNQ channels are important in cardiac repolarization, regulation of neuronal activity, auditory function, modulation of smooth and skeletal muscle contractions, and endocrine function (Barrese et al., 2018). Due to the important yet diverse physiological roles of KCNQs, channelopathies are often linked in human disease, including cardiac arrythmias, epilepsies, neurodevelopmental delays, and abnormal smooth muscle and endocrine function (Barrese et al., 2018). Often, channelopathies arise from disrupted voltage-sensitivity, ion selectivity and conductance, surface expression, and/or channel regulation (Maljevic et al., 2010).

KCNQ channel regulation

Kv channels are regulated by diverse mechanisms that control surface expression, biophysical properties, tetrameric assembly, ubiquitination and degradation, and cellular localization (Capera et al., 2019). Kv channels possess signature motifs that make them susceptible to these kinds of regulation, mediated by lipids, regulatory proteins, post-translational modifying enzymes, and other ion channel subunits (Capera et al., 2019). KCNQ channels have large intracellular C-terminal domains containing four regulatory helices A-D (Barrese et al., 2018). The four helices enable interactions with essential regulatory factors, including CaM, PIP_2, and other KCNQ subunits to form tetrameric channels (Barrese et al., 2018). Mutations that affect KCNQ channel regulation have been implicated in cardiac arrythmias and neurological disorders (Haitin and Attali, 2008; Maljevic et al., 2010).

PIP_2

Phosphatidylinositol-4,5-bisphosphate (PIP_2) is a relatively abundant (~ 1% of membrane lipids) anionic lipid found exclusively in the inner leaflet of the lipid bilayer (McLaughlin et al., 2002; Rusten and Stenmark, 2006). PIP_2 is synthesized from phosphatidylinositol (PI) by two stepwise phosphorylation reactions mediated by PI_4 kinase to produce PIP, and PI_5 kinase to produce PIP_2 (Rusten and Stenmark, 2006; Suh and Hille, 2007). PIP_2 levels in the membrane are balanced by phospholipase C (PLC), phosphatases, and PI_3 Kinase (Czech, 2000; Rusten and Stenmark, 2006). Interestingly, the M-current – later discovered to be primarily produced by neuronal KCNQ2 and KCNQ3 channels – was initially identified due to its suppression by M1 receptor activation and subsequent phospholipase C-mediated PIP_2 hydrolysis (Robbins et al., 1993; Zhang et al., 2003). Application of wortmannin, inhibitor PI4 kinase, suppresses M-currents in a similar way by reducing membrane levels of PIP_2 through synthesis (Suh and Hille, 2007). On the flip side, activation of a voltage sensitive phosphatase (*Ciona Intestinalis* VSP) that cleaves PIP_2 to PI_4P in oocytes expressing KCNQ2/KCNQ3 suppresses M-currents generated from these heteromeric channels (Kim et al., 2017), further demonstrating M-channel dependence on membrane levels of PIP_2. Both neuronal (KCNQ2-5) and cardiac (KCNQ1) KCNQ subtypes require PIP_2 for channel

conductance (Zhang et al., 2003; Zaydman and Cui, 2014). Specifically, PIP_2 is essential for the functional coupling of the voltage sensing and pore domains of KCNQ channels (Zaydman and Cui, 2014; Kim et al., 2017; Sun and MacKinnon, 2017). This coupling is further demonstrated by the MacKinnon group's 2017 crystal structure of KCNQ1 in the absence of PIP_2, resulting in KCNQ1 in an uncoupled state – the channel exhibited an activated voltage sensor but a closed pore (Sun and MacKinnon, 2017). In this uncoupled state, the contact between the S4-S5 linker and the S6 helix is reduced, and likely reduces the sensitivity of the gate hinge to respond to conformational changes in the voltage sensor (Sun and MacKinnon, 2017).

PIP_2 mediates coupling of the voltage sensor and the pore through a binding pocket believed to be formed by basic residue contributions from the S2-S3 linker, the S4-S5 linker, the intracellular region of S6, helix A and B linker of the proximal C-terminus, and helix C and D of the distal C-terminus (Zaydman and Cui, 2014). Variations exist in the putative PIP_2 binding site between KCNQ subtypes, and is likely why differences exist in KCNQ channel binding affinities for PIP_2 and sensitivities to $G_{q/11}$-GPCR mediated channel regulation (Delmas and Brown, 2005; Li et al., 2005; Zaydman and Cui, 2014). Mutations that eliminate positively charged residues in the putative PIP_2 binding pocket can weaken voltage sensor and pore coupling, reducing or eliminating the KCNQ channel response to changes in voltage (Zaydman and Cui, 2014). Finally, recent work demonstrated the importance of PIP_2 binding on KCNQ channel pharmacology, and showed that mutating a positively charged KRRK putative PIP_2-binding motif in the inner S6 helix at the membrane-cytosol interface influenced the channel's response to externally applied retigabine (RTG), a first-in-class KCNQ opener (Kim et al., 2017). The same study determined that KCNQ opener drugs may protect PIP_2 from phosphatase-mediated degradation, and could be the underlying mechanism by which certain drugs open KCNQ channels (Kim et al., 2017). Therefore, it is important to consider PIP_2 when studying both KCNQ channel function and pharmacology.

M1 muscarinic receptors allow for the physiological regulation of M-channel activity (Zhang et al., 2003; Delmas and Brown, 2005; Li et al., 2005). Outlined in Figure 1.3, activation of M1 receptors by acetylcholine (Ach) leads to a signaling cascade mediated by activated $G_{q/11}$ α and $\beta\gamma$ subunits (Mizuno and

Itoh, 2009). PLC is directly activated by the GTP-bound $G_{q/11}$ α subunit, resulting in the cleavage of PIP_2 into DAG and IP_3 (Mizuno and Itoh, 2009). This cleavage directly reduces membrane PIP_2, suppressing M-channel activity (Robbins et al., 1993; Zhang et al., 2003). In addition, recent work has also shown the reduction in M-channel affinity for PIP_2 mediated by Ca^{2+}-bound CaM (Kosenko and Hoshi, 2013). IP_3 released from PIP_2 hydrolysis can activate IP_3-sensitive Ca^{2+} channels at the SR/ER to liberate intracellular Ca^{2+} stores, increasing the proportion of Ca^{2+}-bound CaM in the cytosol (Mizuno and Itoh, 2009). Ca^{2+}-bound CaM can further suppress M-channel activity by reducing channel affinity for PIP_2 (Kosenko and Hoshi, 2013).

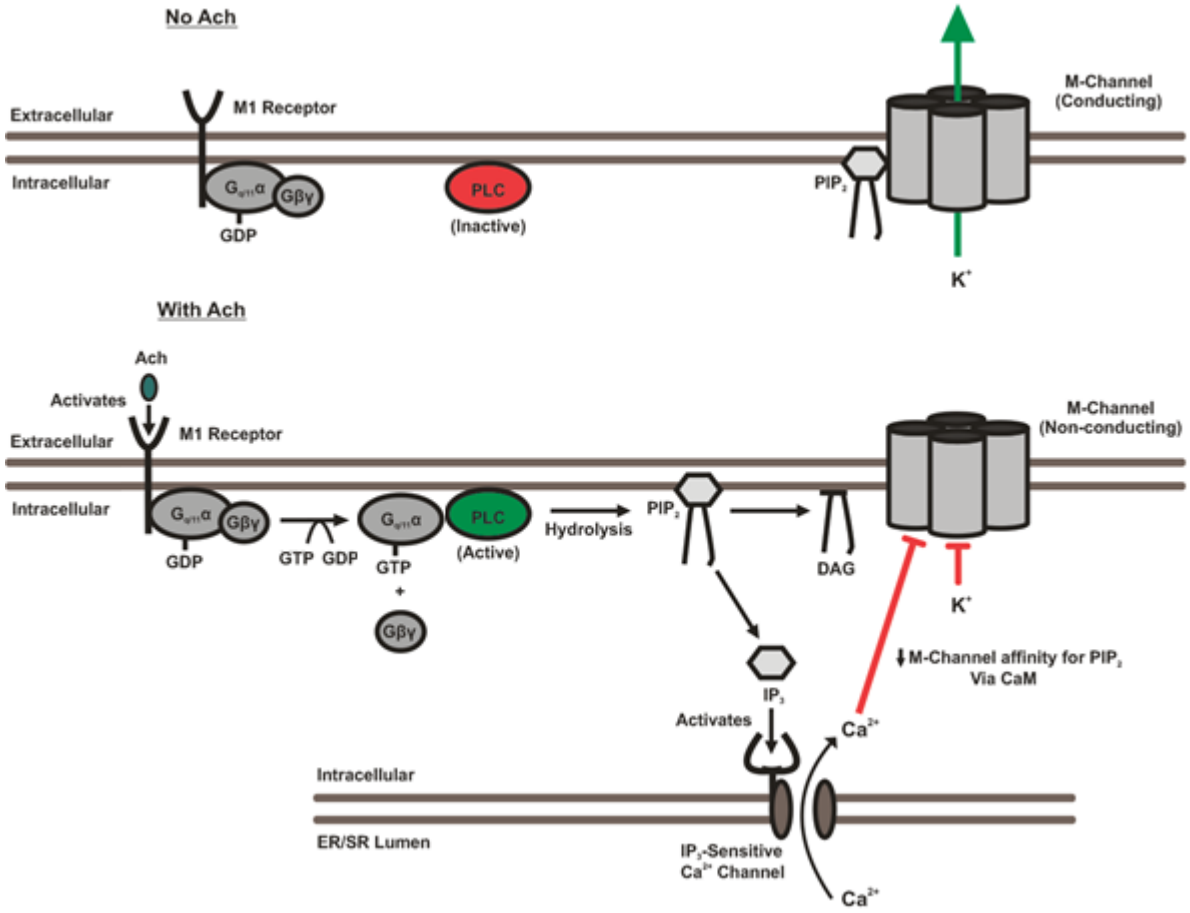

Figure 1.3: Activation of M1 muscarinic receptors suppress M-channel currents. M-channels require interaction with PIP_2 to conduct K^+. Cholinergic stimulation of the 7-transmembrane domain G-protein coupled M1 muscarinic receptor (simplified as a generic receptor in this figure) activates the $G_{q/11}$ signaling pathway, and the subsequent activation of phospholipase C (PLC) cleaves membrane PIP_2, directly suppressing M-currents. Additionally, IP_3-mediated Ca^{2+} efflux from the ER/SR increases Ca^{2+}-bound CaM, further suppressing M-currents by decreasing channel affinity for PIP_2.

Calmodulin

Calmodulin (CaM) is highly conserved in the eukaryotic kingdom, with no amino acid sequence differences between vertebrate species (Friedberg and Rhoads, 2001). CaM is a small soluble regulatory and signaling protein that interacts with diverse cytosolic and membrane-associated proteins (Friedberg and Rhoads, 2001). Being able to respond to physiological changes in [Ca^{2+}], CaM is a mediator of Ca^{2+}-dependent signal transduction pathways, including the M1 receptor pathway in Figure 1.3 (Grundström, 1999; Friedberg and Rhoads, 2001). In addition to the enzymes and signaling protein CaM interacts with, it also interacts with a diverse range of ion channels, often regulating them in a Ca^{2+}-dependent manner (Shah et al., 2006).

CaM is an essential co-factor to all KCNQ channels (Chung, 2014). CaM interacts with IQ motifs in helix A and B of the proximal C-terminus in KCNQ channels (Wen and Levitan, 2002; Yus-Najera et al., 2002; Sun and MacKinnon, 2017). Interestingly, the ability to bind Ca^{2+} does not influence the interaction between CaM and KCNQ channels, as the Ca^{2+}-binding deficient mutant $CaM_{1,2,3,4}$ and wild type CaM bind channels equally well (Wen and Levitan, 2002). However, wild type CaM can sense changes in cytosolic [Ca^{2+}] and influence KCNQ2/3 channel affinity for PIP_2, thereby controlling channel function in a Ca^{2+}-dependent manner (Kosenko and Hoshi, 2013). CaM influences trafficking, folding, and function of cardiac and neuronal subtypes of KCNQ channels, often in subtype-specific ways (Haitin and Attali, 2008; Chung, 2014). For example, while CaM similarly facilitates the trafficking of both KCNQ1 and KCNQ2, the application of bradykinin which produces a rise in intracellular [Ca^{2+}] (and therefore Ca^{2+}-bound CaM) activates KCNQ1 channels by shifting channel voltage-dependence in the hyperpolarizing direction, but suppresses KCNQ2 channel current expression (Gamper and Shapiro, 2003; Shamgar et al., 2006). Finally, recent studies have also identified residues in CaM near the voltage sensor of KCNQ1, where mutations can influence channel voltage-dependence of this channel (Sun and MacKinnon, 2017), suggesting that interactions other than those with helices A and B may be involved. It is not currently known if CaM mutations that affect KCNQ1 voltage-dependence can also influence neuronal KCNQ channels.

KCNQ channel assembly

KCNQ channels form functional homomeric and heteromeric tetramers at the cell membrane (MacKinnon, 1991; Papazian, 1999). KCNQ channels are selective for the subtypes they assemble with to form tetrameric channels (Howard et al., 2007). For instance, KCNQ1 will only assemble with itself to form homotetramers (Schwake et al., 2003), while KCNQ3 can heteromerically assemble with KCNQ2, 4, and 5 (Wang et al., 1998; Kubisch et al., 1999; Schroeder et al., 2000). Despite being limited to only five members, the variation in tetrameric channel composition produces KCNQ channels that are functionally diverse and biophysically distinct (Howard et al., 2007). To further increase channel diversity, variable subtype stoichiometries exist within any subtype combination, each of which exhibits unique biophysical and pharmacological properties (Schwake et al., 2003).

Unlike the *Shaker* K^+ channel, KCNQ channels do not have N-terminal T1 domains to drive channel assembly (Schmitt et al 2000). Assembly of KCNQ channels is believed to be driven instead by a subunit interacting domain – *sid* in the distal C-terminus (Schwake et al., 2003). The *sid* region exists within helices C and D in Figure 1.1, and contains sequences believed to adopt coiled-coil structures. These coiled-coil elements are believed to drive KCNQ channel assembly and impart specificity for KCNQ subtypes (Maljevic et al., 2003; Schwake et al., 2003; Howard et al., 2007). KCNQ chimeric studies further dissected the *sid* region into two domains: the relatively conserved A domain required for all KCNQ assembly, and the notably variable B-domain that influences subunit specificity (Schwake et al., 2003; Howard et al., 2007).

It is also recognized that the regulatory protein CaM, an obligate subunit in KCNQ channels, may contribute to channel assembly (Ghosh et al., 2006). Ghosh et al. (2006) truncated the KCNQ1 C-terminus at amino acid position 555, which eliminated the A- and B-domains attributed to KCNQ1 assembly (Schmitt et al., 2000). It was determined through DSG crosslink experiments that CaM can drive the tetramerization of the C-terminally truncated KCNQ1 (Ghosh et al., 2006). KCNQ1 C-terminus in-vitro affinity chromatography experiments allowed Ghosh et al. (2006) to test several mutations identified in the KCNQ1 C-terminus. The S373P, R518X, and R539W mutations in helix A and B disrupted CaM-KCNQ1

interactions. In cells expressing these mutated channels, current levels decreased significantly despite showing a wild type level of protein expression: a characteristic that supports a reduced channel assembly, but can also be due to reduced intrinsic channel function (Ghosh et al., 2006).

KCNQ1 is critical for cardiac function

KCNQ1 is primarily expressed in cardiac tissue where it generates the slow delayed rectifier current (I_{Ks}) important for mediating cardiac repolarization and controlling cardiac rhythm (Barhanin et al., 1996; Sanguinetti et al., 1996). While the heterologous expression of KCNQ1 yields functional homomeric channels, KCNQ1 is rarely expressed alone in human tissue. Instead, KCNQ1 is typically co-assembled with its auxiliary β subunit, KCNE1, to generate the I_{Ks} current (Sanguinetti et al., 1996; Sesti and Goldstein, 1998). KCNE1 influences KCNQ1 function by enhancing channel currents, slowing channel activation, right-shifting the voltage-dependence of activation, and slowing C-type inactivation (Barhanin et al., 1996; Sanguinetti et al., 1996; Yang et al., 1997; Sesti and Goldstein, 1998; Tristani-Firouzi and Sanguinetti, 1998; Wu et al., 2010). Physiologically, the I_{Ks} current begins to activate during Phase 0 depolarization, and becomes a prominent hyperpolarizing K^+ current in Phases 3 and 4 of the cardiac myocyte action potential (Tristani-Firouzi et al., 2001). The identification of KCNQ1 was important as it guided the discovery of the neuronal KCNQ2-5 genes (Jentsch, 2000). The KCNQ1 crystal structure ((Sun and MacKinnon, 2017) also continues to guide the modelling of other KCNQ subtypes, which has been particularly useful for the work in this thesis.

KCNQ1 is implicated in LQTS

Shortly after the identification of KCNE1, KCNQ1 became the first KCNQ subtype to be identified and cloned due to its link to an inherited form of cardiac arrythmia - long QT syndrome type 1 (LQT1) (Wang et al., 1996). LQT is a condition that prolongs the Q-T interval observed on an electrocardiogram, which translates to significant delay between ventricular depolarization and repolarization (Wang et al., 1996; Tristani-Firouzi et al., 2001). This can have serious consequences on the cardiac rhythm of patients

and can result in syncope and ventricular arrythmias (Tristani-Firouzi et al., 2001). Patients with LQTS are also limited in the pharmacological agents they can use for other illnesses, since many drugs can exacerbate their condition by desynchronizing cardiac electrical activity and causing life-threatening arrythmias people without LQTS rarely experience (Fazio et al., 2013). LQT1 and LQT5 occur from KCNQ1 and KCNE1 mutations respectively, both characterized by the reduced expression of cardiac I_{Ks} (Tristani-Firouzi et al., 2001). Alternatively, KCNQ1 and KCNE1 mutations that enhance I_{Ks} can also cause cardiac issues, including short QT syndrome (SQT) and familial atrial fibrillation (Rothenberg et al., 2016; Whittaker et al., 2018).

KCNQ1 is also implicated in auditory disease

KCNQ1 and KCNE1 are also involved in auditory function by maintaining ionic homeostasis in the cochlea of the inner ear (Neyroud et al., 1997). K^+ ions leave the endolymph during auditory stimulation, and KCNQ1/KCNE1 channels are believed to facilitate K^+ recycling in the endolymph to maintain auditory function (Neyroud et al., 1997; Bleich and Warth, 2000; Casimiro et al., 2001). Therefore, mutations that sufficiently reduce KCNQ1/KCNE1 channel function can have implications in both LQTS and auditory disease, as seen in patients with Jervell and Lange-Nielsen Syndrome (JLNS) (Casimiro et al., 2001).

KCNQ2-3 encode the neuronal 'M-current'

The M-channel, encoded primarily by the KCNQ2 and KCNQ3 genes, was initially identified by Brown and Adams (1980) in frog sympathetic ganglia and named due to its suppression by muscarinic receptor activation (Brown and Adams, 1980). Due to their ankyrin G binding region in the C-terminus, KCNQ2 and KCNQ3 cluster to the axon initial segment and nodes of Ranvier along with voltage-gated sodium channels (Nav) in neurons (Pan et al., 2006). Several hallmark features of M-channels have been described: activation at subthreshold potentials around – 60 mV, slow rates of activation requiring tens to hundreds of milliseconds, lack of inactivation, and sensitivity to cholinergic suppression via muscarinic GPCRs (Constanti and Brown, 1981; Selyanko et al., 2000; Brown and Passmore, 2009). These properties

allow M-channels to generate a sustained K^+ conductance to suppress repetitive firing of neurons in an activity-dependent manner, and also to be physiologically regulated by acetylcholine to fine tune neuronal activity (Brown and Passmore, 2009).

M-channels are likely formed by the heteromeric assembly of KCNQ2 and KCNQ3 (Brown and Passmore, 2009). Several pieces of evidence support this idea. First, KCNQ2 and KCNQ3 are co-localized to axon initial segments and nodes of Ranvier in neurons (Cooper, 2011; Benned-Jensen et al., 2016). Next, KCNQ2 and KCNQ3 have a propensity to co-immunoprecipitate when expressed heterologously and lysates from native neurons (Cooper et al., 2000). Co-expressed KCNQ2 and KCNQ3 produce currents that are biophysically comparable to M-currents, and display similar attenuation of TEA-mediated suppression of M-currents, where homomeric KCNQ2 channels are strongly suppressed (Wang et al., 1998). KCNQ2 can also be functionally expressed in heterologous systems, but KCNQ3 expresses very poorly unless a specific [A315T] pore mutation is introduced to promote efficient membrane trafficking (Gómez-Posada et al., 2010). Finally, homomeric KCNQ2 channels differ biophysically and pharmacologically when compared to M-channels (Wang et al., 1998; Hadley et al., 2000; Selyanko et al., 2000; Shapiro et al., 2000). Therefore, due to the differences when compared to homomeric KCNQ2 and KCNQ3, and the similarities to co-expressed heteromeric KCNQ2/KCNQ3 channels, M-channel likely formed by the heteromeric assembly of KCNQ2 and KCNQ3.

In humans, M-channels are expressed abundantly in central and peripheral neurons to facilitate the efflux of K^+ and suppress neuronal excitability (Jentsch, 2000; Robbins, 2001). M-channels are expressed extensively in the cerebrum, cerebellum, and hippocampus of the central nervous system, regulating the activities of these brain regions (Brown and Passmore, 2009). M-channels are also expressed in the dorsal root ganglia of the peripheral nervous system, where it suppresses nociceptive neurons and produces analgesic effects when activated (Brown and Passmore, 2009). Its diverse functions make M-channels a viable therapeutic target for the treatment or management of neurological and sensory disorders. In addition, mutations that disrupt M-channel function can result in neurological disease (Robbins, 2001).

Mutations in KCNQ2 and KCNQ3 can cause neonatal epilepsies and encephalopathies

Benign familial neonatal epilepsy (BFNE) is an autosomal dominant form of epilepsy that affects 1:100,000 patients (Rogawski, 2000). BFNE produces generalized seizures involving both sides of the cerebrum, and are often associated with breathing difficulties, abnormal heart rates, general confusion, seizures, stiffening of muscles, and jerking movements (Weckhuysen et al., 2013). The seizures begin within the first week of life, but usually self-resolve within the first few months of life (Weckhuysen et al., 2013). It is not understood why BFNE is self-resolving, other than speculations that sufficient compensatory mechanisms may have developed in patients during development (Rogawski, 2000). While many of the seizure characteristics are concerning, BFNE often does not usually disrupt brain development or leave permanent neurological damage (Rogawski, 2000). In fact, most patients experience normal neurological development, and only <16% of patients are at greater risk for seizures later in life (Robbins, 2001). It is difficult to treat BFNE, but patients may be given anti-convulsants (e.g. phenobarbital, phenytoin, or sodium valproate) to manage the seizures. However, due to the transient nature of BFNE, patients are eventually weaned off of anti-convulsants with little to no complications (Rogawski, 2000).

KCNQ2 was identified as a BFNE-linked gene on chromosome 20 and named due to its similarity to the already identified KCNQ1 (Leppert et al., 1989; Charlier et al., 1998; Singh et al., 1998). KCNQ3 was similarly identified on chromosome 8 due to its link to BFNE and contribution to the M-current (Lewis et al., 1993; Biervert et al., 1998). Mutations in KCNQ2 or KCNQ3 that reduce M-channel conductance by 20-30% are sufficient to cause BFNE (Schroeder et al., 1998). Many BFNE-linked mutations have been identified, and typically occur in regions important for channel function. BFNE-linked mutations often influence the voltage-dependence, gating properties, and ionic selectivity of the M-channel (Jentsch, 2000). Several dominantly inherited BFNE-linked mutations identified in KCNQ2 and KCNQ3 produces channels with decreased or eliminated function, and only occur on one copy of the respective gene. It is unclear how BFNE is caused by such mutations, but two possibilities have been proposed: either the haploinsufficiency

of functional KCNQ2 or KCNQ3, or dominant-negative effects caused by assembly of loss-of-function mutants with functional channels (Rogawski, 2000).

While mild mutations in KCNQ2 typically result in BFNE, severe mutations that significantly impair KCNQ2 or M-channel function can cause epileptic encephalopathy (EE) (Weckhuysen et al., 2013). EE may resemble BFNE due to its characteristic onset of seizures in the first week of a patient's life (Weckhuysen et al., 2013). However, EE is much more severe, and can cause bradycardia and apnea with potential to severely impair neurological development. Unlike BFNE, EE may cause lifelong neurological or intellectual impairments, and even death (Weckhuysen et al., 2013).

KCNQ4 channels contribute to hearing and other diverse functions

KCNQ4 was originally identified through studies on hereditary hearing loss, and later was found to be heavily expressed in the cochlear and vestibular tissue. In both tissues, KCNQ4 contributes to auditory functions by mediating the efflux of K^+ to control intracellular K+ concentrations (Kubisch et al., 1999). Despite KCNQ4 presence in the vestibule, it does not seem to contribute to spatial orientation or the ability to balance typically associated with vestibular function (Kubisch et al., 1999). In the lower brain regions where KCNQ4 is expressed in neurons, it can affect the release of neurotransmitters by regulating fusion of synaptic vesicles (Kharkovets et al., 2000). Finally, KCNQ4 is expressed in mechanoreceptors, and may be important for touch sensation (Heidenreich et al., 2011).

KCNQ5 may contribute to the neuronal 'M-current'

KCNQ5 shares the lowest sequence similarity (~40%) with other KCNQ subtypes. KCNQ5 is expressed broadly in the brain, and often in similar brain regions as KCNQ2 and KCNQ3 (Schroeder et al., 2000). KCNQ5 is believed to heteromerically assemble with KCNQ2 or KCNQ3 to conduct an M-like current (Schroeder et al., 2000). *Xenopus laevis* oocyte studies demonstrated that KCNQ5 functionally assembles with KCNQ3 to enhance current expression by 4-5-fold but does not appear to interact with KCNQ2 (Schroeder et al., 2000). KCNQ3/5 channels display similar functional and pharmacological

characteristics as the classical KCNQ2/3 M-channels (Schroeder et al., 2000). If KCNQ5 can heteromerically assemble into M-like channels physiologically, it may contribute to the same regulation of neuronal excitability as classical M-channels. Little is known regarding KCNQ5 assembly with other KCNQ subtypes. In the periphery, KCNQ5 expression has been detected in sympathetic ganglia and in skeletal muscles, both of which have a KCNQ3 presence (Schroeder et al., 1998).

There are no clear physiological roles of KCNQ5 as of the writing of this thesis, though evidence of KCNQ5's physiological importance is implied through links to hereditary disease. Mutations in KCNQ5 have been linked to autosomal dominant forms of EE and intellectual disability (Lehman et al., 2017), supporting its potential role as a contributor to neuronal M-currents.

KCNQ CHANNEL PHARMACOLOGY

Epilepsy and pharmacoresistance to AEDs

Epilepsy is an excitatory neurological disorder that affects about 60 million people worldwide. Epileptic patients exhibit a spectrum of symptoms, from mild confusion to unprovoked debilitating seizures. These are caused by the excessive and often synchronous firing of neurons (Stafstrom and Carmant, 2015). It is difficult to predict the onset of such seizures, which can endanger the patient and their surroundings when seizures occur unexpectedly (Stafstrom and Carmant, 2015). In addition, epileptic patients can experience indirect harms both economically and socially caused by the symptoms of the illness and costs associated with its management (Stafstrom and Carmant, 2015). The molecular causes of epilepsy are diverse, including but not limited to head injuries, tumors, autoimmune disorders, malnutrition, drug and alcohol use, and genetic mutations (Stafstrom and Carmant, 2015). However, for most patients, the underlying cause of epilepsy is poorly understood or unknown (Stafstrom and Carmant, 2015).

The diversity in its causes and gaps in the understanding of epilepsy make this disorder difficult to treat and manage (Stafstrom and Carmant, 2015). Antiepileptic drugs (AEDs) are typically used to manage the severity or frequency of seizures by suppressing the firing of neurons, but they do not treat the underlying disorder (Shorvon et al., 2015). AEDs are prescribed to patients as monotherapies, though patients who are resistant or refractory to treatment may move to combination therapies. Many epileptic patients (~30%) are resistant to AED treatments, even with combination therapies (Shorvon et al., 2015). These patients often undergo more individualized and specialized treatments (e.g. surgical intervention), or simply leave their epilepsies unmanaged (Shorvon et al., 2015).

An explanation for the high prevalence of pharmacoresistant epilepsy is while approximately ~30 AEDs exist and are currently approved for clinical use, they share similar molecular targets: inhibition of Na^+ channels, modulation of GABA receptors, inhibition of AMPA receptors, and rarely through inhibition of Ca^{2+} channels (Rogawski, 2013; Shorvon et al., 2015; Stafstrom and Carmant, 2015). Hence, for patients

with pharmacoresistant epilepsy, there remains a need to study and develop AEDs that target novel targets and/or pathways. The goal is to develop novel pharmacotherapies that can be used independently or in combination with other drugs to allow the effective management pharmacoresistant epilepsy without the need for medically invasive procedures. Recently, the neuronal KCNQ channels have emerged as targets for the management of pharmacoresistant epilepsy (Gunthorpe et al., 2012). Retigabine (RTG) was the first-in-class drug approved by the FDA for the clinical management of pharmacoresistant epilepsy, and its effectiveness has motivated the study and ongoing development of novel KCNQ activating compounds (e.g. ICA-069673 and ML-213).

Retigabine: first-in-class pore targeted KCNQ channel activator

RTG is the first Kv channel activator approved for the treatment of epilepsy. While RTG proved effective in treating pharmacoresistant epilepsy in some patients, it was used without a full understanding of its mechanism of action (Gunthorpe et al., 2012). Several important properties of RTG include its selectivity towards neuronal Kv7/KCNQ channels, ability to shift voltage-dependence of channels to more negative voltages, hyperpolarization of neurons, and suppression of action potential frequency (Yue and Yaari, 2004; Gunthorpe et al., 2012). RTG proved useful for many patients in their management of pharmacoresistant epilepsy (Gunthorpe et al., 2012). However, GlaxoSmithKline announced the discontinuation of RTG production for clinical use in 2017. This decision was partly due to RTG's many side effects and safety issues in patients, including eye abnormalities and skin discoloration, which led to low rates of RTG usage in patients and low financial incentive for the company. Many of these side effects were likely due to the off-target activation of KCNQ channels outside the central nervous system (Gunthorpe et al., 2012).

Mechanistic insights on RTG and the use of voltage clamp fluorometry (VCF)

Since its approval by the FDA for clinical use, studies have elucidated important details describing the binding site and mechanistic properties of RTG. RTG binds to an essential Trp residue (W236 in KCNQ2

and W265 in KCNQ3) in the S5 helix of the pore domain via a critical hydrogen bond (Schenzer et al., 2005; Lange et al., 2009; Kim et al., 2015). This interaction stabilizes the open conformation of neuronal KCNQ channels and shifts voltage-dependence of activation to more negative voltages (Schenzer et al., 2005; Lange et al., 2009). The critical Trp residue is conserved in neuronal KCNQ2-5 but is absent in the RTG-insensitive KCNQ1, explaining the absence of significant cardiac effects caused by this drug. Interestingly, partial RTG-sensitivity can be restored upon an analogous L266W mutation in KCNQ1 (Schenzer et al., 2005). Having characterized its binding site, RTG was later determined through concatenated channel tetramers to require only one sensitive subunit to elicit near-maximal channel-opening effects, demonstrating the potency of RTG-mediated channel effects (Yau et al., 2018).

RTG's mechanism was further elucidated by Kim et al. (2017) through the use of voltage-clamp fluorometry (VCF). In this study, RTG was shown to enhance the interaction between KCNQ3 and PIP_2, resulting in the resistance of PIP_2 to hydrolysis by a voltage sensitive phosphatase (CiVSP) (Kim et al., 2017). This subsequently led to the channel's resistance to phosphatase-mediated current rundown (Kim et al., 2017). RTG seems to strengthen the coupling between the voltage sensor and the pore by increasing channel affinity for PIP_2, and this strengthened coupling improved the pore's sensitivity to voltage sensor conformational changes (Kim et al., 2017). Conversely, mutations that eliminate putative PIP_2 binding KRRK sequence in the S6 helix can moderately reduce RTG's channel opening effects, suggesting PIP_2's role in coupling RTG binding in the pore to changes in channel voltage sensitivity (Kim et al., 2017).

ICA-73: voltage sensor targeted KCNQ channel activator

ICA-069673 (ICA-73) is another KCNQ activating compound with distinct properties from RTG. ICA-73 mediates its channel opening effect through a mechanism independent of RTG-sensitivity, as the RTG-insensitive KCNQ2[W236F] mutant retains full sensitivity to ICA-73 (Wang et al., 2017). Instead, ICA-73 relies on two currently identified residues – F168 and A181 – in the voltage sensors of sensitive channels (Wang et al., 2017). Only KCNQ2 and KCNQ4 are sensitive to ICA-73 channel opening effects, despite all neuronal KCNQs being sensitive to RTG, further supporting a differential mechanism between

the two drugs (Boehlen et al., 2013; Brueggemann et al., 2014). In contrast to RTG, application of saturating ICA-73 to KCNQ2 causes unique effects on channel function: a larger hyperpolarizing shift in channel voltage-dependence, significant deceleration of channel closure, and potentiation of currents (whereas RTG may attenuate currents instead) (Kim et al., 2015; Wang et al., 2017).

Recent studies identified unique pharmacological properties currently known to be specific to ICA-73. The understanding of these properties was critical for my thesis work in Chapters 3 and 4. These properties were exploited in my thesis work to detect the functional assembly of heteromeric KCNQ channels and for understanding the link between KCNQ mutations and human disease.

Subtype selectivity

ICA-73 is selective for KCNQ2 and KCNQ4, with little to no effect on other KCNQ subtypes (Boehlen et al., 2013; Brueggemann et al., 2014). Wang et al. (2017) determined that a chimera containing the KCNQ2 voltage sensor and the KCNQ3 pore produced channels sensitive to ICA-73. Further chimeric experiments isolated the determinants of ICA-73 sensitivity to be within the S3-S4 helix of the voltage sensing domain (Wang et al., 2017). Finally, two critical positions were identified in the KCNQ2 voltage sensor: F168 and A181 (L and P respectively in the ICA-73 insensitive KCNQ3). Mutating these positions to the residues found in KCNQ3 abolished (F181L) or weakened (A181P) ICA-73 effects (Wang et al., 2017). Conversely, mutating KCNQ3 at L198 and P211 to residues found in KCNQ2 (F and A respectively) produced ICA-73 sensitive KCNQ3 channels (Wang et al., 2017). Therefore, sensitivity to ICA-73 appears to be dependent on two critical residues, Phe and Ala in the voltage sensing domain normally found in KCNQ2 and KCNQ4, but not in KCNQ3.

State dependence

ICA-73 can only mediate its channel opening effects after channels have been activated through depolarization; this was described as state-dependence of ICA-73 effects (C. K. Wang et al., 2018). The extent of ICA-73 effects positively correlates with the extent of voltage dependent activation, producing a

voltage-dependence of drug effects that overlaps closely with the voltage-dependence of channel activation (C. K. Wang et al., 2018). It is currently believed that the activation of the voltage sensor exposes a normally occluded drug binding site, allowing ICA-73 to bind stabilize the activated channel conformation and prevent closure (C. K. Wang et al., 2018). Closure of channels likely requires the drug to unbind. Due to ICA-73's slow rate of unbinding, it significantly extends the time required for full channel closure (C. K. Wang et al., 2018). State-dependence can be a useful therapeutic property, as ICA-73 is more likely to target hyperactive neurons rather than neurons at rest. Hyperactive neurons are more frequently depolarized, resulting in a greater proportion of activated KCNQ2 channels available for drug binding. ICA-73 may therefore produce fewer side effects in the management of epilepsy when compared to RTG, due to its selectivity for KCNQ2 and KCNQ4, as well as state-dependence (C. K. Wang et al., 2018).

Stoichiometric dependence

Four drug-sensitive KCNQ subunits are required for ICA-73 to elicit its maximal channel opening effect (A. W. Wang et al., 2018). A.W. Wang et al. (2018) showed that KCNQ2 and KCNQ3 have attenuated sensitivity to ICA-73's channel opening effects relative to KCNQ2 alone (A. W. Wang et al., 2018). Additionally, WT KCNQ2 and KCNQ2[F168L] tetrameric concatemers became increasingly sensitive to ICA-73 with increasing KCNQ2:KCNQ2[F168L] stoichiometric ratios (A. W. Wang et al., 2018). The stoichiometric dependence property of ICA-73 is important in my thesis work as any assembly between KCNQ2 and ICA-73 insensitive channels can be detected as an attenuation of ICA-73's channel opening effects.

The unique properties of ICA-73 can potentially guide the development of novel KCNQ-targeted AEDs with greater subtype selectivity, state-dependence, and reduced side effects. My thesis work also demonstrates its potential to be used scientifically for understanding ion channel function, studying human disease, and improving our understanding of KCNQ pharmacology. Table 1.1 outlines key differences between RTG and ICA-73.

	Retigabine (RTG)	ICA-069673 (ICA-73)
Binding site	Pore	Voltage sensor
Critical residues	W236 (KCNQ2) W265 (KCNQ3)	F168 and A181P (KCNQ2)
Subtype selectivity	Neuronal KCNQ2-5	KCNQ2, KCNQ4
State dependence	No	Yes
# of drug sensitive subunits required for maximal effect	1	4

Table 1.1: Known differences between RTG and ICA-73. Postulated drug binding site, critical residues required for drug effect, subtype selectivity, state dependence, and drug-sensitive subunits required for maximal effect.

SCOPE OF THESIS INVESTIGATION

As an emerging class of anti-epileptic drug, KCNQ channel openers and their mechanism of action are gradually being understood. While no KCNQ openers are currently produced for clinical use (2019), the two subtypes of KCNQ openers – voltage sensor-targeted (e.g. ICA-73) or pore-targeted (e.g. RTG) drugs – demonstrate the potential to use as therapeutics for the treatment of pharmacoresistant epilepsies, and to guide the development of more potent, selective, and efficacious KCNQ openers. In addition to their clinical potential, these drugs can be utilized as pharmacological tools in ion channel research. Two chapters in this thesis investigates KCNQ channel mutations, their effects on channel assembly, and relation to human disease using an ICA-73 pharmacological assay. The final chapter investigates an approach to improve the use of voltage-clamp fluorometry in KCNQ channels, through an approach that can potentially be applied to other channels, and help enable future KCNQ functional and pharmacological studies.

In Chapter 3, we collaborated with Dr. Elysa Marco in investigating a KCNQ3 truncation mutation observed in a child patient. We were interested in this mutation because while the patient exhibits autistic and ataxic phenotypes, studies on KCNQ channel assembly imply that such a mutation will eliminate the mutant's ability to assemble into M-channels with KCNQ2. To determine whether phenotypes are due to haplo-insufficiency or dominant negative suppression of endogenous wild type channels, we created a pharmacological assay using ICA-73 and detected the unexpected assembly of heteromeric M-channels between KCNQ3 truncations and KCNQ2.

In Chapter 4, we collaborated with Dr. Billie Au, Dr. Juan Appendino, and Dr. Marvin Braun in investigating a BFNE-linked KCNQ3 mutation [T313I]. Using the same pharmacological assay established in Chapter 3, we detected the assembly of functional heteromeric M-channels between KCNQ3[T313I] and wild type KCNQ2 channels. In addition, we constructed KCNQ3[T313I] M-channel concatemers and observed a suppression of M-channel currents relative to wild type KCNQ3, which may have caused the BFNE observed in the proband.

Lastly, in Chapter 5, we investigated a methodical approach to improve the strength and consistency of voltage-clamp fluorometry (VCF) signals from KCNQ3 channels. Using the structure and sequence of KCNQ1 as guide, a channel that consistently produces massive VCF signals, we constructed KCNQ3 VCF mutants with significantly improved VCF consistency and signal strength, which can be applied to future functional and pharmacological studies on KCNQ3. Our approach for improving VCF signals from KCNQ3 can be potentially applicable to other KCNQ channels (particularly KCNQ2), and perhaps also other classes of ion channels.

Overall, this thesis addresses gaps in our understanding of KCNQ3 channel function, and highlights how we can use an improved understanding of KCNQ-targeted drugs to explore the details of M-channel assembly and study the relation between KCNQ mutations and human disease. In addition, we improved upon the VCF technique that has been valuable for understanding the pharmacology of KCNQ openers and demonstrated an approach that may enable future functional and pharmacological studies of other ion channels.

CHAPTER 2: MATERIALS AND METHODS

Ion channel constructs and molecular biology

Human KCNQ2 and KCNQ3 cDNAs in the pTLN expression vector were gifts of Dr. M. Taglialatela and Dr. T. Jentsch. The KCNQ3-FS534 truncation and KCNQ3[T313I] was generated by their corresponding mutagenic primers using the two-step overlapping PCR approach, and subcloned into the original pTLN vector using NotI and EcoRI restriction enzymes. The artificial KCNQ3 truncations were generated through introduction of a TAG stop codon at amino acid positions 369, 532, 571, and 830 through a one-step PCR approach, and subcloned into the original pTLN vector using NotI and KpnI restriction enzymes to produce KCNQ3-ΔC503, KCNQ3-ΔC340, KCNQ3-ΔC301, and KCNQ3-ΔC42 respectively.

The human KCNQ3[A315T] channel trafficks more efficiently to the cell membrane than wild type KCNQ3 and was used for the homomeric expression of KCNQ3 channels. KCNQ3[A315T] was cloned into the pSRC5 vector and were gifts of Dr. M. Taglialatela and Dr. T. Jentsch. KCNQ3[A315T]-FS534 and KCNQ3[A315T][T313I], and KCNQ3[A315T][Q218C] (referred to as KCNQ3*VCF) mutant channels were generated by their corresponding mutagenic primers using the two-step overlapping PCR approach, and subcloned into the original pSRC5 vector using NotI and EcoRI restriction enzymes.

The KCNQ2 tetrameric concatemer was generated in pCDNA3.1(-) in a previous study (A. W. Wang et al., 2018). Wild type KCNQ3 or KCNQ3[T313I] were amplified through a flanking PCR, restriction digested using NheI and XbaI, and finally inserted into the original KCNQ2 concatemer by replacing the first KCNQ2 channel gene. The overall design summarized is: NheI-(KCNQ3 or KCNQ3[T313I])-XbaI-(KCNQ2)-EcoRV-(KCNQ2)-EcoRI-(KCNQ2)-BamHI-(GFP)-(STOP CODON)-HindIII.

Sequences for all KCNQ channel constructs were verified by Sanger sequencing through the University of Alberta's Applied Genomics Core (TAGC). Mutagenic primers are listed in Table 2.1: forward

and reverse flanking primers, forward primers for site-directed mutagenesis, and reverse primer for introducing the TAG stop codon are shown in Table 2.1.

Oocyte harvesting and microinjection

Mature *Xenopus laevis* females were obtained from the University of Alberta Department of Biological Sciences. Lobes of stage V-VI oocytes were harvested surgically and dissected into fragments of 10-20 oocytes in filtered OR2 solution (82.5 mM NaCl, 2.5 mM KCl, 1 mM $MgCl_2$, 5 mM HEPES, pH 7.6). Fragments were transferred into an OR2 solution containing 3 μg/mL type IV collagenase (Worthington Biochemical Corporation) and diluted to a final enzyme concentration of 2 μg/mL in 50 mL falcon tubes. Oocytes were defolliculated on a rotator for 2 hours at a rotation frequency of 0.5 Hz. After 2 hours, oocytes were checked on every 15 minutes to ensure that most oocytes have been defolliculated. Defolliculated oocytes were rinsed with 25 mL of OR2 solution four times prior to incubation in a filtered OR3 solution (500 mL Liebovitz's L-15 medium, 15 mM HEPES, 1 mM L-glutamine, 0.5 mM gentamycin, pH 7.6) and allowed to rest for at least 4 hours in 18˚C prior to sorting and mRNA microinjections.

cDNAs were linearized with MluI for pTLN(KCNQ2), HpaI for pTLN(KCNQ3), and ApaLI for pSRC5(KCNQ3[A315T]) and ethanol precipitated to concentrate templates for RNA transcription. Concentrated mRNAs were transcribed from linearized cDNAs using the SP6 (for channels pTLN) or T7 (for channels in pSRC5) mMessage mMachine kit (Ambion). All mRNAs were diluted to experimental concentrations to ensure that the correct amounts of mRNA can be injected through a 50 nL injection. After microinjections, oocytes were incubated for 24-72 hours at 18˚C before recording using two electrode voltage clamp electrophysiology.

Frog surgeries, oocyte handling, and mRNA injections were done under the approval of University of Alberta Animal Care Protocol AUP00001752.

Mammalian cell culture and transfection

Mouse LM (tk-) fibroblasts (ATCC), referred to in this thesis as LM cells, were cultured in 50 mL polystyrene tissue culture flasks (Falcon) in Dulbecco's Modified Eagle Medium – DMEM (Invitrogen) supplemented with 10% fetal bovine serum and 1% penicillin and streptomycin. LM cells were transferred into six-well plates and transfected with plasmids encoding concatenated tetrameric channels using the jetPRIME DNA transfection reagent (Polyplus). Successfully transfected cells were identified visually due to the C-terminal GFP tag in our constructs. Cells were incubated at 37˚C in 5% CO_2, and for 24 hours after transfection to allow sufficient channel expression for whole cell patch-clamp recordings.

Two electrode voltage-clamp electrophysiology

Recording pipettes were pulled from borosilicate glass tubes (Harvard Apparatus LTD) using a Sutter P-97 puller (Sutter Instrument), and had resistances between 0.1-1 MΩ. Recordings were filtered at 5 kHz and sampled at 10 kHz using a Digidata 1440A (Molecular Devices) controlled by pClamp 10 software (Molecular Devices). Recordings were done in modified Ringer's solution (116 mM NaCl, 2 mM KCl, 1 mM $MgCl_2$, 0.5 mM $CaCl_2$, 5 mM HEPES, pH 7.4). Pipettes were filled with 3M KCl solution.

Voltage-clamp fluorometry

VCF requires oocytes to incubate for 3 days post-microinjection to allow sufficient channel expression. The Alexa-488 maleimide cysteine-reactive fluorophore was stored as 3 µL aliquots and diluted to 100 µM with depolarizing high K^+ Ringer's solution (100 mM KCl, 1mM $MgCl_2$, 0,5 mM $CaCl_2$, 5 mM HEPES, pH 7.6) each experimental day. Oocytes expressing KCNQ3*VCF constructs were labeled in the fluorophore solution for 20 minutes on ice, rinsed using standard Ringer's solution, and finally kept on ice in modified Ringer's solution prior to recordings. VCF was performed with two electrode voltage-clamp on an Olympus IX51 inverted microscope. A PhlatLight LED (Luminus Devices) served as the light source and was directed to the dark poles of oocytes. Fluorescence from the oocyte was filtered and converted into

an electrical signal by a PIN040-A photodiode (OSI Optoelectronics). The electrical signal was sent to a patch-clamp unit, where the signal was amplified and sent to the pClamp 10 software for recording.

Whole cell patch-clamp

Patch pipettes were pulled from soda lime capillary glass tubes (Fisher) using a Sutter P-97 puller (Sutter Instrument) and had resistances of 1-3 MΩ. Recordings were filtered at 5 kHz and sampled at 10 kHz, and manually compensated for capacitance and series resistance. Recordings were done on cells immersed in bath solution (135 mM NaCl, 5 mM KCl, 1 mM $CaCl_2$, 1 mM $MgCl_2$, 10 mM HEPES, pH 7.4). Pipettes were filled with an internal solution (135 mM KCl, 5 mM K-EGTA, 10 mM HEPES, pH 7.2).

Drug solutions

Retigabine was purchased from Toronto Research Chemicals, and ICA-069673 was obtained from Tocris. Both drugs were dissolved in DMSO to produce 100 mM stock solutions. Drug stock solutions were diluted into respective extracellular solutions each experimental day.

Data analysis

Conductance-voltage relationships for channels were fit using a standard single component Boltzmann equation in the form:

$$\frac{G}{Gmax} = \frac{1}{1 + e^{-(\frac{V - V1/2}{k})}}$$

Where $V_{1/2}$ is the voltage where channels exhibit half-maximal activation, k is the slope factor reflecting the voltage range over which an e-fold change in the open probability (P_o) is observed, and G/Gmax is the proportion of channels in the open and conducting state. Fractional instantaneous currents were determined as the ratio of the instantaneous current divided by the maximal current in the presence or absence of ICA-73. Statistical tests and significance are described in figure legends throughout the thesis.

Student's T-test was used for one comparison of mean between two groups. Non-parametric Kruskal-Wallis one-way ANOVA was used for comparing ranks on fractional instantaneous current and current amplitude data. Dunnett's post-hoc test was used to compare means to a control mean. Tukey's post-hoc test was used to compare every mean with multiple control means.

Molecular modelling

Molecular models of KCNQ2 and KCNQ3 were generated using the online SWISS-MODEL tool (Waterhouse et al., 2018), using the 2017 cryo-EM structure of KCNQ1 as guide (Sun and MacKinnon, 2017). These models are for illustration only and have not undergone refinement or development beyond this web-based homology modelling tool.

Primer name	Sequence of forward primer (5' to 3')	Primer name	Sequence of reverse primer (5' to 3')
KCNQ3 FF	GGC GAC GTG GAG CAA GTC ACC	**KCNQ3 RF**	TAA GGC CTC AAA GTC TCC TTG
KCNQ3 tetrameric insert FF	GGG GGC TAG CAT GGG GCT CAA GGC GCG C	**KCNQ3 tetrameric insert RF**	GGG GTC TAG AAA TGG GCT TAT TGG AAG G
KCNQ3-FS534	CCG TCT CTA TAA AAA AAA AAT TCA AGG AGA C	**KCNQ3-ΔC503**	GCG CGG TAC CCT ACT CAA AGT GCT TCT GAC G
KCNQ3 T313I	GCC TGA TCA TAC TGG CCA CCA TTG GC	**KCNQ3-ΔC340**	GCG CGG TAC CCT AAT AGA GAC GGA ATT GTA G
KCNQ3 A315T T313I	GCC TGA TCA TAC TGA CCA CCA TTG GC	**KCNQ3-ΔC301**	GCG CGG TAC CCT AAA TCA TAT CTA TTC TCG TC
KCNQ3 L156W L157F	CGG GAG ACT GGT GGT TCT TAC TGG AGA C	**KCNQ3-ΔC42**	GCG CGG TAC CCT AGC TTC TCC CTC ATC CAG C
KCNQ3 Q218C L222F	GGA AAC TGC GGC AAT GTT TTC GCC ACC TCC		
KCNQ3 Q218C L222W	GGA AAC TGC GGC AAT GTT TGG GCC ACC TCC		

Table 2.1: List of mutagenic primers. Forward primers are used with the corresponding reverse flanker, and vice versa for reverse primers. FF = forward flanker, RF = reverse flanker. Constructs requiring the two-step PCR method used corresponding flanking primers in the second step. All constructs were generated using the listed primers.

CHAPTER 3: PHARMACOLOGICAL DETECTION OF HETEROMERIC ASSEMBLY OF TRUNCATED KCNQ3 CHANNELS

BACKGROUND

KCNQ2 and KCNQ3 are the primary molecular correlates of the neuronal M-current, a hyperpolarizing potassium current that controls threshold and burst firing properties of neurons (Brown and Adams, 1980; Wang et al., 1998; Cooper et al., 2000; Shapiro et al., 2000). M-channels are physiologically regulated by membrane levels of PIP_2, which are controlled by M1 acetylcholine receptor-mediated activation of $G_{q/11}$ and phospholipase C (Zhang et al., 2003; Suh and Hille, 2007). Since these channels are expressed broadly in the central nervous system and play an important role in controlling neuronal excitability, then it is no surprise that mutations in KCNQ2 and KCNQ3 have been linked to a spectrum of childhood epileptic conditions (Biervert et al., 1998; Charlier et al., 1998; Singh et al., 1998). KCNQ3 mutations are most commonly associated with benign familial neonatal epilepsy (BFNE); a mild form of childhood epilepsy that is responsive to conventional anti-epileptic drugs and typically resolves in the first few years of life with no structural or cognitive impairment (Maljevic and Lerche, 2014; Miceli et al., 1993). In contrast, despite its similar involvement in M-channels, KCNQ2 mutations are linked to far more severe neurological defects including pharmacoresistant seizures, epileptic encephalopathy (EE), and global neurodevelopmental delay (Miceli et al., 1993; Weckhuysen et al., 2012; Lerche et al., 2013; Maljevic and Lerche, 2014; Millichap et al., 2016).

Assembly of KCNQ2 and KCNQ3 produces heteromeric channels biophysically distinct from either homomeric channels, including unique voltage-dependence, current expression, and altered sensitivity to pharmacological agents (Shapiro et al., 2000; Wang et al., 1998). It is generally believed that the C-terminus of KCNQ channels govern subtype-specific channel assembly. KCNQ1 and KCNQ3 channels are not normally compatible and do not generate functional heteromeric channels, but this exclusion can be overcome by the chimeric swapping of the C-terminal regions between KCNQ subtypes (Schmitt et al., 2000; Maljevic et al., 2003; Schwake et al., 2003, 2006). Specifically, the C-terminal helices C and D

contains segments with high probabilities for the formation of coiled-coiled domains thought to contribute to tetrameric assembly and influence subtype specificity (Howard et al., 2007). However, there remains significant uncertainty regarding the determinants of subtype-selective assembly of KCNQ2-5 channels.

ClinVar and RIKEE databases report a variety of KCNQ2/KCNQ3 frameshift and truncation mutations summarized visually in Figure 3.1 A. KCNQ2 truncations often cause severe phenotypes (e.g. epileptic encephalopathy, red symbols in Figure 3.1 A) compared to similar KCNQ3 truncations (e.g. benign familial neonatal epilepsy, green symbols in Figure 3.1 A). In these cases of KCNQ-related disease, it is unclear if abnormal channel function arises from haploinsufficiency of functional KCNQ channels versus dominant negative effects from the assembly of mutated subunits with normal subunits. In other words, truncation of one copy of KCNQ2 or KCNQ3 may reduce the number of normal subunits available to form functional M-channels, reducing M-current expression, or alternatively, truncated subunits may assemble with wild type subunits and suppress function in a dominant negative manner, also reducing M-current expression. Additionally, heteromerization of KCNQ2 and KCNQ3 influences sensitivity to certain types of Kv7/KCNQ activators, so studying their assembly and how sensitivity to pharmacological agents is changed can influence the selection of therapies for managing patient epilepsies.

Lauritano et al. (2019) recently identified a homozygous KCNQ3 truncation at amino acid 534 in a patient with intellectual disability and pharmacodependent epilepsy (Lauritano et al., 2019). We investigated a patient with an identical KCNQ3 mutation (but heterozygous and *de novo*), to study the effects of KCNQ3 channel truncations on M-channel assembly and function. Using the subtype specific actions of the voltage sensor targeted ICA-069673 (ICA-73) (Padilla et al., 2009; Wang et al., 2017; A. W. Wang et al., 2018), we devised a pharmacological strategy to assess heteromeric channel assembly. ICA-73 drastically decelerates the deactivation of homomeric KCNQ2 channels, but this effect is significantly attenuated when KCNQ2 and KCNQ3 are co-assembled (A. W. Wang et al., 2018; C. K. Wang et al., 2018). We used the ICA-73 assay to test heteromeric assembly of KCNQ2 with the disease linked KCNQ3 truncation, along with a series of artificial KCNQ3 truncations. Pharmacological characterization offers unambiguous

evidence that significant truncations of KCNQ3 retain the ability to assemble and form heteromeric channels with KCNQ2, similar to WT KCNQ3. The findings in this chapter suggest that heteromeric assembly may occur in patients and can potentially contributes to a dominant-negative effect on M-channels in disease states.

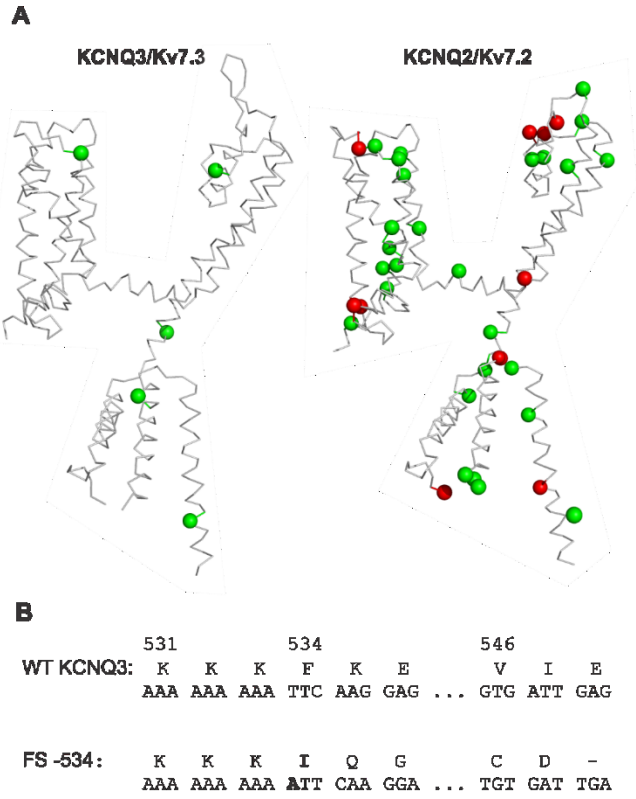

Figure 3.1: Truncation and frameshift mutations of KCNQ2 and KCNQ3. (A) Locations of frameshift and truncation mutations in KCNQ2 and KCNQ3 reported on ClinVar and RIKEE databases. Mutations associated with BFNE are highlighted in green, whereas mutations associated with epileptic encephalopathy or other severe syndromes are highlighted in red. **(B)** A *de novo* adenine insertion in KCNQ3 was identified in a patient exhibiting traits of autism and neurodevelopmental delay. The patient sequence is presented along with the reference WT KCNQ3 sequence. The frameshift causes premature truncation at amino acid position 548, leading to the modification of 14 amino acids and truncation of 324 amino acids.

RESULTS

Clinical features of a heterozygous KCNQ3-FS534 child

The heterozygous KCNQ3-FS534 mutation was initially observed in an 8-year-old male at first evaluation at an academic center's child neurology division. He exhibits Autism Spectrum Disorder (ASD) and Attention Deficit Hyperactivity Disorder (ADHD) according to DSM-5 criteria, but he also shows global developmental challenges. He exhibited intact gross motor milestones at 12 months of age but exhibited delays in language development. At 2 years of age, he stopped making communicative utterances. At 8 years of age, he exhibited gross motor skills (e.g. running, climbing, swimming), struggled with fine motor skills (e.g. writing, dressing independently), and his capacity to use language was limited to single words to express his needs and wants. At 11 years of age, his inattention and hyperactivity became more prominent, significantly impacting his ability to use fine motor control and following instructions. At the time of this study, his language remained limited to single word expressions, and he continues to struggle orienting to social stimuli, reciprocal interaction, imitation, and general social interactions.

Exome sequencing revealed a *de novo* KCNQ3 gene truncation in our patient, arising from a frameshift at amino acid position 534 that resulted from a single adenine insertion in a repetitive polyadenine region shown in Figure 3.1 B. This frameshift modified 14 amino acids, and prematurely truncated the protein at amino acid position 548. A GeneDX array, mitochondrial DNA sequencing, fragile X screening, and chromosome microarray did not reveal other noteworthy findings. The patient's family have members previously diagnosed with dyslexia and ASD traits, though not with comparable severity as observed in the patient. Interestingly, this patient does not exhibit BFNE typically observed in patients with disease-linked KCNQ3 mutations.

The recent report by Lauritano et al. (2019) highlighted an identical frameshift KCNQ3 mutation, but with a pattern of recessive inheritance in a female patient (Lauritano et al., 2019). This female patient was homozygous for this frameshift and unlike our patient, exhibited neonatal epilepsy that have been

effectively treated with various anticonvulsants including sodium valproate. Similar to our male patient, this female patient exhibits speech delay, motor difficulties, little autonomy, and mild learning difficulties, reflecting a form of ASD (Lauritano et al., 2019). In our case, the KCNQ3-FS534 appeared *de novo* in the male child. Therefore, the penetrance of neurological phenotypes despite a heterozygous phenotype reflect complexities, perhaps genetic or environmental factors throughout the child's development, that influenced the severity of illness caused by the KCNQ3-FS534 mutation. This may not be surprising as KCNQ2 and KCNQ3 channels likely have shifting patterns of expression and functional importance during development (Kanaumi et al., 2008).

Functional characterization of the KCNQ3-FS534 mutation in *Xenopus laevis* oocytes

The C-terminus of KCNQ channels has been implicated in many studies as the mediator of channel assembly and subtype specificity, particularly in studies focusing on the exclusion of cardiac KCNQ1 by neuronal KCNQ2 or KCNQ3. However, there is not a clear understanding of features that drive the assembly, maturation, or subtype specificity of neuronal KCNQ channels, including M-channels formed by KCNQ2 and KCNQ3. The KCNQ3-FS534 was used as a starting point for this study, where we aimed to study the effects of KCNQ3 truncations on assembly of heteromeric M-channels. We first reconstituted the KCNQ3-FS534 mutation in both WT KCNQ3 and the KCNQ3[A315T] background channels (the [A315T] mutation enhances KCNQ3 currents >30 fold when compared with WT KCNQ3) (Etxeberria et al., 2004; Gómez-Posada et al., 2010), and examined the effects on current expression and function. Similar to Lauritano et al. (2019), we observed that the KCNQ3 truncation leads to a pronounced reduction of total current equivalent to background uninjected levels in *X. laevis* oocytes (Figure 3.2 A, B, C). In addition, the non-selective AED retigabine (RTG) was unable to rescue channel function (Figure 3.2 B, C).

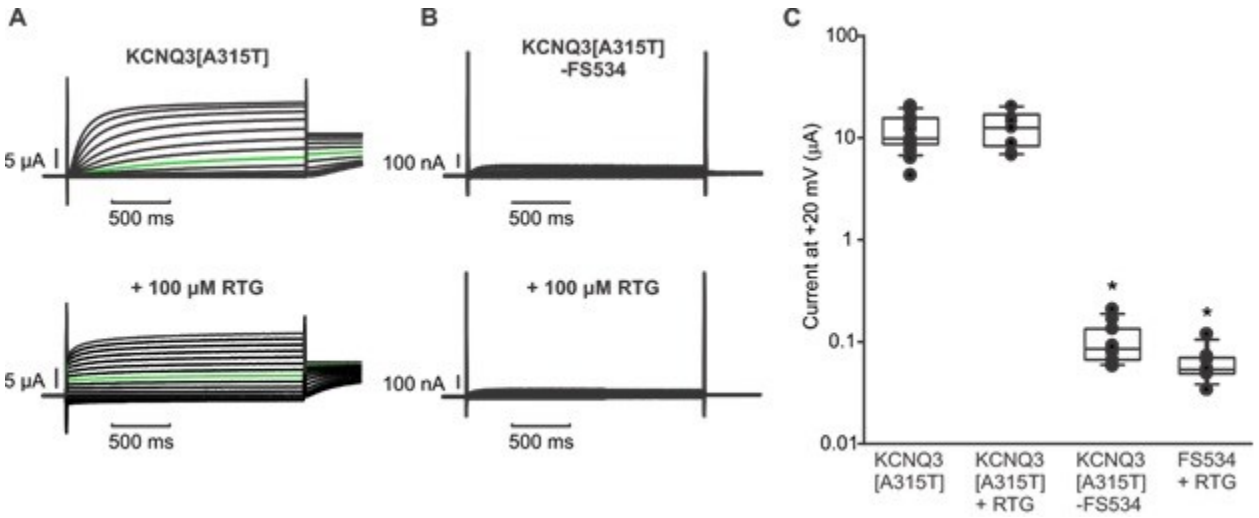

Figure 3.2: Frameshift mutation FS534 abolishes KCNQ3 currents and channel response to RTG. (A and B) Exemplar two-electrode voltage-clamp records for KCNQ3[A315T] and KCNQ3[A315T]-FS534 channels in *X. laevis* oocytes, in control conditions (upper trace) and 100 µM RTG (lower trace). A total of 50 ng of mRNA was injected per oocyte. Injected oocytes were held at -80 mV, pulsed for 2 s between voltages of +20 mV to -140 mV, followed by a -20 mV test pulse (start-to-start interval, 3 s). Traces in green indicate a 2 s pulse to -30 mV. **(C)** Current magnitude comparison between KCNQ3[A315T] and KCNQ3[A315T]-FS534, in control or 100 µM RTG, plotted on a logarithmic scale. Each data point represents a unique oocyte recording (n = 8-19). Current magnitudes were compared using the Kruskal Wallis one-way ANOVA on ranks, followed by Dunn's post-hoc test to compare with the KCNQ3[A315T] control group. (* indicates $p < 0.05$ relative to KCNQ3[A315T]).

We then used the KCNQ3-FS534 mutation on the WT KCNQ3 background to test its effects upon co-expression with KCNQ2 in the formation of heteromeric M-channels. After 48 hours of expression time, we observed clearly resolvable currents in oocytes expressing WT KCNQ2 homomeric channels, but no observable currents can be produced by KCNQ3-FS534 alone (Figure 3.3 A, B). Co-expression of WT KCNQ2 and WT KCNQ3 in a 1:1 mRNA ratio produced a synergistic increase of total current relative to KCNQ2 or KCNQ3 alone (Figure 3.3 A, D). The same combination of KCNQ2 and KCNQ3-FS534 failed to recapitulate this current increase (Figure 3.3 A, C). Interestingly, KCNQ3-FS534 did not suppress channel currents either, resulting in currents that are similar in amplitude as KCNQ2 homomeric channels (Figure 3.3 A). These results cannot distinguish if KCNQ3-FS534 fails to assemble with and influence KCNQ2, or if KCNQ3-FS534 assembles with KCNQ2 but fails to enhance current expression of heteromeric channels.

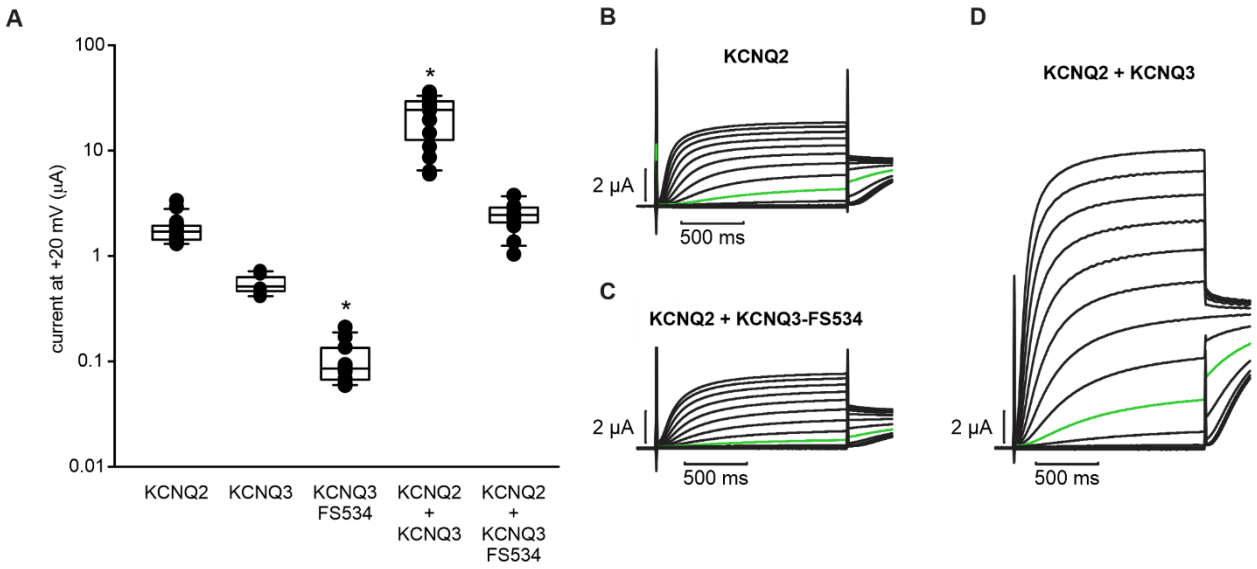

Figure 3.3: Frameshift mutant KCNQ3-FS534 does not enhance KCNQ2 currents. (A) Current magnitude comparison at +20 mV for the injected combinations of channel mRNAs in *X. laevis* oocytes on a logarithmic scale. A total of 50 ng of mRNA was injected per oocyte, and the heteromeric combinations were injected in a 1:1 mRNA ratio. Each data point represents a unique oocyte recording (n = 8-16). Current magnitudes were compared using a Kruskal Wallis one-way ANOVA on ranks followed by Dunnett's post-hoc test comparing against the KCNQ2 control. **(B-D)** Exemplar two-electrode voltage-clamp records for KCNQ2, KCNQ2 + KCNQ3-FS534, and KCNQ2 + KCNQ3 channels, as indicated, with a protocol identical to the one described in Figure 3.2. Traces in green indicate a 2 s pulse to -30 mV. (* indicates $p < 0.05$ relative to KCNQ2)

Biophysical assessment of assembly of KCNQ3-FS534 with KCNQ2

Conductance-voltage (GV) relationships were fit using the standard single-component Boltzmann described in Chapter 2, and were used to determine if KCNQ3-FS534 can influence channel gating or RTG sensitivity when co-injected with KCNQ2 (Figure 3.4). With no application of RTG, KCNQ2 homomeric channels exhibited a half maximal activation ($V_{1/2}$) of -36.6 mV +/- 2.7 mV, whereas the KCNQ2 + KCNQ3-FS534 combination exhibited a right-shifted $V_{1/2}$ of -25.6 mV +/- 3.3 mV. In Ringer's solution containing saturating levels of RTG (we used 100 μM of RTG), neuronal KCNQ2-5 channels exhibit a marked hyperpolarizing shift of voltage-dependence (Tatulian et al., 2001; Tatulian and Brown, 2003; Kim et al., 2015). We observed an RTG-mediated gating shift of -41.2 mV in KCNQ2 homomeric channels, and a moderately smaller gating shift of -36.2 mV in co-expressed KCNQ2 + KCNQ3-FS534 channels (Figure 3.4 D). In contrast, WT KCNQ2 + WT KCNQ3 heteromeric channels exhibited a larger RTG-mediated

gating shift of -59.7 mV, from a $V_{1/2}$ of -37.5 +/- 4.6 mV in control conditions (Figure 3.4 D). GV relationships for wild type homomeric KCNQ2 and the wild type heteromeric KCNQ2 + KCNQ3 are superimposed (grey curves in Figure 3.4 C). for comparison with KCNQ2 + KCNQ3-FS534. Although the effects of KCNQ3-FS534 are small, they are statistically significant and provided the first hint that KCNQ3-FS534 may assemble with KCNQ2 to moderately influence the GV and RTG-sensitivity of expressed channels. Interestingly, Lauritano et al. (2019) did not report any biophysical effects of KCNQ3-FS534 using similar approaches but in mammalian Chinese hamster ovary (CHO) cells instead of *X. laevis* oocytes (Lauritano et al., 2019).

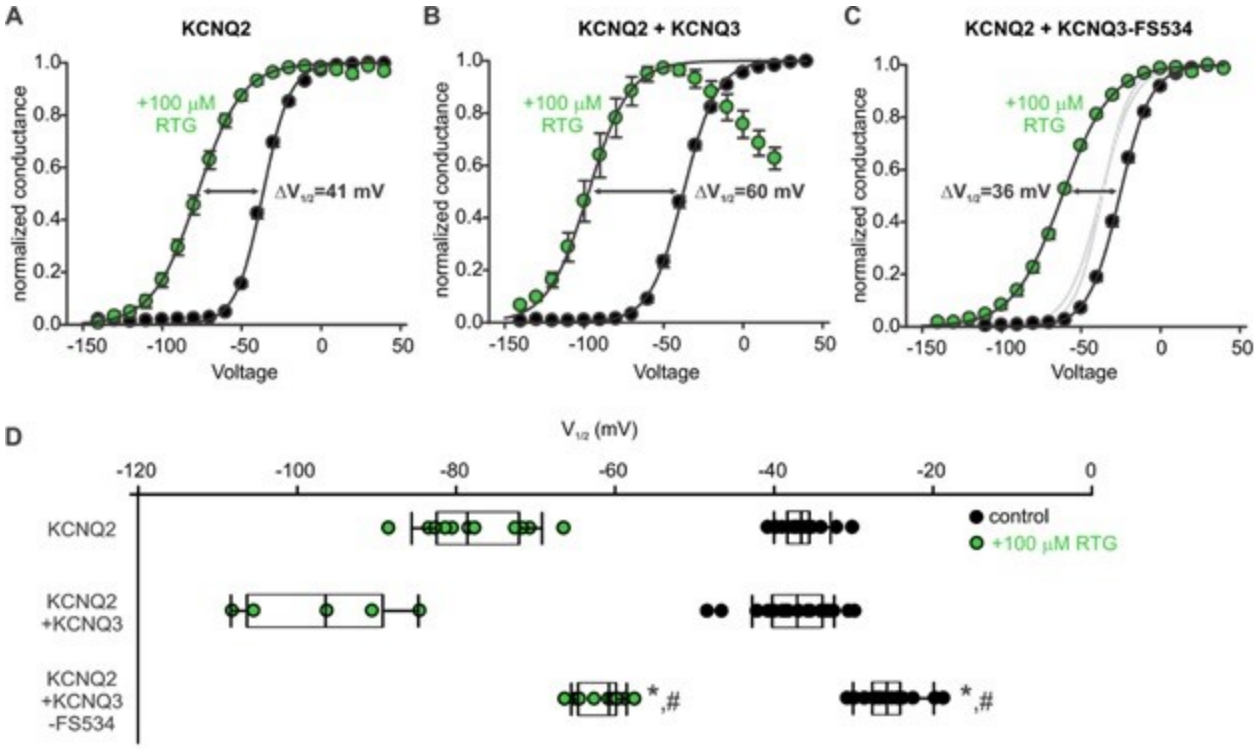

Figure 3.4: Altered voltage-dependence and RTG response of KCNQ2 co-expressed with KCNQ3-FS534. (A-C) Summary conductance-voltage relationships from KCNQ2 **(A)**, KCNQ2 + KCNQ3 **(B)**, and KCNQ2 + KCNQ3-FS534 **(C)**, expressed in *X. laevis* oocytes. **(D)** Cell-by-cell illustration of $V_{1/2}$ for each channel combination in the presence or absence of 100 µM RTG. Fitted gating parameters for KCNQ2 were (no RTG: $V_{1/2}$ = -36.6 +/- 2.7 mV, k = 8.6 +/- 1.1; 100 µM RTG: $V_{1/2}$ = -77.8 +/- 6.6 mV, k = 14.1 +/- 4.3). KCNQ2 + KCNQ3 fitted gating parameters were (no RTG: $V_{1/2}$ = -37.5 +/- 4.6 mV, k = 10.5 +/- 1.7; 100 µM RTG: $V_{1/2}$ = -97.2 +/- 9.9 mV, k = 12.9 +/- 2.0). KCNQ2 + KCNQ3-FS534 fitted gating parameters were: (no RTG: $V_{1/2}$ = -25.6 +/- 3.3 mV, k = 9.9 +/- 1.5; 100 µM RTG: $V_{1/2}$ = -61.8 +/- 2.8 mV, k = 15.4 +/- 3.4). Data are mean +/- SEM. $V_{1/2}$ compared between channel combinations in control and RTG conditions using a one-way ANOVA and the Holm-Sidak post-hoc test. (* indicates $p<0.05$ relative to KCNQ2, # indicates $p<0.05$ relative to KCNQ2 + KCNQ3 heteromeric combination).

The ICA-73 pharmacological assay and detection of KCNQ2/KCNQ3 channel assembly

Lauritano et al. (2019) reported that the KCNQ3-FS534 mRNA may be prone to significant nonsense-mediated mRNA decay, and a reduced expression of this truncated channel may have minimized the appearance of the biophysical effects in their experiments (Lauritano et al., 2019). Since we observed biophysical effects from a co-expressed KCNQ3-FS534, we suspected that expression of KCNQ3-FS534, at least in oocytes, were not reduced to the same degree as shown by Lauritano et al. (2019). We wanted to devise an alternative approach to clearly detect the heteromeric assembly of KCNQ2 and KCNQ3. As discussed in Chapter 1, recent studies have identified several characteristics of the voltage-sensor targeted ICA-73 KCNQ channel activator, including its selectivity for KCNQ2 and KCNQ4, dependence on activated channels, and stoichiometric dependence of drug effects (Wang et al., 2017; A. W. Wang et al., 2018; C. K. Wang et al., 2018).

A.W. Wang et al., (2018) reported how subunit composition alters the sensitivity of channels to the subtype-selective ICA-73 channel activator (A. W. Wang et al., 2018). We first assessed the differences in drug responses by exposing homomeric and heteromeric KCNQ2/KCNQ3 channels to saturating levels of ICA-73 in Ringer's solution (we used 100 μM ICA-73), and delivering voltage-step protocols to microinjected *X. laevis* oocytes as described in Figure 3.5. Each protocol began with the full activation of channels at +20 mV to allow ICA-73 binding, due to the drug's strict dependence on activated channels (C. K. Wang et al., 2018). Following this, channels were exposed to a repolarization step to a range of voltages (-20 mV to -120 mV in 20 mV steps), to allow drug unbinding and channel closure. Finally, we stepped to +20 mV to assess the magnitude of instantaneous current, which reflects the extent of drug unbinding and deactivation that occurred during the repolarizing step, highlighted with arrows in Figure 3.5 A, B. This assay clearly distinguishes homomeric KCNQ2 and heteromeric KCNQ2/KCNQ3, based on differences in the magnitude of instantaneous current relative to the total current. While ICA-73 causes extremely slow deactivation of KCNQ2, and hence a large instantaneous current (Figure 3.5 B), this effect is largely attenuated in co-expressed KCNQ2/KCNQ3 channels (Figure 3.5 A, C). Over the range of hyperpolarization

voltages used in this study, the weaker ICA-73 sensitivity of heteromeric KCNQ2/KCNQ3 channels is apparent (Figure 3.5 D), resulting in a less prominent instantaneous current compared to homomeric KCNQ2 channels.

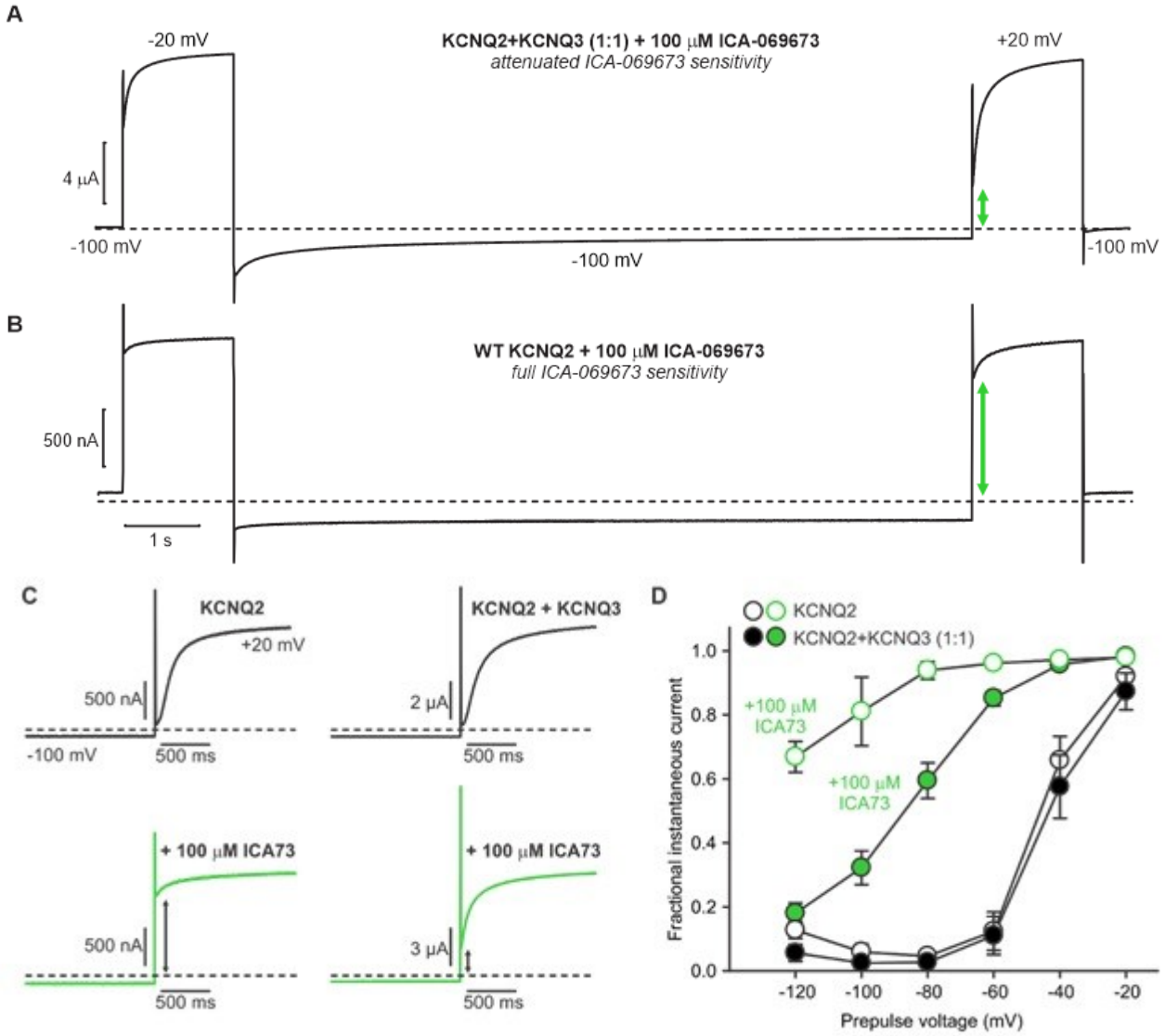

Figure 3.5: Attenuated effects of ICA-73 on heteromeric KCNQ2 + KCNQ3 channels. (A-B) Exemplar *X. laevis* oocyte two-electrode voltage-clamp records for measurement of instantaneous current. Injected oocytes were held at a prepulse voltage of -100 mV for 10 s, then pulsed to + 20 mV for 2 s. Green arrows highlight measurement of instantaneous current fraction. **(C)** Exemplar traces illustrating channel activation after -100 mV prepulses in the absence and presence of ICA-73 (5.9 +/- 0.9 % and 81.1 +/- 3.8 % respectively for KCNQ2, 2.5 +/- 0.3 % and 32.3 +/- 2.0 % respectively for KCNQ2 + KCNQ3). **(D)** Fractional instantaneous current was measured after a range of prepulse voltages (n = 7-12). Data in **(C)** are presented as mean +/- SEM.

Determination of assembly of C-terminally truncated KCNQ3 with KCNQ2

Next, we used ICA-73 as a pharmacological tool to investigate assembly of KCNQ3-FS534 with KCNQ2, and extended this approach to a variety of artificial KCNQ3 C-terminal truncations (Figure 3.6). Since our ICA-73 assay can clearly demonstrate if KCNQ3 or its truncation mutants can functionally assemble with KCNQ2, it may be valuable tool for future studies of KCNQ channel assembly or characterizing biophysical and pharmacological effects of channel mutations. However, the use of this assay can be limited if KCNQ3 forms non-functional channels with KCNQ2. In these cases, observable currents are only generated by homomeric KCNQ2 channels, and it becomes unclear if a mutated KCNQ3 is dominantly suppressing currents through assembly, or if assembly is lost. However, alteration of ICA-73 sensitivity relative to homomeric KCNQ2 channels remains as strong evidence that a mutated KCNQ3 may effectively and functionally assemble with KCNQ2.

We applied this ICA-73 assay and observed that KCNQ3 truncations, even significant ones predicted to abolish channel assembly, are well-tolerated and can assemble with KCNQ2 (Figure 3.6). Representative instantaneous currents after a repolarization step to -100 mV are shown in Figure 3.6 A, organized according to the positions of these mutations on the KCNQ3 channel. The mean data for instantaneous currents across a range of repolarization voltages is also shown in Figure 3.6 B, C. Truncations as large as 340 amino acids in the KCNQ3-ΔC340 mutant (out of the total 872 amino acids in KCNQ3), resulting in the deletion of the C and D helices, still supported prominent assembly with KCNQ2 as reflected by the reduction in instantaneous currents (Figure 3.6 B, C). Only the truncation of helices A and B in KCNQ3-ΔC503 – required for CaM binding – completely abolished functional assembly of KCNQ2 and KCNQ3 (Figure 3.6 A). Despite producing an attenuated response to ICA-73 (i.e. a reduction in instantaneous current), KCNQ3-FS534 and KCNQ3-ΔC340 only partially reduced instantaneous current, suggesting that the region between ΔC340 and ΔC301 has an important influence on KCNQ2/KCNQ3 heteromeric assembly, even if it is not the only region that drives assembly.

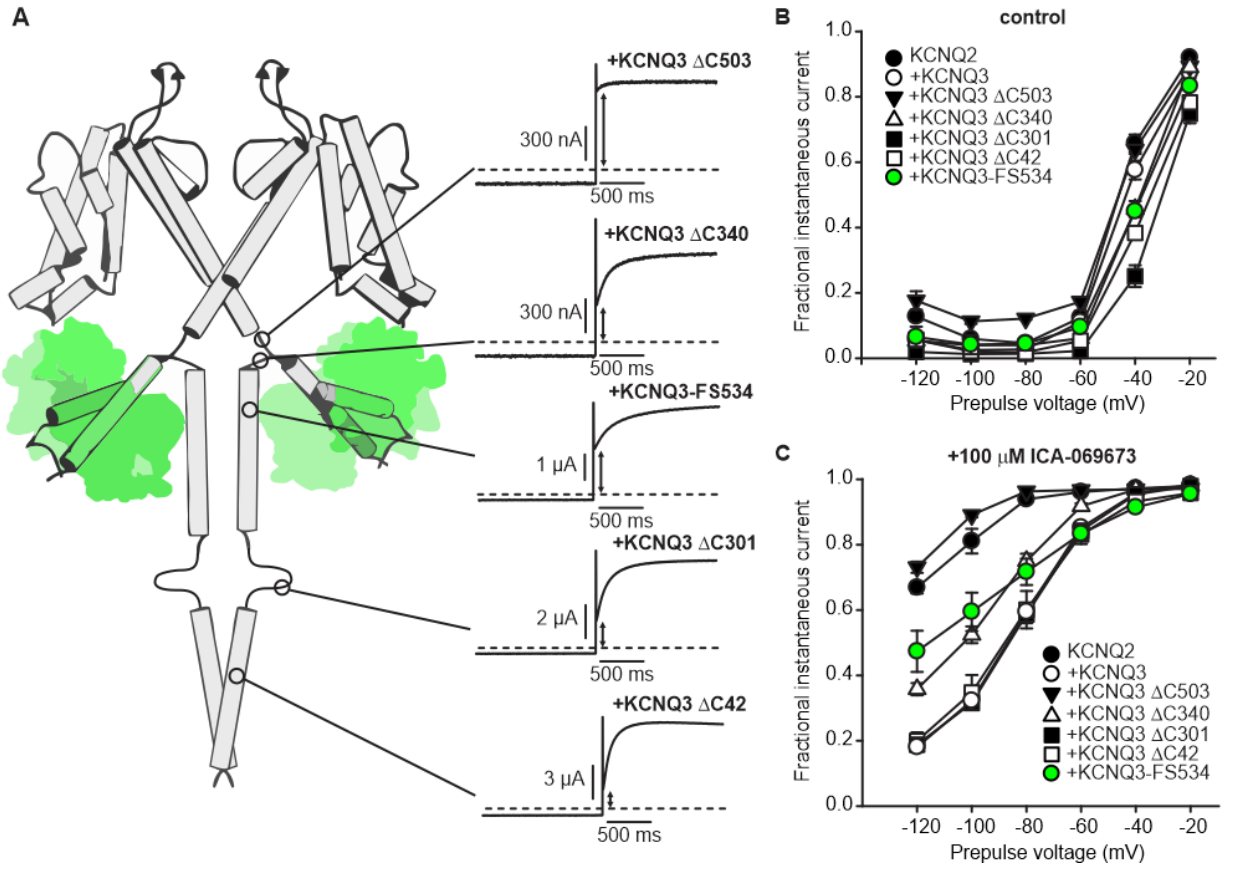

Figure 3.6: Functional assessment of assembly of KCNQ3 truncations with KCNQ2. (A) KCNQ structural model illustrating the location of KCNQ truncations tested in the study. Exemplar two-electrode voltage-clamp records illustrating instantaneous current for KCNQ2 + KCNQ3 truncations with respect to the positions of truncations. CaM is illustrated in green. Co-injections were controlled for total mRNA at 50 ng, with a 1:1 KCNQ2:KCNQ3 ratio. **(B and C)** Instantaneous currents were measured after a range of prepulse voltages, using the same protocol as Figure 3.5 A, B. Instantaneous currents were measured in **(B)** control or **(C)** 100 μM ICA-73 (n = 4-12 for control, n = 7-11 for drug condition). Data in **(B)** and **(C)** are presented as mean +/- SEM.

Titration of KCNQ2/KCNQ3 channel ratios

Since we are overexpressing KCNQ2 and KCNQ3 (WT or truncated) in a heterologous system, their expression levels may be significantly higher than physiological levels in native neurons. This overexpression may be driving interactions which normally would not occur, allowing channels to overcome the loss of important structural elements important for driving assembly. To address this uncertainty, we injected oocytes significantly smaller ratios – 4:1 ratios – of KCNQ2:KCNQ3 (WT, ΔC301, and ΔC340), halved the total mRNA injected to 25 ng per oocyte, and investigated current magnitude and ICA-73

sensitivity using the same assay described in Figure 3.5 and 3.6. Although the data is not shown, the 4:1 KCNQ2:KCNQ3 ratio was determined through experimentation, where several ratios of KCNQ2:KCNQ3 were tested, to retain similar propensity to heteromerically assemble as the 1:1 ratio injection. We found that co-expressing KCNQ2 with WT KCNQ3 at a 4:1 ratio still caused prominent current enhancement (Figure 3.7 B) and substantial attenuation of ICA-73 effects (Figure 3.7 A). similar to levels observed for the 1:1 co-expression at double the total mRNA. Co-expressing the same 4:1 ratio of KCNQ2 with KCNQ3-ΔC301 did not enhance current magnitude to the same extent as WT KCNQ3, but exhibited a similar degree of attenuation of ICA-73 sensitivity as WT KCNQ3 (Figure 3.7 A, B), suggesting a strong propensity for this truncation mutant to assemble with KCNQ2. However, the KCNQ3-ΔC340 demonstrated attenuated assembly with KCNQ2 (Figure 3.7 A, B), consistent with the findings in Figure 3.6.

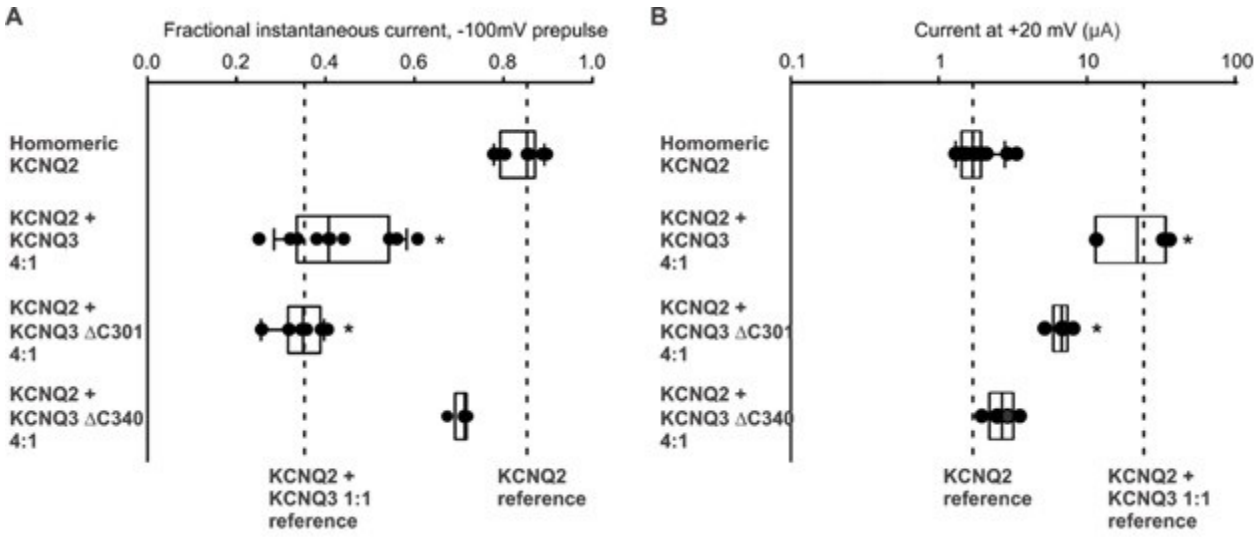

Figure 3.7: KCNQ3-ΔC301 and WT KCNQ3 have a similar propensity to assemble with KCNQ2. (A) Fractional instantaneous currents in 100 μM ICA-73 for indicated channel combinations (25 ng total RNA injection) using the experimental protocol described in Figure 3.5A). Dotted reference lines indicate the mean fractional instantaneous currents of homomeric KCNQ2 (mean = 81.1 +/- 3.8 %, n = 8) and heteromeric KCNQ2 + KCNQ3 1:1 mixture (mean = 32.3 +/- 2.0 %, n = 7). Each data point represents a unique oocyte recording (n = 4-10). **(B)** Current amplitudes of the same oocytes when pulsed to +20 mV. Dotted reference lines indicate the mean current amplitude of homomeric KCNQ2 and heteromeric KCNQ2 + KCNQ3 1:1 mixture. Each data point represents a unique oocyte recording (n = 4-16). Data were compared using a Kruskal-Wallis ANOVA on ranks, followed by Dunnett's post-hoc test (* indicates $p < 0.05$ relative to homomeric KCNQ2).

Despite retaining the ability to assemble with KCNQ2, we realized that most KCNQ3 truncations were unable to restore current expression to wild type KCNQ2 + KCNQ3 levels. In Figure 3.8, we summarized the effects of 1:1 co-injection of various KCNQ3 truncations with KCNQ2, highlighting patterns related to assembly versus current expression of these different subunit combinations. We observed that the progressive truncation of KCNQ3 caused a gradual reduction of total current expression (Figure 3.8 B). Modest truncations (e.g. KCNQ3-ΔC42) supported wild type levels of current potentiation, but this effect is lost with truncations of ΔC301 or greater. Therefore, there is a mismatch between the effect of KCNQ3 truncations on current expression and the effect on ICA-73 sensitivity, particularly with KCNQ3-ΔC301 in which assembly with KCNQ2 appears equally favourable as with WT KCNQ3.

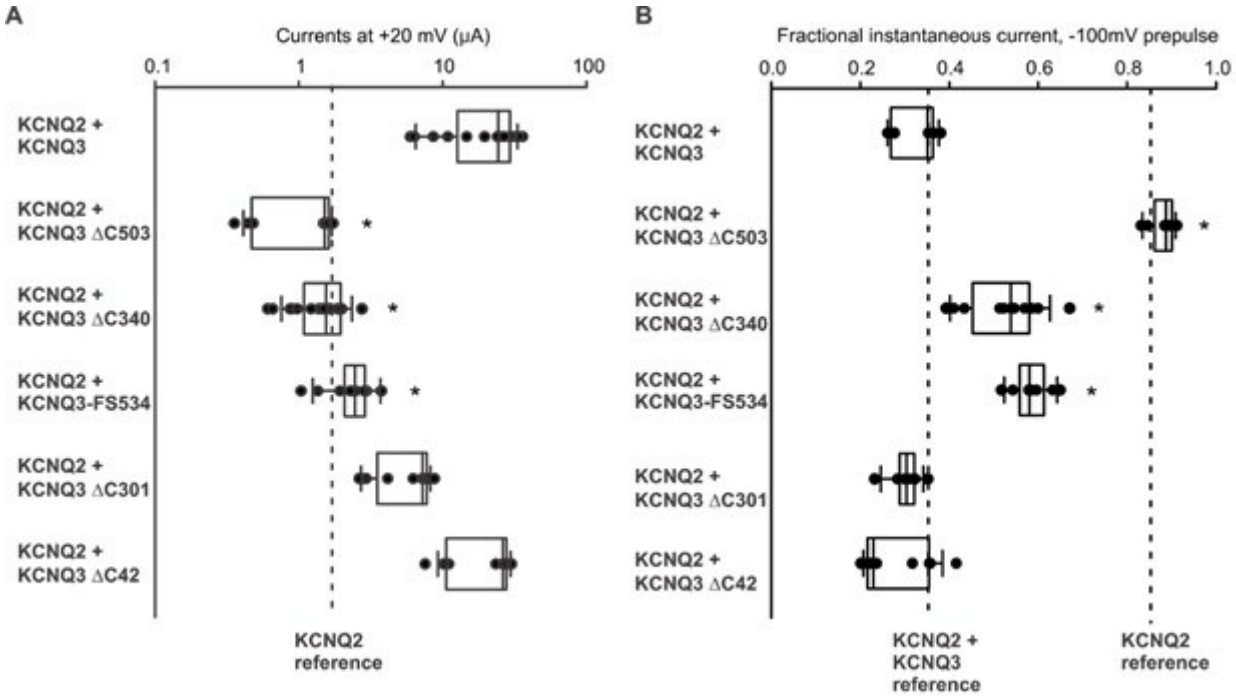

Figure 3.8: Most KCNQ3 truncations cannot enhance current to wild type heteromeric KCNQ2 + KCNQ3 levels. (A) Current amplitudes of various 1:1 KCNQ2-KCNQ3 co-injections in *X. laevis* oocytes when pulsed to +20 mV. While KCNQ3-ΔC503 is the only construct unable to assemble with KCNQ2, having the ability to assemble is not sufficient to return current levels back to normal. Each data point represents a unique oocyte recording (n = 12-20 for co-injections). The dotted line reflects the average current amplitude of KCNQ2 homomers (mean = 1.81 +/- 0.14 μA, n = 16) in *X. laevis* oocytes. **(B)** Fractional instantaneous current in 100 μM ICA-73, for indicated 1:1 co-injections of KCNQ2 + KCNQ3 (wild type or truncated). Dotted reference lines indicate the mean fractional instantaneous currents of homomeric KCNQ2 and heteromeric KCNQ2 + KCNQ3 1:1 mixture. Data were compared using a Kruskal-Wallis ANOVA on ranks, followed by Dunnett's post-hoc test (* indicates $p < 0.05$ relative to heteromeric KCNQ2 + KCNQ3).

DISCUSSION

In previous studies, the subtype-specific assembly of KCNQ channels was determined to be primarily driven by structural elements within the C-terminal helices C and D (Howard et al., 2007; Haitin and Attali, 2008; Sun and MacKinnon, 2017). We investigated assembly through a series of C-terminally truncated KCNQ3, using a subtype-selective KCNQ2 activating compound, ICA-73. ICA-73 clearly distinguished homomeric KCNQ2 and heteromeric KCNQ2/KCNQ3, and revealed that significant C-terminal truncations in KCNQ3, including the disease-linked KCNQ3-FS534, can functionally assemble with KCNQ2.

Unlike most Kv channels (Kv1-6,8,9), which have an N-terminal T1 domain in regulating channel function and subtype-specific assembly, Kv7/KCNQ channels lack this domain and must have other determinants for controlling assembly (Li et al., 1992; Kreusch et al., 1998; Schwake et al., 2003, 2006). There are many unanswered questions in the control of subtype selectivity and exclusion in assembly, and subunit stoichiometries in assembled channels. Native M-channels are believed to contain KCNQ2 and KCNQ3 in a 1:1 ratio, as determined by sensitivity to TEA-mediated channel block (Hadley et al., 2000, 2003). However, this is little understanding of how M-channel assembly is controlled, and if variable subunit stoichiometries can occur (Bal et al., 2008; Stewart et al., 2012). Similarly, it is generally accepted that KCNQ2 and KCNQ5 do not functionally assemble, but there is little understanding of how this exclusion is controlled. It is only known that KCNQ1 is excluded from assembly with the non-cardiac KCNQ2-5, and this exclusion can be manipulated by the chimeric swapping of C-terminus between KCNQ subtypes (Schwake et al., 2003, 2006; Howard et al., 2007).

Our motivation to investigate C-terminal regulation of M-channel assembly began with the identification of a C-terminal KCNQ3 truncation in a male patient diagnosed with ASD and general neurodevelopmental delay but lacked seizures. This was clinically interesting as KCNQ3 loss-of-function mutations are typically observed in children with neonatal epilepsy, but this phenotype was absent in our

patient. In addition, Lauritano et al. (2019) recently reported an identical frameshift mutation in a female patient, from a family with consanguineous marriage, resulting in a homozygous inheritance of the mutation and prominent penetrance of neurological features, including epilepsy (Lauritano et al., 2019). Interestingly, the parents who were heterozygous for the mutation were only modestly affected by this significant truncation of the KCNQ3 C-terminus (Lauritano et al., 2019). In contrast, the patient in our study exhibited much more severe and notable autistic traits and neurological disability, including challenges with social reciprocity, receptive and expressive language, fine motor skills, and markedly reduced sustained attention. These findings suggest that differences in their genetic or environmental background may have affected the penetrance of the neurological defects emerging from the KCNQ3-FS534 mutation.

Consistent to the findings of Lauritano et al. (2019), we found that the major defect attributed to the KCNQ3-FS534 mutation is reduced current expression from heteromeric KCNQ2/KCNQ3 channels. Lauritano et al. (2019) provided compelling evidence that the KCNQ3-FS534 mutation is poorly expressed in heterologous CHO cells and patient-derived fibroblasts (Lauritano et al., 2019). They also observed little evidence that KCNQ3-FS534 can functionally assemble with KCNQ2. In our study using *X. laevis* oocytes, and through a pharmacological approach using ICA-73, we observed substantial assembly of KCNQ2 with a wide range of truncated forms of KCNQ3, including KCNQ3-FS534. However, we find it noteworthy that the KCNQ3-FS534 did assemble less prominently than KCNQ3-ΔC301, suggesting that assembly may be disrupted if not eliminated. Our work may benefit from surface expression experiments (e.g. cell-surface biotinylation) to determine the effects of truncation mutations and the role of the C-terminus in channel trafficking and surface stability, to enable comparisons with the results from Lauritano et al. (2019) regarding the expression of KCNQ3-FS534, and for expression data to be used to complement our electrophysiological data. Since the ankyrin G binding region is truncated in KCNQ3-FS534, it is likely surface expression and localization is affected.

We demonstrated an alternative approach to detect the heteromerization of KCNQ2 with KCNQ3 (and can be potentially applied to other KCNQ subtypes) based on channel sensitivity to the voltage sensor-

targeted drug ICA-73. Wang et al., (2017) demonstrated that ICA-73 effects rely on the subunit composition of M-channels. While the deactivation of KCNQ2 can be strongly decelerated by ICA-73, requiring ~20 s hyperpolarizing steps to allow drug unbinding and permit channel closure, heteromeric KCNQ2/KCNQ3 channels are much more resistant to ICA-73 effects, exhibiting faster and more complete channel closure upon hyperpolarization (Wang et al., 2017; A. W. Wang et al., 2018; C. K. Wang et al., 2018). While the mechanism underlying this effect is not clear, the effect is clearly useful for diagnosing the assembly of KCNQ2 with other ICA-73 insensitive subtypes. Previous studies have exploited differential sensitivity to TEA-mediated block of KCNQ2 and KCNQ3 channels (Hadley et al., 2000, 2003). Our pharmacological assay provides an alternative approach to determine assembly, and may benefit from ICA-73's channel specificity. It was also useful to show how KCNQ-activating compounds with therapeutic potential can influence the function of disease-linked channels.

Lastly, the demonstration of efficient assembly of some C-terminally truncated KCNQ3 with KCNQ2 was unexpected, particularly since both KCNQ3-FS534 and KCNQ3-ΔC340 lack the subunit interacting domain (*sid*) previously found to strongly influence subtype-specific assembly (Maljevic et al., 2003; Schwake et al., 2003, 2006). It is noteworthy that these prior studies used chimeric strategies to replace C-terminal segments of KCNQ1 with KCNQ2 or KCNQ3, and used current potentiation as a marker of M-channel assembly with KCNQ3 and KCNQ2 respectively (Maljevic et al., 2003; Schwake et al., 2003, 2006; Howard et al., 2007). While these studies clearly identified important elements in the C-terminus, it is not clear if effects on current expression arose from altered assembly or reduced channel maturation and trafficking. Nakajo and Kubo (2008) was the first to produce evidence that prominent C-terminal deletions of KCNQ2 or KCNQ3 can retain the propensity to functionally assemble using differential TEA-sensitivity (Nakajo and Kubo, 2008). Structural studies also indicate that the C-termini of Kv7/KCNQ channels can assemble into protein-interacting coiled-coil structures, and may promote tetrameric channel assembly and act as a scaffold for association with regulatory proteins (Howard et al., 2007; Sun and MacKinnon, 2017). Our findings indicate that KCNQ channel assembly and trafficking are likely controlled by distinct channel

regions, and pharmacological assays using selective drugs can be useful to study the composition of functional tetramerized channels in future studies.

In summary, our study introduces a new and useful pharmacological approach to investigate heteromerization of KCNQ channels using the subtype-selective ICA-73. Our findings illustrate that significant truncations of the KCNQ3 C-terminus are well tolerated in terms of assembly with KCNQ2, but may cause neurological phenotypes due to a failed promotion of functional current expression observed with WT KCNQ3.

CHAPTER 4: BENIGN FAMILIAN NEONATAL EPILEPSY CAUSED BY THE KCNQ3[T313I] SELECTIVITY FILTER MUTATION

BACKGROUND

Many epileptic disorders, ranging from benign familial neonatal epilepsy (BFNE) to epileptic encephalopathy (EE), have been linked to mutations identified in the KCNQ2 and KCNQ3 voltage gated potassium channels (Jentsch, 2000; Rogawski, 2000; Robbins, 2001; Cooper and Jan, 2003; Soldovieri et al., 2011; Weckhuysen et al., 2012; Lerche et al., 2013; Maljevic and Lerche, 2014). One clinical issue often encountered is how to best predict long term outcomes and management approach for neonates with new-onset seizures. Although genetic sequencing is becoming more accessible, clinicians who identify genetic links to epilepsy often do not have sufficient information to best predict phenotypes from genotypes, particularly for mutations in KCNQ2 and KCNQ3, which presents a wide range of epileptic severity.

KCNQ2 and KCNQ3 heteromerically assemble into the neuronal M-channel, which controls threshold and burst firing of neurons. One hallmark feature of the heteromeric M-channel is the potentiation of current expression >10 fold relative to KCNQ2 and KCNQ3 homomeric channels. Dysfunction in both KCNQ2 and KCNQ3 can lead to pathological states in patients. BFNE is a mild form of childhood epilepsy that begins in the first few postnatal days, and are typically self-resolving and do not interfere with structural or cognitive development. BFNE is associated with mutations in both KCNQ2 and KCNQ3 (Leppert et al., 1989; Lewis et al., 1993; Singh et al., 2003; Maljevic and Lerche, 2014). In contrast, EE is a severe form of epilepsy and typically causes long-term neurological disabilities, decreased motor function, and propensity towards pharmacoresistant epilepsies later in life; EE is typically associated with mutations in KCNQ2 rather than KCNQ3 (Weckhuysen et al., 2012). In general, disease-linked mutations in KCNQ2 are more frequently reported than KCNQ3, and are generally more severe.

KCNQ3 mutations have been reported throughout the channel sequence, including the voltage sensing domain, the pore domain, and C-terminal regions important for tetramerization, PIP_2 association, and calmodulin binding. Figure 4.1 A highlights the locations of pathogenic point mutations of KCNQ3

reported in ClinVar and RIKEE databases, on the structural template of the recently reported KCNQ1 cryo-EM structure (Sun and MacKinnon, 2017). The green shaded SF region in Figure 4.1 A reflects the cluster of validated disease-linked mutations in the KCNQ3 selectivity filter, an important region for ion selectivity and permeation. The geometry and stability of the selectivity filter is determined by several intra- and intersubunit interactions that are widely conserved among Kv channels (MacKinnon and Yellen, 1990; Doyle et al., 1998; Zhou et al., 2001; Pless et al., 2013). In *Drosophila melanogaster Shaker* channels, which are prone to a slow C-type inactivation (analogous to the human Kv1.3), disruption of these selectivity filter stabilizing bonds leads to pronounced acceleration of inactivation and significant reduction in channel conductance (Perozo et al., 1994; Y. Yang et al., 1997; Kurata and Fedida, 2006; Pless et al., 2013). In contrast, M-channels are not normally inactivating, and many selectivity filter mutations have relatively mild effects on overall channel function (Brown and Adams, 1980; Wang et al., 1998).

In this study, we investigated a previously unreported KCNQ3[T313I] mutation in the selectivity filter region identified in a child patient previously diagnosed with BFNE. An analogous mutation in KCNQ2 was previously reported (KCNQ2[T274M]), but was associated with severe clinical outcomes, including profound global developmental delay, motor dysfunction, and remitting seizures characteristic of EE (Weckhuysen et al., 2012; Orhan et al., 2014; Milh et al., 2013, 2015). We characterized the electrophysiological effects of the [T313I] mutation in KCNQ3 in homomeric and heteromeric KCNQ2/KCNQ3 channels, to describe the effects of the selectivity filter mutation in KCNQ3 on channel function. We applied the same ICA-73 pharmacological assay used in Chapter 3 to detect the functional assembly between KCNQ2 and KCNQ3[T313I]. Our findings highlight that KCNQ2/KCNQ3 heteromeric channels are relatively tolerant of the mutation that is extremely disruptive in other Kv channels (e.g. *D.melanogaster Shaker* channels), and this likely explains the mild disease pathology associated with KCNQ3 selectivity filter mutations.

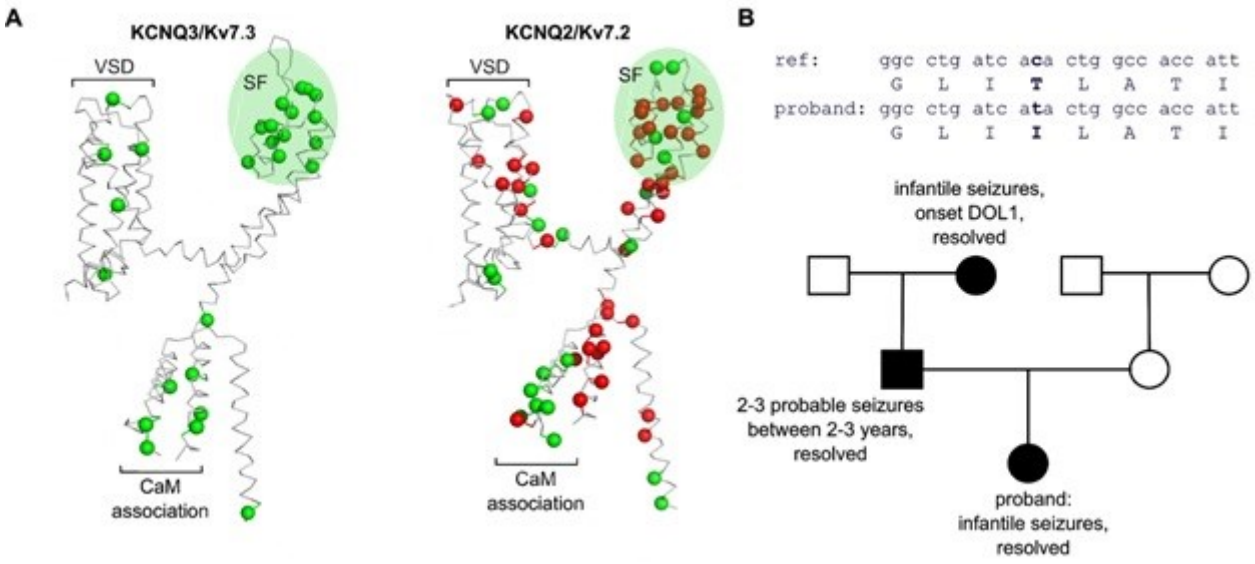

Figure 4.1: Inheritance of KCNQ2 and KCNQ3 mutations associated with epilepsy. (A) Mutations in KCNQ2 or KCNQ3 associated with a documented case of epilepsy (compiled from ClinVar or RIKEE databases) are highlighted on molecular models of each channel. Mutations are color coded based on severity (green = BFNE, red = epileptic encephalopathy or other severe outcomes). Mutations that do not map to structural elements defined in the KCNQ1 cryo-EM structure have been omitted (VSD = voltage-sensing domain, SF = selectivity filter, CaM = Calmodulin). **(B)** Pattern of inheritance of a neonatal seizure phenotype in a family carrying the KCNQ3[T313I] mutation. Upper, sequence alignment of the reference KCNQ3 gene and KCNQ3 protein in relation to the proband. The identified mutation [T313I] is highlighted in bold type. Lower, pedigree for the family characterized in our study with filled symbols indicating affected individuals.

RESULTS

Clinical features of a heterozygous KCNQ3[T313I] child

The patient proband was initially identified as a baby girl born after a normal pregnancy and uncomplicated vaginal delivery. Four days after birth, she exhibited abnormal breathing patterns and body tremors. The frequency of these events increased, eventually requiring patient hospitalization. Through video-EEG monitoring, frequent seizures were recorded for the patient during sleep and wakefulness. The seizures were determined to be characteristic of BFNE. As the seizures continued, the patient was eventually prescribed anti-epileptic therapies, including phenobarbital, which eventually stopped the seizures.

Neurological examinations of this patient revealed a normal non-dysmorphic infant with normal brain anatomy. The family members who carried this mutation experienced a history of childhood seizures and ADHD, but like the proband, exhibited no severe neurological or structural defects. Several months after the seizures, the patient remained event-free, and a repeat EEG revealed normal brain activity. Eventually, phenobarbital was weaned at 8 months of age. At 2 years of age, the proband developed normally in all domains, suggesting a clinical presentation consistent with BFNE.

KCNQ3[T131I] mutation eliminates homomeric channel function

The KCNQ3[T313I] mutation was intriguing to us from a biophysical and physiological perspective due to its positioning in the selectivity filter. Due to the functional importance of the selectivity filter, mutations in this region of KCNQ3 often result in disease (D305, A306, W309, G310, I317, Y319, G320 reported in ClinVar associated with BFNE), particularly the relatively mild and self-resolving BFNE. One previous study of an analogous mutation in *Shaker* channels highlighted the importance of this particular site in stabilizing the selectivity filter (Pless et al., 2013). The KCNQ3 T313 is analogous to the *Shaker* T439, which is likely involved in an intersubunit hydrogen bond with the selectivity filter residue Y455 (in the conserved GYG motif of Kv channels) of a neighbouring subunit, highlighted in Figure 4.2 A. In *Shaker* channels, disruption of T439 in even one subunit is sufficient to suppress channel currents, and accelerates

the rate of inactivation by ~100 fold (Pless et al., 2013). It is likely that the powerful effect of mutating T439 is due to a propagated effect from the mutated subunit to neighbouring subunits, resulting in a suppression of channel function in an allosteric manner (Pless et al., 2013). Consistent with the effects of the *Shaker*[T439V] mutation on channel currents, the KCNQ3[T313I] mutation abolishes channel currents when expressed in *X. laevis* oocytes. Even when we used KCNQ3[A315T] background to enhance the surface of KCNQ3 surface expression, we were unable to detect functional channels from homomeric KCNQ3[T313I][A315T] channels (Figure 3.2 A, B).

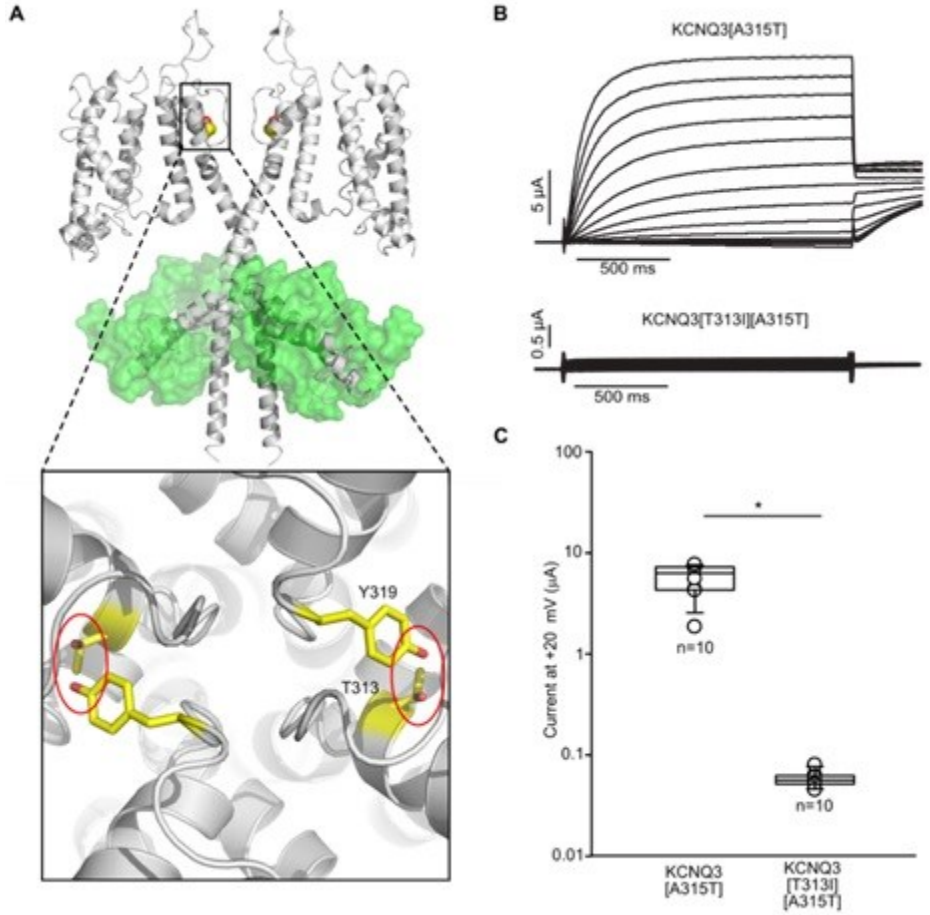

Figure 4.2: KCNQ3[T313I] abolishes KCNQ3 function. (A) Molecular model of essential intersubunit hydrogen bond between conserved residues T313 and Y319 located in the selectivity signature sequence. **(B)** Two-electrode voltage-clamp recordings from *Xenopus laevis* oocytes expressing KCNQ3[A315T] and KCNQ3[A315T][T313I]. Oocytes were held at −80 mV and depolarized for 1.5 s to voltages between −140 mV and +40 mV (in 10 mV steps) followed by repolarization to −20 mV test pulse. **(C)** Cell-by-cell comparison of current amplitudes of KCNQ3[A315T] and KCNQ3[A315T][T313I] at +20 mV, plotted on a logarithmic scale. KCNQ3[A315T] and KCNQ3[A315T][T313I] groups were compared using Student's t-test (* indicates $p < 0.05$ relative to the KCNQ3[A315T] control).

KCNQ3[T313I] attenuates currents in heteromeric KCNQ2/KCNQ3 channels

We wanted to address the effects of the KCNQ3[T313I] mutation on M-channel function, due to the predominance of heteromeric KCNQ2/KCNQ3 channels *in vivo*. We expressed KCNQ2, KCNQ3, and KCNQ3[T313I] independently and together to simulate the heteromeric assemblies that may occur *in vivo*. Wild type heteromeric KCNQ2 and KCNQ3 channels co-expressed at a 1:1 mRNA injection ratio significantly potentiated currents relative to homomeric KCNQ2 or KCNQ3 channels. However, co-expression of KCNQ2 and KCNQ3[T313I] at the 1:1 mRNA ratio was unable to potentiate currents, but instead produced currents similar in amplitude as homomeric KCNQ2 channels (Figure 4.3 A, B).

In our proband, the KCNQ3[T313I] mutation was inherited paternally, and a normal KCNQ3 was inherited maternally. Therefore, to mimic the heterozygous genotype of the proband, we tested the mixed expression of WT KCNQ3 and KCNQ3[T313I] with KCNQ2 using a 2:1:1 (KCNQ2:WT KCNQ3:KCNQ3[T313I]) mRNA injection ratio. We observed that the presence of KCNQ3[T313I] in the triple injection did not suppress current magnitude relative to co-expressed KCNQ2 and WT KCNQ3, but instead produced currents that resemble the wild type 1:1 KCNQ2/KCNQ3 co-expressed channels (Figure 4.3 A, B). However, current magnitudes in these experiments can be variable due to the complex stoichiometries of channel subunits in assembled channels (e.g. one KCNQ3 assembled with three KCNQ2 subunits, amongst all other combinations between KCNQ2 and KCNQ3). In all co-injections with KCNQ3[T313I], no effects on voltage-dependence of channel activation were observed in *X. laevis* oocytes (Figure 4.3 C). Due to the similarity in channel gating and current magnitude between homomeric KCNQ2 channels and co-expressed KCNQ2/KCNQ3[T313], it was not clear if the currents we observed in co-injected oocytes were due to homomeric KCNQ2 channels or functionally assembled KCNQ2/KCNQ3[T313I] channels. This detail is important for characterizing the nature of selectivity filter mutations on heteromeric KCNQ2/KCNQ3 channels.

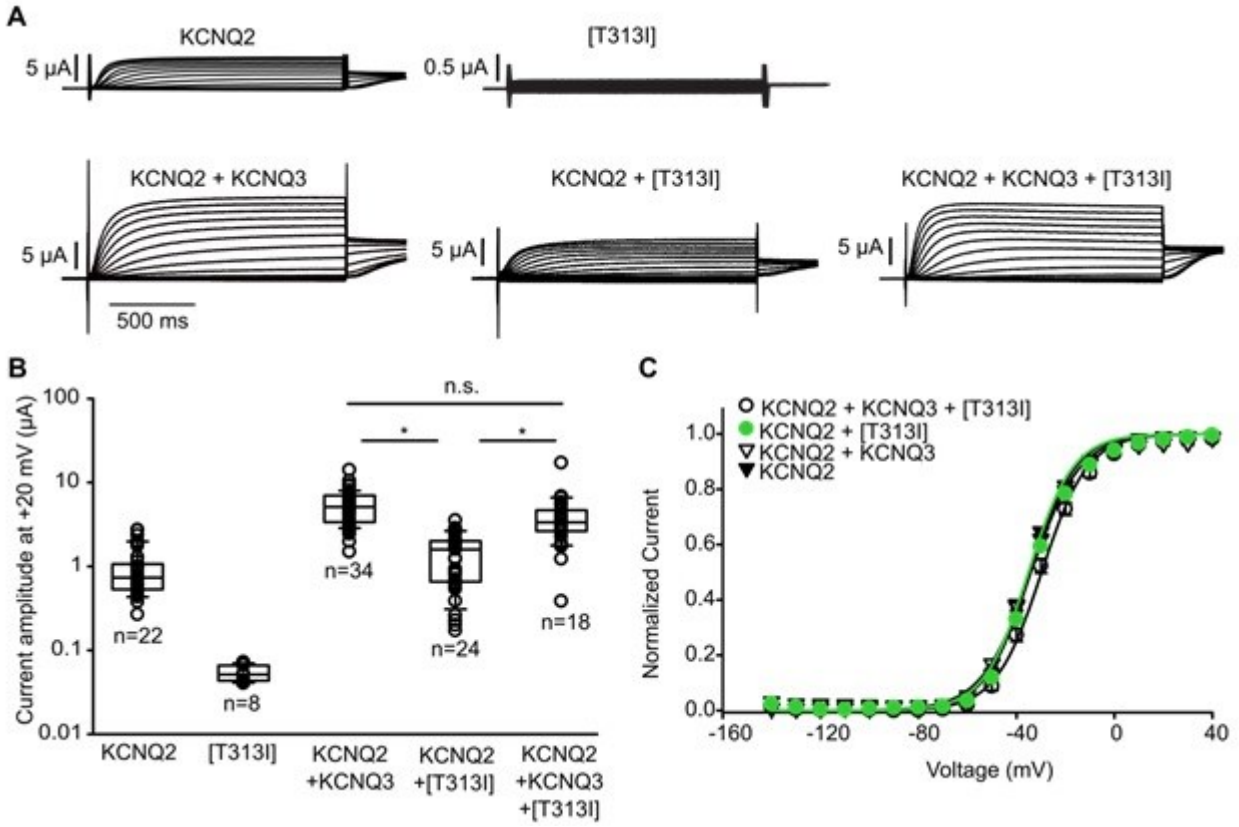

Figure 4.3: Co-expression with KCNQ2 and KCNQ3[T313I] reduces heteromeric channel function with no effect on gating. (A) Two-electrode voltage-clamp sample traces from oocytes expressing various combinations of KCNQ2 and KCNQ3 (injected with a total of 50 ng of mRNA per group). The voltage step protocol is the same as Figure 4.2B. **(B)** Current amplitudes after a 1.5 s +20 mV voltage step, plotted on a logarithmic scale. Current magnitudes were compared using one-way ANOVA, followed by Tukey's post-hoc test (* indicates $p < 0.05$). **(C)** Conductance-voltage relationships were collected using the protocol in panel (A), using tail current magnitudes (-20 mV) to assess the extent of channel opening during the conditioning step. Fitted gating parameters are shown as mean +/- S.E.M.: for KCNQ2 + KCNQ3 + KCNQ3[T313I], k = 9.4 +/- 0.3 mV, $V_{1/2}$ = -29.7 +/- 1.0 mV; for KCNQ3 + KCNQ3[T313I], k = 9.1 +/- 0.3 mV, $V_{1/2}$ = -35.1 +/- 0.5 mV; for KCNQ2 + KCNQ3, k = 10.2 +/- 0.3 mV, $V_{1/2}$ = -34.2 +/- 0.3 mV; for KCNQ2 homomers, k = 9.2 +/- 0.2 mV, $V_{1/2}$ = -34.2 +/- 0.6 mV. No significant differences in gating parameters were detected.

Heteromeric composition of KCNQ2:KCNQ3[T313I] determined by ICA-73 sensitivity

Discussed in Chapters 1 and 3, KCNQ2 channels exhibit pronounced deceleration of deactivation in the presence of ICA-73, whereas the effects are attenuated in heteromeric KCNQ2/KCNQ3 channels due to the presence of ICA-73 insensitive KCNQ3 (Wang et al., 2017; A. W. Wang et al., 2018; C. K. Wang et al., 2018). We used the same pharmacological assay discussed in Chapter 3 to investigate whether currents observed in the KCNQ2/KCNQ3[T313I] condition were generated by homomeric KCNQ2 or heteromeric

channels. We depolarized oocytes to +20 mV to open channels and allow ICA-73 binding, followed by repolarization to a range of voltages from -20 mV to -120 mV. We depolarized oocytes again to +20 mV to assess the extent of the deceleration of channel deactivation caused by the drug, as reflected by the relative magnitude of instantaneous current at this step. As observed in Chapter 3, homomeric KCNQ2 channels exhibit high sensitivity to ICA-73, resulting in significant deceleration of deactivation and large instantaneous current fractions. In contrast, wild type heteromeric KCNQ2/KCNQ3 channels deactivate considerably faster, producing smaller instantaneous currents (Figure 4.4 A, B, C). While KCNQ2/KCNQ3[T313I] exhibited an intermediate instantaneous fraction compared to wild type homomeric and heteromeric channels (Figure 4.4 A, B, C), these channels behaved distinctively from KCNQ2, suggesting that KCNQ3[T313I] can functionally assemble with KCNQ2, even if it cannot potentiate currents to wild type heteromeric levels.

Though we have not directly tested this, it is unlikely that KCNQ2/KCNQ3 assembly is affected by the KCNQ3[T313I] mutation. Therefore, the intermediate response to ICA-73 is likely due to a mixture of homomeric KCNQ2 – which exhibit maximum responses to ICA-73, and heteromeric KCNQ2/KCNQ3[T313I] – which exhibits attenuated responses to ICA-73, where homomeric and heteromeric channels are comparable in the magnitudes of the current they conduct. Co-expression of the 2:1:1 (KCNQ2: WT KCNQ3: KCNQ3[T313I]) displayed similar ICA-73 response to the wild type heterozygous control (Figure 4.4 A, B, C).

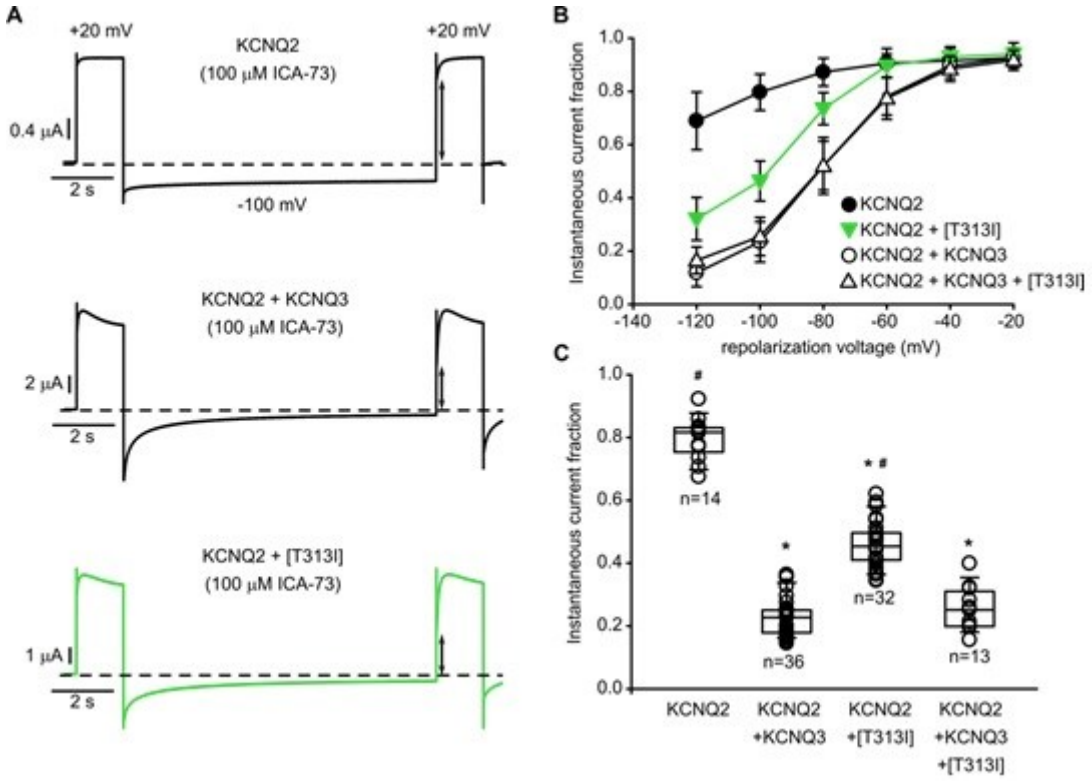

Figure 4.4: Reduced ICA-73 sensitivity of KCNQ2/KCNQ3[T313I] heteromeric channels. (A) Example currents of two-electrode voltage-clamp recordings. Oocytes were depolarized to +20 mV and hyperpolarized for 12 s in a step-down manner (-20 mV per sweep), followed by another +20 mV depolarizing pulse to determine instantaneous current at -100 mV. **(B)** Fractional instantaneous current after incubation with 100 μM ICA-73 was measured as indicated by the arrows in panel (A). **(C)** Fractional instantaneous current for various combinations of KCNQ2, KCNQ3, and KCNQ3[T313I]. Instantaneous current fractions were compared using one-way ANOVA, followed by Tukey's post-hoc test (* indicates $p < 0.05$ relative to KCNQ2, # indicates $p < 0.05$ relative to KCNQ2 + KCNQ3).

KCNQ3[T313I] effects in concatenated tetrameric channels

To eliminate uncertainties caused by mixed channel stoichiometries, we generated concatenated channel constructs to fix the subunit composition of channel tetramers (A. W. Wang et al., 2018), and directly test the effects of the KCNQ3[T313I] mutant on tetrameric current expression and gating properties. The three concatemers tested either had four covalently linked KCNQ2 protomers, or one WT KCNQ3/KCNQ3[T313I] subunit at the first protomer position linked to three KCNQ2 protomers. Therefore, variation only exists in the first subunit of the concatemer. The channel containing WT KCNQ3 as the first protomer exhibited larger currents relative to the concatenated homomeric KCNQ2 channel (Figure 4.5 A,

B). Unlike the concatemer containing WT KCNQ3, the concatemer containing KCNQ3[T313I] as the first protomer was unable to enhance currents, but instead produced currents comparable to the concatenated homomeric KCNQ2 channel (Figure 4.5 A, B), similar to the current suppression effect observed in *X. laevis* oocytes (Figure 4.3 B). Finally, he KCNQ3[T313I] containing concatemer produced a statistically significant rightward shift in channel voltage-dependence relative to the WT KCNQ3 containing concatemer (Figure 4.5 C). Although the shift in voltage-dependence is relatively small (~7.5 mV) between WT KCNQ3 and KCNQ3[T313I] containing concatemers, it was interesting as we did not observe this effect in monomerically expressed channels in oocytes.

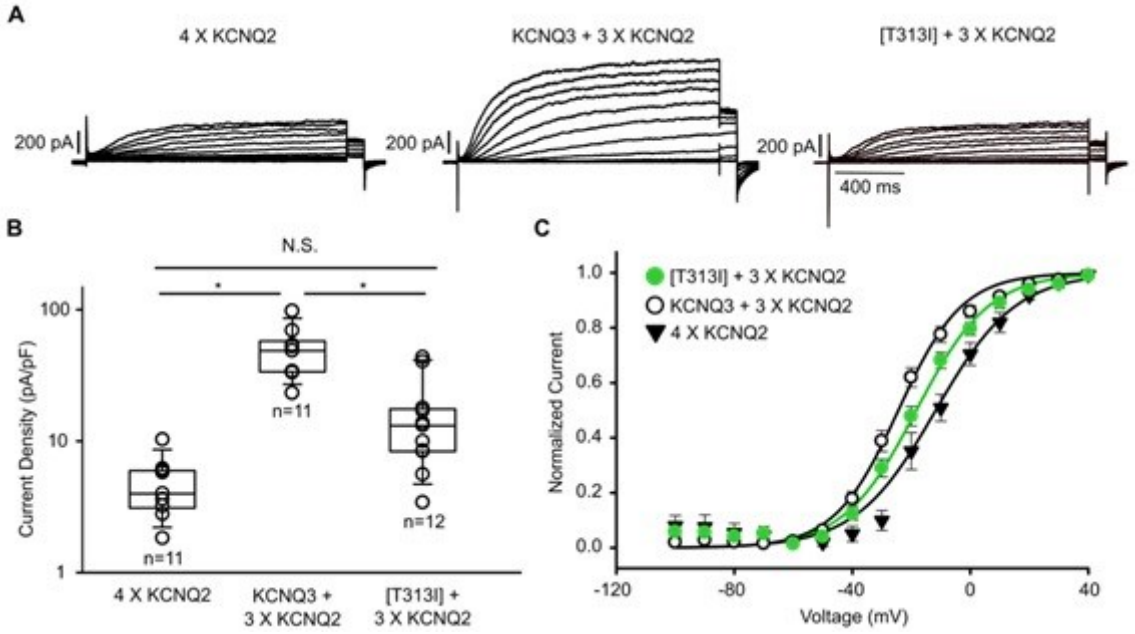

Figure 4.5: Fixed stoichiometry of KCNQ2/KCNQ3 determined one mutated subunit trends towards current suppression. (A) Exemplar patch clamp traces of tetrameric constructs, example traces were chosen based on the mean values. LM cells were transfected and allowed to incubate for 24 hours before patch data was obtained. **(B)** Cell-by-cell current density comparison at +20 mV accounting for variations in cell capacitance, plotted on a logarithmic scale. Current density was compared using a one-way ANOVA and Tukey's post-hoc test (* indicates $p < 0.05$). **(C)** Normalized GV curves of concatemeric constructs were collected 24 hours after incubation, using the same protocol as Figure 3A. Fitted gating parameters were (mean +/- S.E.M.): for KCNQ3[T313I] + 3X KCNQ2, k = 12.3 +/- 0.6 mV, $V_{1/2}$ = -18.3 +/- 0.6 mV; for KCNQ3 + 3X KCNQ2, k = 10.8 +/- 0.5 mV, $V_{1/2}$ = -29.4 +/- 1.6 mV; for 4X KCNQ2, k = 13.6 +/- 0.7 mV, $V_{1/2}$ = -11.4 +/- 1.9 mV.

DISCUSSION

There is significant interest in determining the genotype-phenotype correlation of mutations in KCNQ2 and KCNQ3 for understanding the prognosis and pathogenesis of affected patients. Scientifically, the characterization of these channel mutants is valuable for understanding the assembly, function, and regulation of native M-channels, which are important regulators of neuronal excitability. Clinically, understanding KCNQ-linked disease at a molecular level can guide clinical decisions for the treatment or management of M-channel related illnesses in patients. In this chapter, we reported a novel mutation in the selectivity filter region of KCNQ3 predicted to disrupt a stabilizing intersubunit interaction previously reported in *Shaker* channels. This KCNQ3[T313I] mutation was identified in a patient who exhibited BFNE, and there is likely a close relationship between the current suppressing of this mutation and the BFNE phenotype.

Interestingly, while the analogous T439 in *Shaker* channels, or its hydrogen bonding partner Y445 (in the conserved GYG motif of the selectivity filter) were fundamental in stabilizing the selectivity filter to allow ion conduction, the KCNQ3 T313 likely plays a similar role. The intersubunit nature of this interaction made *Shaker* channels particularly intolerant to mutations at residues T439 and Y445, in contrast to the greater tolerance for mutations that disrupt the *intra*subunit interactions in the selectivity filter (e.g W434F mutant). This is likely due to the propagation of loss-of-function effects to neighbouring subunits, or subunit cooperativity, when *inter*subunit interactions are disrupted, resulting in disease outcomes.

KCNQ3 T313 is likely part of a critical intersubunit hydrogen bond with Y319, since KCNQ3[T313I] are completely unable to functionally assemble, even on the highly expressing KCNQ3[A315T] background (Figure 4.2). However, it appears that the effects of the T313I mutation is less pronounced in heteromeric conditions, as KCNQ2/KCNQ3[T313I] can clearly functionally assemble (Figure 4.4). KCNQ3[T313I] moderately reduced heteromeric channel currents with KCNQ2, with no differences in gating properties when compared with wild type heteromeric KCNQ2/KCNQ3 when co-

expressed (Figure 4.3), or expressed in a concatemer (Figure 4.5). Our observations are distinct from the powerful effects of disrupting the intersubunit hydrogen bond in *Shaker* channels, and other unidentified interactions may be important in stabilizing the selectivity filter of KCNQ channels.

While the KCNQ3[T313I] is linked to the relatively mild BFNE, the analogous KCNQ2[T274M] is linked to severe epileptic encephalopathy and global developmental delay (Weckhuysen et al., 2012; Orhan et al., 2014; Milh et al., 2013, 2015). Interestingly, the functional characterization of KCNQ2[T274M] in *X. laevis* oocytes produced similar outcomes as our observations for KCNQ3[T313I] in the same cells: partial suppression of heteromeric current levels and no gating effects (Orhan et al., 2014). However, despite having similar functional outcomes, the KCNQ2 mutation (and KCNQ2 mutations in general) is much more severe phenotypically. The severe phenotypes associated with KCNQ2 mutations have been attributed to: more important physiological roles of KCNQ2 homomeric channels, greater contributions to channel stoichiometries, or its involvement with other channel or protein assemblies (Bal et al., 2008; Robbins et al., 2013; Soh et al., 2014). Although it was interesting to see a small rightward shift in voltage dependence for the KCNQ3[T313I]-containing tetrameric concatemer compared to the WT KCNQ3-containing control (Figure 4.5 C), when expressed in LM cells, suggesting that gating shifts may appear depending on cell type and raises the possibility that voltage dependence shifts may be present in our proband. As small as the shift in voltage dependence is (~ 7.5 mV shift), it may have been sufficient when combined with the current suppression effect to cause the mild BFNE observed in our proband. Since we have observed inconsistencies in heterologous expression systems (oocytes vs LM cells), it would be interesting, and may perhaps improve the translatability of our findings if we studied the effects of T313I expressed in more physiologically relevant systems (e.g. neurons).

Experiments with concatenated channels have their limitations. While the subunit composition within a concatemer can be strictly controlled, it is often difficult to ensure that proper channel folding can be achieved with novel structural constraints introduced through covalent linkage of protein subunits. Misfolded proteins may have altered function and/or pharmacological sensitivities, producing results that

may be different from properly folded and assembled channels. Additionally, it is unclear if all four subunits in a functional channel are from the same concatemer, or if the fully assembled channels are composed of subunits from multiple concatenated channels (e.g. the first subunit from four concatemers assembling into a functional channel). While the differences in current densities caused by KCNQ3[T313I] in Figure 4.5 are statistically significant, these are the limitations that must be considered when interpreting our results.

Finally, we highlighted another useful application of the pharmacological approach for detecting functional assembly of heteromeric KCNQ channels using ICA-73. In addition to detecting the functional assembly of KCNQ2 with KCNQ3[T313I], we were able to make inferences on potential current suppression effects caused by the disease-linked KCNQ3 mutant on heteromeric M-channels. Clinically, studying this mutant will enable more accurate predictions in patient outcomes caused by similar mutations to the KCNQ3 selectivity filter. It provides useful information for clinicians in patient care should the same or similar pathogenic KCNQ3 variants are identified in patients.

In summary, our study reports a BFNE-linked mutation in the KCNQ3 selectivity filter, which eliminates the functional assembly of homomeric channels, suppresses the currents of heteromeric channels, and have no significant effect on voltage-dependence of heteromeric channels in *X. laevis* oocytes. We unambiguously detected the functional assembly of heteromeric KCNQ2/KCNQ3[T313I] channels using ICA-73, and determined that the biophysical consequences of this KCNQ3 mutation are less severe than the analogous mutation reported in *D. melanogaster Shaker* potassium channels.

CHAPTER 5: AROMATIC MUTATIONS CAN IMPROVE VOLTAGE-CLAMP FLUOROMETRY SIGNALS IN KCNQ3

BACKGROUND

Voltage clamp fluorometry (VCF) was first employed to optically track conformational changes in the voltage sensor of *Shaker* channels independently from conformational changes in the pore (Mannuzzu et al., 1996). In ion channel voltage sensor studies, VCF typically involves the covalent attachment of a thiol-reactive fluorophore probe to a natural or engineered cysteine site (Mannuzzu et al., 1996; Gandhi and Olcese, 2009; Kim et al., 2017). When exposed to light of a specified wavelength, the fluorophore is excited and reaches a higher energetic state. The subsequent relaxation of the fluorophore emits a light of a longer wavelength relative to the incident light, which can be selectively detected by a detector, and converted into an electrical signal (Mannuzzu et al., 1996; Gandhi and Olcese, 2009). Conformational changes in ion channel voltage sensors shifts the position of the fluorophore, resulting in brightening or dimming of fluorescence that can be measured as a change in fluorescence between two voltage sensor states (ΔF) demonstrated in Figure 5.1 (Gandhi and Olcese, 2009). This change in fluorescence is likely due to the differential quenching of emitted light by the environment surrounding the fluorophore (Gandhi and Olcese, 2009). Additionally, the kinetics of voltage sensor movement can be measured through the rate of the change in fluorescence as the channel responds to changes in voltage (Gandhi and Olcese, 2009). Therefore, VCF can be a powerful technique to complement electrophysiology current data with measures of voltage sensor conformational changes. It is noteworthy that the quantity of fluorescent light that ultimately reaches the detector is variable, and can depend on the intensity of the incident light, the quantity and availability of fluorophores, and the extent of environmental quenching of the fluorescent light (Mannuzzu et al., 1996; Gandhi and Olcese, 2009).

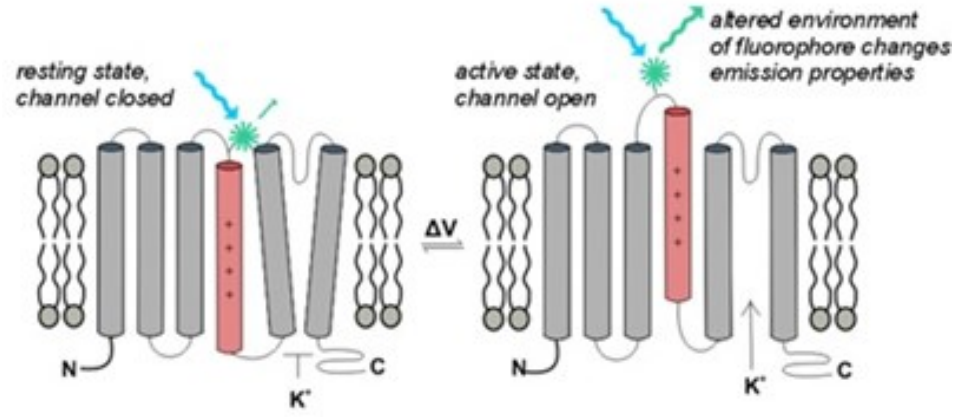

Figure 5.1: Voltage clamp fluorometry (VCF) detects the changes in fluorescence intensity caused by voltage sensor conformational changes. In the left panel, the voltage sensor is in the resting state and the channel is closed. Excitation of the fluorophore results in the emission of fluorescent light, but only small quantities of light can be emitted due to positioning of the fluorophore. In the right panel, the voltage sensor is activated by voltage and the channel is open. Excitation of the fluorophore results in an increased emission of fluorescent light due to changes in the fluorophore environment. (Kim et al., 2017)

Since its first use in *Shaker* channels (Mannuzzu et al., 1996), VCF has been used to study a diverse range of ion channel voltage sensors (Gandhi and Olcese, 2009). VCF has been employed successfully in both the cardiac KCNQ1 and the neuronal KCNQ3 (Zaydman et al., 2013; Nakajo and Kubo, 2015; Cui, 2016; Kim et al., 2017). KCNQ1 channels can consistently produce massive VCF signals (large ΔF-to-noise ratio) (Zaydman et al., 2013; Nakajo and Kubo, 2015; Cui, 2016), but comparatively, KCNQ3 can only produce small VCF signals (small ΔF-to-noise ratio) and inconsistently (Kim et al., 2017). In fact, the first KCNQ3 VCF signal was detected by Kim et al. (2017) after an extensive cysteine mutagenesis scan in the voltage sensor, which led to the construction of the KCNQ3[Q218C][A315T] VCF channel background (Kim et al., 2017) – we will refer to this background as KCNQ3*VCF in this thesis. Until the writing of this Chapter, no VCF signals have been detected from KCNQ2, KCNQ4, or KCNQ5.

The detection of VCF signals from KCNQ3 allowed Kim et al. in 2017 to extensively study the role of PIP_2 in channel function, voltage sensor and pore coupling, and the pharmacology of retigabine. This study described the distinct effects of PIP_2 depletion, disruption of PIP_2 binding, PIP_2 protection by RTG, and PIP_2 dependence of RTG effects (Kim et al., 2017). This study not only generated significant insight

into our understanding of KCNQ3 and its pharmacology, but the KCNQ3[Q218C][A315T] has since been used in other studies for a deeper understanding of KCNQ3 disease-linked mutations (Barro-Soria, 2019). There is also significant interest in using VCF to study the effects of Kv7/KCNQ targeted anti-epileptic compounds, particularly the voltage sensor targeted compounds, and how they influence voltage sensitivity of KCNQ channels. Although possible, VCF signals from KCNQ3 remain difficult to obtain (as will be shown in Figure 5.4), creating a need to improve the strength and consistency of VCF signals in KCNQ3. We wanted to develop an approach that can improve VCF for KCNQ3, and perhaps enable the use of VCF on KCNQ2, KCNQ4 and KCNQ5.

KCNQ1 can consistently produce large VCF signals (Figure 5.2). Due to sequence and predicted structural similarities between KCNQ1 and KCNQ3, we used the former to guide mutations in KCNQ3 in hopes of recreating a KCNQ1-like environment near the fluorophore attachment site to improve the strength of VCF signals to levels observed in KCNQ1. We identified several positions in KCNQ3 – L156, L157, L222 – near the fluorophore attachment site C218, which are aromatic residues at analogous positions in KCNQ1 (F157, W158, F222 respectively). We mutated our KCNQ3*VCF at L156, L157, and L222 to aromatic residues found in KCNQ1, and screened their effects on channel function, VCF signal strength, VCF signal consistency, and channel response to retigabine. We constructed several KCNQ3*VCF mutants for screening: KCNQ3*VCF[L156W][L157F], KCNQ3*VCF[L156W][L157F][L222F], KCNQ3*VCF[L222F], and KCNQ3*VCF[L222W]. While all mutants showed some degree of improvement, we determined that KCNQ3*VCF[L156W][L157F] is likely the best candidate for future KCNQ3 VCF studies. KCNQ3*VCF[L156W][L157F] provided significant improvements to both VCF signal strength and consistency, with little effect on channel gating, current expression, and retigabine sensitivity. In this study, we define consistency as the ability to detect usable signals ($\%\Delta F/F > \sim 0.5\%$) on an oocyte-to-oocyte basis.

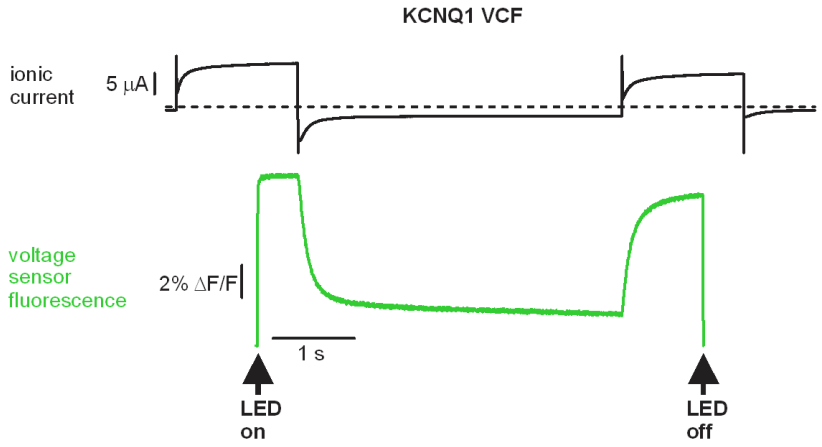

Figure 5.2: KCNQ1 produces massive VCF signals. The top panel shows a representative KCNQ1 current trace. *X. laevis* oocytes are initially depolarized to +20 mV to open channels, hyperpolarized to -140 mV to close channels, and depolarized to +20 mV again to open channels. The bottom panel shows the corresponding fluorescence trace tracking voltage sensor movement. The LED light is turned on with an input of 2 V when channels are fully active, measuring the fluorescence of fully activated voltage sensors. Closure of the channel changes the fluorophore environment, reducing the fluorescence detected from channels. Subsequent depolarization of closed channels increases the fluorescence back to activated levels. The fluorescence change is measured relative to the fluorescence when channels are fully closed. In this trace, $\Delta F/F = 8$ % between the fully activated and deactivated states.

RESULTS

Identification of positions near the fluorophore attachment site C218 for mutagenesis

Through our sequence alignment, we identified three Leu residues near the C218 fluorophore attachment site in a model of the KCNQ3 structure in Figure 5.3 B (based on the Sun and Mackinnon 2017 KCNQ1 cryo-EM structure) (Sun and MacKinnon, 2017). We mutated these residues into aromatic Trp and Phe residues found in KCNQ1, producing several KCNQ3*VCF aromatic constructs: KCNQ3*VCF[L156W][L157F], KCNQ3*VCF[L222F], KCNQ3*VCF[L222W], and KCNQ3*VCF[L156W][L157F][L222F]. We will use the Alexa-488 dye described in Chapter 2 for all VCF experiments discussed in this chapter.

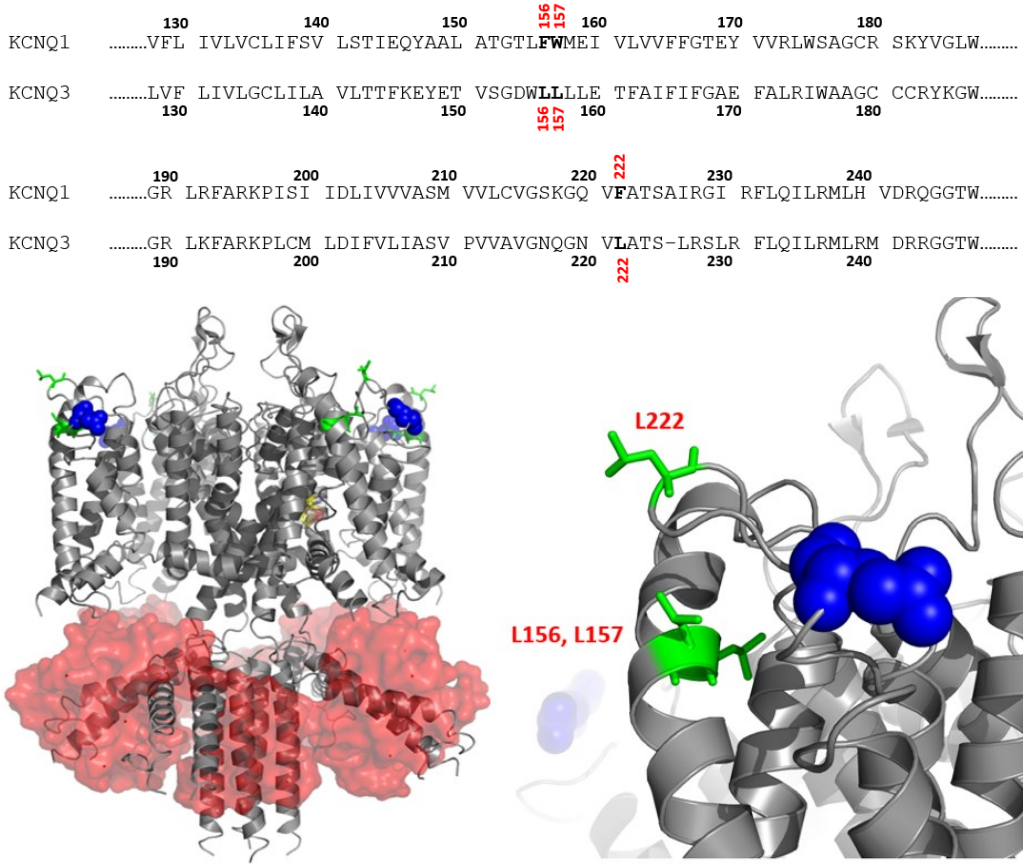

Figure 5.3: Sequence alignment and identification of KCNQ3 residues for aromatic mutation.
The top panel shows the aromatic F156, W157 and F222 residues present in KCNQ1 but are Leu in KCNQ3. The bottom panel shows the structural model of KCNQ3 in grey, calmodulin in red, Leu residues identified from sequence alignment in green, and Q218 (mutated to C218 in KCNQ3*) in blue. L156, L157, and L222 are in close proximity to the fluorophore attachment position 218, and are good candidates for aromatic mutagenesis.

Aromatic mutations near C218 can significantly improve VCF signal strength and consistency

To our surprise, all KCNQ3*VCF mutants we constructed significantly improved VCF strength and/or consistency, though to various degrees. Similar to previous studies, we struggled obtaining VCF signals from the KCNQ3*VCF control channel, and observed mostly small or undetectable VCF signals most of the time. However, we can occasionally obtain signals %ΔF/F > 0.5 %. The average %ΔF/F is the smallest for KCNQ3*VCF (mean %ΔF/F = 0.4 +/- 0.1 %), and we often observed no changes in fluorescence despite observing large ionic currents indicating efficient surface expression of channels (Figure 5.4 A, B). For the KCNQ3*VCF control, we observed a %ΔF/F range between 0 to 1.6 %, with most recordings being closer to the lower end. KCNQ3*VCF[L222F] improved signal consistency (we rarely observed %ΔF/F < 0.5 %) and increased the mean magnitude of %ΔF/F to an intermediate level (mean %ΔF/F = 1.0 +/- 0.1 %) relative to all the mutants we tested, with a %ΔF/F range of 0.3 to 1.6% (Figure 5.4 A, B). KCNQ3*VCF[L156W][L157F] significantly improved signal consistency (%ΔF/F is rarely < 1.0 %) and increased the mean magnitude of %ΔF/F to the highest level (mean %ΔF/F = 2.0 +/- 0.1 %) relative to all other mutants we tested, with a %ΔF/F range of 0.9 to 4.2 % (Figure 5.4 A, B). Since both the L222F and L156W/L157F mutations improved VCF signals from KCNQ3, we constructed a channel with all three mutations to see if VCF signals can be further improved. When compared to KCNQ3*VCF[L156W][L157F], KCNQ3*VCF[L156W][L157F][L222F] produced a similar mean magnitude of %ΔF/F (mean %ΔF/F = 1.6 +/- 0.1 %), produced %ΔF/F > 1 % relatively consistently, with a %ΔF/F range of 1.2 to 1.9 %. All %ΔF/F are compared between KCNQ3*VCF mutants on a cell-by-cell basis on Figure 5.4 B. Although not all the data is shown in Figure 5.5 for the mutants we tested, we only detected moderate changes in channel voltage dependence and current expression. Nevertheless, KCNQ3*VCF[L156W][L157F] produced the strongest and most robust VCF signals that are not further improved by an additional [L222F] mutation.

While we are uncertain of its usefulness, the KCNQ3*VCF[L222W] mutant is interesting. Although the mutation is in the same position as KCNQ3*VCF[L222F], the aromatic amino acid identity, either Trp or Phe, had dramatically different effects on fluorescence behaviour. KCNQ3*VCF[L222W] produced stronger VCF signals than the KCNQ3*VCF control (data not shown but is clear when comparing representative traces in Figure 5.4 A), as did the KCNQ3*VCF[L222F] mutant. However, a higher level of fluorescence is associated with the deactivated voltage sensor, rather than the typically observed activated voltage sensor (Figure 5.4 B); in other words, the fluorescence associate with channel states is flipped. Furthermore, we observed the highest fluorescence not when voltage sensors are fully activated or deactivated, but somewhere in-between these two states (i.e. channel fluorescence is low when voltage sensors are active, but channels undergoing voltage dependent closure will emit high fluorescence transiently before stabilizing with an intermediate level of fluorescence upon full voltage sensor deactivation). Although we are unsure about the importance of this finding, or how it can be applied to study voltage sensor function, this fluorescence behaviour has not been previously observed in KCNQ channels.

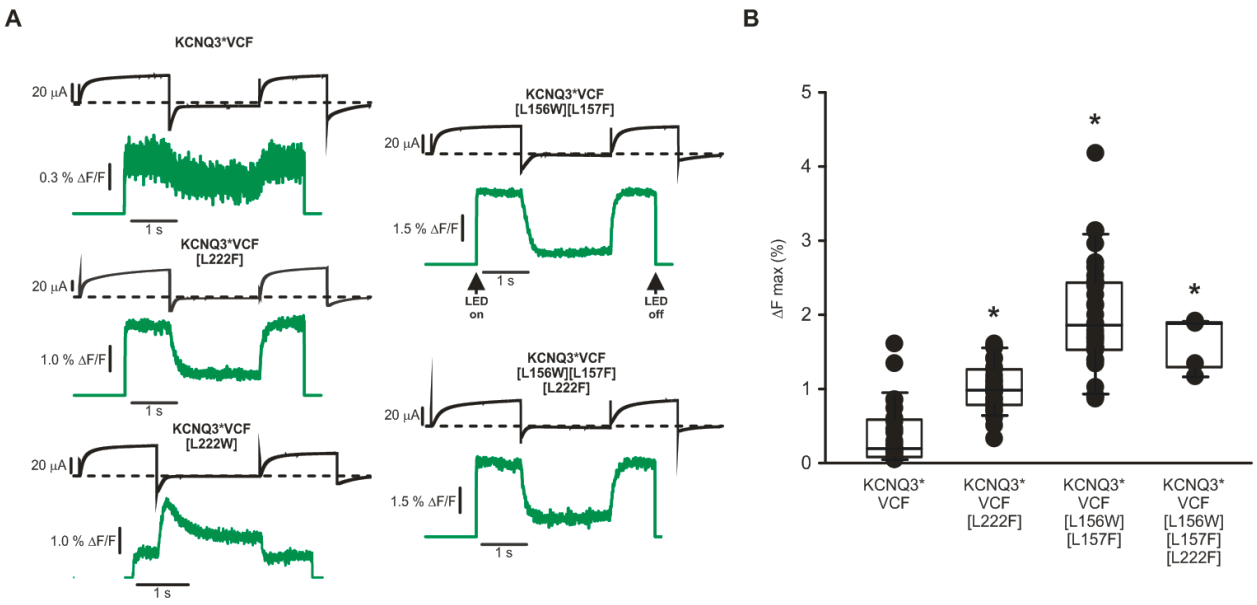

Figure 5.4: KCNQ3*VCF[L156W][L157F] channels produce the largest ΔF/F, and significantly improves consistency of signals > 0.5 % ΔF/F. (A) Representative ionic current and fluorescence traces from oocytes injected with 50 ng of KCNQ3*VCF control or aromatic mutant mRNA and were recorded from 72 hours after injection for channel overexpression. Recordings are obtained using the same protocol outlined in Figure 5.2. **(B)** Cell-by-cell comparison of maximum %ΔF/F between KCNQ3*VCF and aromatic mutants. KCNQ3*VCF[L222W] is excluded from this comparison due to its complex fluorescence behaviour during channel gating. Each data point represents a unique oocyte recording (n = 5-37). Data are mean +/- SEM, and are as follows: KCNQ3*VCF (mean = 0.4 +/- 0.1 %), KCNQ3*VCF[L222F] (mean = 1.0 +/- 0.1 %), KCNQ3*VCF[L156W][L157F] (mean = 2.0 +/- 0.1 %), and KCNQ3*VCF [L156W][L157F][L222F] (mean = 1.6 +/- 0.2 %). Data were compared using a Kruskal-Wallis ANOVA on ranks, followed by Dunnett's post-hoc test (* indicates $p<0.05$ relative to the KCNQ3*VCF control).

KCNQ3[L156W, 157F] has no effect on channel gating and but moderately enhances RTG effects

Finally, we wanted to determine if the L156W and L157F mutation affects channel function or responses to RTG. We observed no departure in channel gating behaviour caused by these aromatic mutations, and only a moderate increase in the RTG-mediated hyperpolarizing shift (by an additional -20.8 mV when compared with the KCNQ3*VCF control in voltage-dependence). Since there is no drastic departure from normal KCNQ3*VCF behaviour, the KCNQ3*VCF[L156W][L157F] is a good KCNQ3 VCF background candidate to consider for future studies.

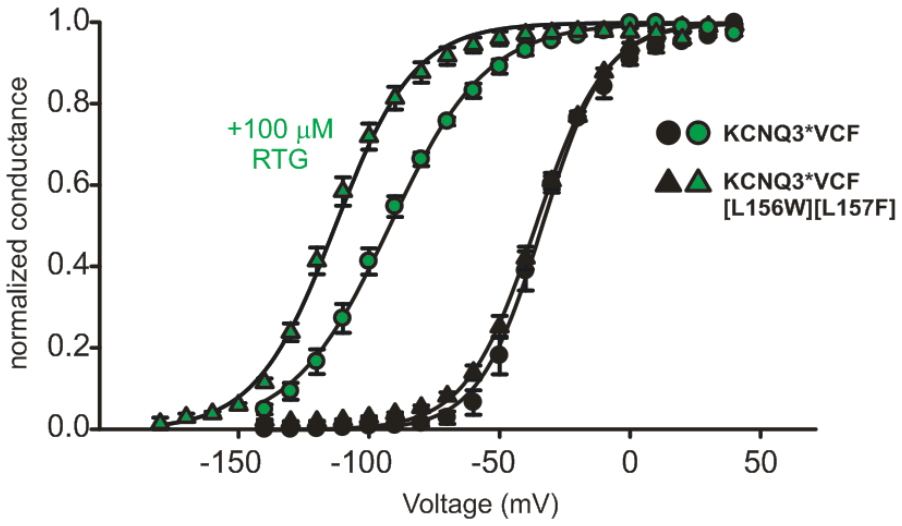

Figure 5.5: The L156W and L157F double mutation has no effect on channel gating, and slightly increases channel response to RTG. The black data points reflect data in the absence of RTG, and green data points reflect data in the presence of 100 μM RTG. Normalized conductance is obtained from the instantaneous tail current at -40 mV after depolarizing channels to the voltages in the graph. All four curves are fitted with their respective GV fits using the one-component Boltzmann equation discussed in Chapter 2. Fitted gating parameters for KCNQ3* were (no RTG: $V_{1/2}$ = -33.7 +/- 2.2 mV, k = 12.2 +/- 2.5; 100 μM RTG: $V_{1/2}$ = -92.1 +/- 3.5 mV, k = 18.6 +/- 2.2). Fitted gating parameters for KCNQ3*[L156W][L157F] were (no RTG: $V_{1/2}$ = -36.2 +/- 3.7 mV, k = 13.3 +/- 1.7; 100 μM RTG: $V_{1/2}$ = -113.0 +/- 6.7 mV, k = 15.2 +/- 3.1). Data are mean +/- SEM (n = 8-11).

DISCUSSION

The study of voltage-dependent channels has been dramatically improved since the conceptualization of voltage-clamp fluorometry; due to the ability it gives to researchers in tracking the behaviour of voltage sensors independently from the pore (Gandhi and Olcese, 2009). Despite its usefulness, VCF has always been a challenge in neuronal KCNQ channels. There have been no reports of VCF signals obtained from KCNQ2,4,5, and only few reports of weak and inconsistent signals obtained from KCNQ3 (Kim et al., 2017; Barro-Soria, 2019). This chapter explored a mutagenic approach using aromatic residues to improve VCF signals in KCNQ3 channels, that can be applied to other KCNQ as well. This approach clearly improves both the signal strength and the consistency of large signals (> 1 %) for the KCNQ3.

Due to the Kv7/KCNQ's emergence as a target for treating pharmacoresistant epilepsies, scientists and industries have been interested in applying VCF to KCNQ3, and if possible, KCNQ2, to facilitate the study and development of compounds with greater potency and decreased side effects. The crystal structure of KCNQ1 generated by Sun and MacKinnon (2017) enabled the modeling of the KCNQ3 structure, and combined with sequence alignment, allowed us to identify sequence differences between the VCF-friendly KCNQ1 and the VCF-unfriendly KCNQ3 near the latter's fluorophore attachment site. We made these mutations hoping to increase the differential quenching between activated and deactivated voltage sensors, so that changes in fluorescence can be more easily detected.

We found that all the KCNQ3 aromatic mutants we tested had altered, strengthened, and/or improved the consistency of VCF signals from channels. Not only did we identify a useful tool that can be applied to study KCNQ3's PIP_2-dependence or pharmacology (KCNQ3*VCF[L156W][L157F]), these findings also increased our confidence in the structural model of KCNQ3. Due to the success of this study, we will apply this novel mutagenic approach to KCNQ2,4,5, perhaps producing the first VCF signals detected in these channel subtypes.

In summary, we successfully improved the strength and consistency of VCF signals in KCNQ3 through our mutagenic approach. We found that the KCNQ3*VCF[L156W][L157F] construct can be a useful tool due to its strong and consistent VCF signals, and minimal effects on channel gating and pharmacology. We will likely use this construct for future studies of KCNQ3's PIP_2-dependence and the pharmacology of novel KCNQ3-targeted compounds.

CHAPTER 6: DISCUSSION

GENERAL DISCUSSION

Kv7/KCNQ channels are emerging targets for the treatment of pharmacoresistant epilepsy. Recent studies have uncovered significant insight into the mechanisms of the first-in-class drug retigabine, and of several other KCNQ activators including ICA-73 (Lange et al., 2009; Gunthorpe et al., 2012; Kim et al., 2015; Wang et al., 2017; A. W. Wang et al., 2018; C. K. Wang et al., 2018; Yau et al., 2018). Differences were identified between the pore-targeted RTG and the voltage sensor targeted ICA-73, including distinct binding regions and sequence determinants of drug effects (Kim et al., 2015; Wang et al., 2017; A. W. Wang et al., 2018b; C. K. Wang et al., 2018). Understanding the properties of these drugs not only guides the investigation and development of their analogues, but also enables their use in research to identify functional properties and stoichiometries of KCNQ channels (A. W. Wang et al., 2018; Yau et al., 2018), including the work discussed in this thesis. Findings in this thesis exploit the properties of ICA-73 to improve our understanding of the KCNQ-related neurological diseases, KCNQ channel assembly, and the structural properties of the channel pore. Additionally, I investigated how aromatic mutations can improve the use of voltage clamp fluorometry for future studies on KCNQ channel function and pharmacology.

In Chapter 3, we investigated the effects of KCNQ3 truncations, their link to disease, and M-channel assembly in *Xenopus* oocytes. We began by characterizing the effects of a disease-linked KCNQ3 truncation mutation KCNQ3-FS534 identified in a child patient, and determined that it suppresses homomeric and heteromeric M-channel function to homomeric KCNQ2 levels (Figures 3.1, 3.2, 3.3, 3.4). Moderate effects were observed in channel voltage-dependent gating and attenuated retigabine-mediated effects were also observed. Next, we demonstrated that the recently identified properties of ICA-73 (state-dependence, selectivity, stoichiometric dependence) can be exploited in an assay to detect the heteromeric assembly of KCNQ2/KCNQ3 M-channels (Figure 3.5). Using this assay, we unambiguously detected the assembly of the disease-linked KCNQ3-FS534 and several artificial KCNQ3 truncations (Figures 3.6, 3.7, 3.8).

Additionally, we showed that having a wild type-like propensity to assemble does not mean M-channel level currents can be restored (Figures 3.7, 3.8), and this may be the underlying reason why we observe autistic and ataxic phenotypes in our child patient. We further eliminated ambiguity caused by overexpression of channels by significantly reducing the expression of mutant KCNQ3, and determined that many truncated forms of KCNQ3 have similar propensity to assemble as WT KCNQ3 (Figure 3.7). Our results suggest that the dominant phenotype observed in the child patient is likely due to a dominant-negative effect caused by the suppression of M-currents from heteromerically assembled KCNQ3-FS534.

In Chapter 4, we investigated the disease-linked T313I mutation in the selectivity filter of KCNQ3, and observed its effects on homomeric and heteromeric M-channel function in *Xenopus* oocytes and mouse LM fibroblasts. This mutation (Figure 4.1) is interesting since the analogous position in the *Drosophila Shaker* stabilizes the selectivity filter through intersubunit hydrogen bonds, and mutation can dramatically suppress channel current and accelerate C-type inactivation (Pless et al., 2013). We determined that KCNQ3[T313I] cannot form functional homomeric channels, and suppresses M-channel currents to KCNQ2 homomeric levels when co-expressed with KCNQ2 (Figure 4.2, 4.3). Since we already established an assay in Chapter 3, using ICA-73 to detect the functional assembly of KCNQ2/KCNQ3 channels, we employed it in this study and unambiguously detected significant assembly of functional KCNQ2/KCNQ3[T313I] heteromeric channels (Figure 4.4). Though functional, currents from heteromeric KCNQ2/KCNQ3[T313I] channels are significantly suppressed compared to wild type KCNQ2/KCNQ3 channels (Figure 4.4). Finally, we constructed tetrameric KCNQ2-KCNQ3 concatemers expressed in mouse LM fibroblasts and determined that a single KCNQ3[T313I] subunit is sufficient to suppress M-channel currents *and* produce a rightward shift in voltage dependence when compared to WT KCNQ3 (Figure 4.5). Interestingly, we did not observe rapid inactivation (Figure 4.2) seen with the analogous mutation in *Shaker* channels (Pless et al., 2013).

Lastly, in Chapter 5, motivated by the potential contributions of voltage clamp fluorometry to understanding channel function and pharmacology, we methodically improved the voltage clamp

fluorometry approach for KCNQ3 channels in a way that can be applied to other KCNQ subtypes. We identified several amino acid differences between KCNQ1 (which consistently produces massive VCF signals – Figure 5.2) and KCNQ3 (which inconsistently produces small VCF signals), near the fluorophore attachment site in the KCNQ3 structural model (Figure 5.3). We mutated these residues to aromatic amino acids to improve differential quenching between activated and deactivated voltage sensors, producing: KCNQ3*VCF[L222F], KCNQ3*VCF[L222W], KCNQ3*VCF[L156W][L157F], and KCNQ3*VCF[L156W][L157F][L222F]. All mutant channels that we tested improved the strength and consistency of VCF signals (Figure 5.4). The KCNQ3*VCF[L156W][L157F] is particularly interesting for future use since it produced the largest improvements to KCNQ3 VCF signals, with minimal effects on channel biophysics and retigabine-mediated effects characteristic of KCNQ3*VCF (Figure 5.4, 5.5).

Understanding the genotype-phenotype correlation of Kv7/KCNQ mutations

An understanding of the genotype-phenotype correlation between mutations and disease can be important for guiding clinical decisions for patients carrying such mutations. We collaborated with clinicians who identified patients carrying a single copy of the FS534 or T313I variant of KCNQ3, and exhibited some form of neurological disorder: neurodevelopmental delay and benign familial neonatal seizures, respectively. When we first began characterizing the KCNQ3-FS534 and the KCNQ3[T313I] mutant channels, we quickly realized a common difficulty. Since we observe dominant neurological phenotypes in both patients, we could not determine if their disorders arose from the haploinsufficiency of functional wild type KCNQ3, or dominant negative effects from assembled mutant KCNQ3 in homomeric and heteromeric channels; in other words, are channels ‘inert’ and do not affect assembled M-channels, or are they suppressing or modifying other functional channels through heteromeric assembly. The difference between the two possibilities lies in the channel’s ability to assemble. Using our understanding of the subtype specificity and stoichiometric dependence of the KCNQ activator ICA-73, we tested both KCNQ3 variants and unambiguously detected the assembly of both variants with KCNQ2. Not only did the KCNQ3 variants assemble with KCNQ2, but they influenced the function of heteromeric channels by suppressing

current expression, shifting channel voltage dependence, and/or influencing channel sensitivity to pharmacological agents. The work in this thesis shows that ICA-73 can likely be applied in future experiments as a relatively easy way to detect assembly of heteromeric channels, and to characterize the effects of KCNQ2 and KCNQ3 mutations on neuronal M-channel function.

Lastly, since we explored the effects of two KCNQ channel openers, retigabine and ICA-73, on channels containing mutated KCNQ3 subunits, our findings may be able to guide the clinical decisions and selection of therapeutics used to manage symptoms in the patients of our study, and they may be applicable to other/future patients who share similar KCNQ3 mutations.

Insights into KCNQ channel assembly

While several studies have investigated C-terminal regions in facilitating KCNQ channel assembly, they all used a similar chimeric approach to swap the C-terminal regions between KCNQ1 and KCNQ2 or KCNQ3 (Schwake et al., 2003, 2006; Howard et al., 2007). While this approach can be useful when channel currents are potentiated – a hallmark feature of co-assembled wild type KCNQ channels (Wang et al., 1998) – it was limited when channel currents were not potentiated. These past studies focused exclusively on the importance of the *subunit interaction domain (sid,* consisting of helix C and D), and its importance for heteromeric KCNQ2/KCNQ3 assembly. We have shown using a more specific pharmacological approach that the loss of *sid*, which may be decreasing the extent of assembly, is not the exclusive determinant of heteromeric channel assembly. Other regions that drive assembly must exist, and may be in the differentiating region between KCNQ3-ΔC501 and KCNQ3-ΔC340. This region consists of helix A and B, which have been shown to be important for interaction with calmodulin and PIP_2 (Wen and Levitan, 2002; Yus-Najera et al., 2002; Zaydman and Cui, 2014b; Sun and MacKinnon, 2017). If this differentiating region is the final contributor to channel assembly, then we can begin investigating if intrinsic elements within this region, calmodulin, and/or PIP_2 are driving channel assembly.

Although it is clearly useful in some circumstances, we understand that the ICA-73 approach to detect heteromeric assembly can also be limited. One requirement of this assay is that assembly can only be detected if heteromeric channels are functional, since ICA-73's effects can only be observed through changes in channel currents. Therefore, while most of the mutants we tested (KCNQ3 truncations or the KCNQ3[T313I]) did functionally assemble into heteromeric channels and attenuated channel response to ICA-73, it is possible that KCNQ3-ΔC503 assembles with KCNQ2 into non-functional channels that cannot be detected using ICA-73. In this case, assembly (or inability to assemble) must be determined using other approaches (e.g. co-immunoprecipitation, BRET…). Combining these other approaches with our ICA-73 assay may finally help isolate the assembly-determining region in KCNQ channels that has long been relatively unclear.

Finally, although different stoichiometries between KCNQ2 and KCNQ3 can assemble into functional M-channels, we are uncertain regarding the specific stoichiometries that formed *in vitro* in our injected oocytes, or *in vivo* in our patient probands. A.W. Wang et al. (2018) showed the stoichiometric dependence of ICA-73 effects: where progressive loss of ICA-73 sensitive subunits led to the progressive attenuation of ICA-73 channel opening effects. This property can perhaps be assessed more closely to determine the types of, and perhaps the dominant stoichiometry, between wild type KCNQ3 or KCNQ3 mutants and KCNQ2.

Differences between KCNQ and *Shaker* channel selectivity filters

Although Kv channels follow a similar channel architecture (6-TM, intracellular N and C-termini), they are functionally and structurally diverse (Miller, 2000; Kuang et al., 2015). The *Drosophila shaker* channel is unique to this genus, but is most homologous the human Kv1 class of channels (Rasmussen and Trimmer, 2018). *Shaker* was the first voltage-gated potassium channel discovered, and its study has generated significant insight into the voltage sensing and ion selective properties of Kv channels (Miller, 2000; Kuang et al., 2015). The selectivity filter of *Shaker* and the intrasubunit/intersubunit hydrogen

bonding interactions have been studied extensively (Pless et al., 2013). The selectivity filter is shown to collapse when the intersubunit hydrogen bonding residues T439 and Y445 are mutated, resulting in dramatic acceleration of channel inactivation and suppression of current (Pless et al., 2013). We determined that the analogous T313I mutation in KCNQ3 likely disrupts a similar intersubunit hydrogen bond that normally stabilizes the selectivity filter, since we observed a similar suppression of channel currents but no appearance of channel inactivation (Figures 4.2, 4.3). It is interesting to observe that inactivation is accelerated in *Shaker* (a channel that normally inactivates) (Hoshi et al., 1991), but not recreated in KCNQ3 (a channel that does not normally inactivate), suggesting a unique underlying mechanism driving inactivation in *Shaker* that is influenced by the disruption of the critical intersubunit hydrogen bond (Pless et al., 2013).

The importance of the intersubunit hydrogen bond is further shown in KCNQ2. The analogous position in KCNQ2 is likely involved in the same intersubunit hydrogen bond, as mutation in this region reported in ClinVar and RIKEE databases is linked to severe epileptic encephalopathy phenotype expected from loss-of-function KCNQ2 mutations. Due to the dramatic effects caused by disrupting this critical intersubunit hydrogen bond in *Shaker*, KCNQ2, and KCNQ3, and the conservation of Thr and Tyr residues amongst Kv channels at these positions (Doyle et al., 1998), this specific mechanism for stabilizing the selectivity filter is likely shared by many Kv channels.

Implications for future drug development and channel studies

With the emergence of novel Kv7/KCNQ targeted anti-epileptic compounds with unique properties and selectivity, it is important to dissect the details of their mechanism of action to guide the continuous development of more potent, selective, and therapeutically beneficial drugs for treating pharmacoresistant epilepsy. It has been shown that retigabine and ICA-73 have drastically different effects on KCNQ channel behaviour (Kim et al., 2015, 2017; A. W. Wang et al., 2017, 2018; C. K. Wang et al., 2018). However, there remains a lack of understanding of the mechanisms of these drugs, particularly with the relatively new voltage sensor targeted compounds (e.g. ICA-73). Voltage clamp fluorometry has been a challenge in its

application for KCNQ channel studies. However, it can provide specific details on the voltage sensor that are normally unobtainable from current data alone (Gandhi and Olcese, 2009). In this thesis, we have shown an approach that dramatically decreased the difficulty in obtaining KCNQ3 VCF signals. Similar aromatic mutations can be made in other KCNQ subtypes, which may enable the use of VCF on these channels. Making VCF usable for these other channels can significantly improve our functional and pharmacological understanding of KCNQ channels, and can potentially accelerate research progress and pharmaceutical development related to these channels.

CONCLUSION

An improved understanding of KCNQ activators has been guiding the development of novel compounds with potentially improved clinical outcomes, but has also improved our overall understanding of KCNQ channels. This thesis highlights the use of KCNQ activators to understand Kv7/KCNQ channel mutations in disease, regions important for channel assembly, and interactions important for maintaining the channel pore.

REFERENCES

Aggarwal, S.K., MacKinnon, R., 1996. Contribution of the S4 segment to gating charge in the Shaker K+ channel. Neuron 16, 1169–1177. https://doi.org/10.1016/s0896-6273(00)80143-9

Bähring, R., Barghaan, J., Westermeier, R., Wollberg, J., 2012. Voltage Sensor Inactivation in Potassium Channels. Front. Pharmacol. 3. https://doi.org/10.3389/fphar.2012.00100

Bal, M., Zhang, J., Zaika, O., Hernandez, C.C., Shapiro, M.S., 2008. Homomeric and Heteromeric Assembly of KCNQ (Kv7) K+ Channels Assayed by Total Internal Reflection Fluorescence/Fluorescence Resonance Energy Transfer and Patch Clamp Analysis. J. Biol. Chem. 283, 30668–30676. https://doi.org/10.1074/jbc.M805216200

Barhanin, J., Lesage, F., Guillemare, E., Fink, M., Lazdunski, M., Romey, G., 1996. K(V)LQT1 and lsK (minK) proteins associate to form the I(Ks) cardiac potassium current. Nature 384, 78–80. https://doi.org/10.1038/384078a0

Barrese, V., Stott, J.B., Greenwood, I.A., 2018. KCNQ-Encoded Potassium Channels as Therapeutic Targets. Annu. Rev. Pharmacol. Toxicol. 58, 625–648. https://doi.org/10.1146/annurev-pharmtox-010617-052912

Barros, F., Dominguez, P., de la Peña, P., 2012. Cytoplasmic Domains and Voltage-Dependent Potassium Channel Gating. Front. Pharmacol. 3. https://doi.org/10.3389/fphar.2012.00049

Barro-Soria, R., 2019. Epilepsy-associated mutations in the voltage sensor of KCNQ3 affect voltage dependence of channel opening. J. Gen. Physiol. 151, 247–257. https://doi.org/10.1085/jgp.201812221

Benned-Jensen, T., Christensen, R.K., Denti, F., Perrier, J.-F., Rasmussen, H.B., Olesen, S.-P., 2016. Live Imaging of Kv7.2/7.3 Cell Surface Dynamics at the Axon Initial Segment: High Steady-State Stability and Calpain-Dependent Excitotoxic Downregulation Revealed. J. Neurosci. 36, 2261–2266. https://doi.org/10.1523/JNEUROSCI.2631-15.2016

Bezanilla, F., 2008. How membrane proteins sense voltage. Nat. Rev. Mol. Cell Biol. 9, 323–332. https://doi.org/10.1038/nrm2376

Bezanilla, F., 2000. The voltage sensor in voltage-dependent ion channels. Physiol. Rev. 80, 555–592. https://doi.org/10.1152/physrev.2000.80.2.555

Bezanilla, F., Stefani, E., 1998. [19] Gating currents, in: Methods in Enzymology, Ion Channels Part B. Academic Press, pp. 331–352. https://doi.org/10.1016/S0076-6879(98)93022-1

Biervert, C., Schroeder, B.C., Kubisch, C., Berkovic, S.F., Propping, P., Jentsch, T.J., Steinlein, O.K., 1998. A potassium channel mutation in neonatal human epilepsy. Science 279, 403–406. https://doi.org/10.1126/science.279.5349.403

Bleich, M., Warth, R., 2000. The very small-conductance K+ channel KVLQT1 and epithelial function. Pflüg. Arch. 440, 202–206. https://doi.org/10.1007/s004240000257

Boehlen, A., Schwake, M., Dost, R., Kunert, A., Fidzinski, P., Heinemann, U., Gebhardt, C., 2013. The new KCNQ2 activator 4-Chlor-N-(6-chlor-pyridin-3-yl)-benzamid displays anticonvulsant potential. Br. J. Pharmacol. 168, 1182–1200. https://doi.org/10.1111/bph.12065

Brown, D.A., Adams, P.R., 1980. Muscarinic suppression of a novel voltage-sensitive K+ current in a vertebrate neurone. Nature 283, 673–676. https://doi.org/10.1038/283673a0

Brown, D.A., Passmore, G.M., 2009. Neural KCNQ (Kv7) channels. Br. J. Pharmacol. 156, 1185–1195. https://doi.org/10.1111/j.1476-5381.2009.00111.x

Brueggemann, L.I., Haick, J.M., Cribbs, L.L., Byron, K.L., 2014. Differential activation of vascular smooth muscle Kv7.4, Kv7.5, and Kv7.4/7.5 channels by ML213 and ICA-069673. Mol. Pharmacol. 86, 330–341. https://doi.org/10.1124/mol.114.093799

Capera, J., Serrano-Novillo, C., Navarro-Pérez, M., Cassinelli, S., Felipe, A., 2019. The Potassium Channel Odyssey: Mechanisms of Traffic and Membrane Arrangement. Int. J. Mol. Sci. 20. https://doi.org/10.3390/ijms20030734

Casimiro, M.C., Knollmann, B.C., Ebert, S.N., Vary, J.C., Greene, A.E., Franz, M.R., Grinberg, A., Huang, S.P., Pfeifer, K., 2001. Targeted disruption of the Kcnq1 gene produces a mouse model of Jervell and Lange– Nielsen Syndrome. Proc. Natl. Acad. Sci. 98, 2526–2531. https://doi.org/10.1073/pnas.041398998

Charlier, C., Singh, N.A., Ryan, S.G., Lewis, T.B., Reus, B.E., Leach, R.J., Leppert, M., 1998. A pore mutation in a novel KQT-like potassium channel gene in an idiopathic epilepsy family. Nat. Genet. 18, 53–55. https://doi.org/10.1038/ng0198-53

Chung, H.J., 2014. Role of calmodulin in neuronal Kv7/KCNQ potassium channels and epilepsy. Front. Biol. 9, 205–215. https://doi.org/10.1007/s11515-014-1305-3

Constanti, A., Brown, D.A., 1981. M-Currents in voltage-clamped mammalian sympathetic neurones. Neurosci. Lett. 24, 289–294. https://doi.org/10.1016/0304-3940(81)90173-7

Cooper, E.C., 2011. Made for “anchorin”: Kv7.2/7.3 (KCNQ2/KCNQ3) channels and the modulation of neuronal excitability in vertebrate axons. Semin. Cell Dev. Biol. 22, 185–192. https://doi.org/10.1016/j.semcdb.2010.10.001

Cooper, E.C., Aldape, K.D., Abosch, A., Barbaro, N.M., Berger, M.S., Peacock, W.S., Jan, Y.N., Jan, L.Y., 2000. Colocalization and coassembly of two human brain M-type potassium channel subunits that are mutated in epilepsy. Proc. Natl. Acad. Sci. 97, 4914–4919. https://doi.org/10.1073/pnas.090092797

Cooper, E.C., Jan, L.Y., 2003. M-channels: neurological diseases, neuromodulation, and drug development. Arch. Neurol. 60, 496–500. https://doi.org/10.1001/archneur.60.4.496

Cui, J., 2016. Voltage-Dependent Gating: Novel Insights from KCNQ1 Channels. Biophys. J. 110, 14–25. https://doi.org/10.1016/j.bpj.2015.11.023

Czech, M.P., 2000. PIP2 and PIP3: Complex Roles at the Cell Surface. Cell 100, 603–606. https://doi.org/10.1016/S0092-8674(00)80696-0

Delmas, P., Brown, D.A., 2005. Pathways modulating neural KCNQ/M (Kv7) potassium channels. Nat. Rev. Neurosci. 6, 850–862. https://doi.org/10.1038/nrn1785

Doyle, D.A., Morais Cabral, J., Pfuetzner, R.A., Kuo, A., Gulbis, J.M., Cohen, S.L., Chait, B.T., MacKinnon, R., 1998. The structure of the potassium channel: molecular basis of K+ conduction and selectivity. Science 280, 69–77. https://doi.org/10.1126/science.280.5360.69

Etxeberria, A., Santana-Castro, I., Regalado, M.P., Aivar, P., Villarroel, A., 2004. Three Mechanisms Underlie KCNQ2/3 Heteromeric Potassium M-Channel Potentiation. J. Neurosci. 24, 9146–9152. https://doi.org/10.1523/JNEUROSCI.3194-04.2004

Fazio, G., Vernuccio, F., Grutta, G., Re, G.L., 2013. Drugs to be avoided in patients with long QT syndrome: Focus on the anaesthesiological management. World J. Cardiol. 5, 87–93. https://doi.org/10.4330/wjc.v5.i4.87

Friedberg, F., Rhoads, A.R., 2001. Evolutionary Aspects of Calmodulin. IUBMB Life 51, 215–221. https://doi.org/10.1080/152165401753311753

Gamper, N., Shapiro, M.S., 2003. Calmodulin mediates Ca2+-dependent modulation of M-type K+ channels. J. Gen. Physiol. 122, 17–31. https://doi.org/10.1085/jgp.200208783

Gandhi, C.S., Olcese, R., 2009. The Voltage-Clamp Fluorometry Technique, in: Lippiat, J.D. (Ed.), Potassium Channels: Methods and Protocols, Methods in Molecular Biology. Humana Press, Totowa, NJ, pp. 213–231. https://doi.org/10.1007/978-1-59745-526-8_17

Ghosh, S., Nunziato, D.A., Pitt, G.S., 2006. KCNQ1 assembly and function is blocked by long-QT syndrome mutations that disrupt interaction with calmodulin. Circ. Res. 98, 1048–1054. https://doi.org/10.1161/01.RES.0000218863.44140.f2

Gómez-Posada, J.C., Etxeberría, A., Roura-Ferrer, M., Areso, P., Masin, M., Murrell-Lagnado, R.D., Villarroel, A., 2010. A Pore Residue of the KCNQ3 Potassium M-Channel Subunit Controls Surface Expression. J. Neurosci. 30, 9316–9323. https://doi.org/10.1523/JNEUROSCI.0851-10.2010

Grundström, T., 1999. Calmodulin – an exceptional protein: Calmodulin and Signal Transduction edited by Linda J. Van Eldik and D. Martin Watterson. Trends Cell Biol. 9, 40. https://doi.org/10.1016/S0962-8924(98)01371-3

Gunthorpe, M.J., Large, C.H., Sankar, R., 2012. The mechanism of action of retigabine (ezogabine), a first-in-class K+ channel opener for the treatment of epilepsy. Epilepsia 53, 412–424. https://doi.org/10.1111/j.1528-1167.2011.03365.x

Hadley, J.K., Noda, M., Selyanko, A.A., Wood, I.C., Abogadie, F.C., Brown, D.A., 2000. Differential tetraethylammonium sensitivity of KCNQ1-4 potassium channels. Br. J. Pharmacol. 129, 413–415. https://doi.org/10.1038/sj.bjp.0703086

Hadley, J.K., Passmore, G.M., Tatulian, L., Al-Qatari, M., Ye, F., Wickenden, A.D., Brown, D.A., 2003. Stoichiometry of expressed KCNQ2/KCNQ3 potassium channels and subunit composition of native ganglionic M channels deduced from block by tetraethylammonium. J. Neurosci. Off. J. Soc. Neurosci. 23, 5012–5019.

Haitin, Y., Attali, B., 2008. The C-terminus of Kv7 channels: a multifunctional module. J. Physiol. 586, 1803–1810. https://doi.org/10.1113/jphysiol.2007.149187

Heginbotham, L., Lu, Z., Abramson, T., MacKinnon, R., 1994. Mutations in the K+ channel signature sequence. Biophys. J. 66, 1061–1067. https://doi.org/10.1016/S0006-3495(94)80887-2

Heginbotham, L., MacKinnon, R., 1993. Conduction properties of the cloned Shaker K+ channel. Biophys. J. 65, 2089–2096. https://doi.org/10.1016/S0006-3495(93)81244-X

Heidenreich, M., Lechner, S.G., Vardanyan, V., Wetzel, C., Cremers, C.W., De Leenheer, E.M., Aránguez, G., Moreno-Pelayo, M.Á., Jentsch, T.J., Lewin, G.R., 2011. KCNQ4 K(+) channels tune mechanoreceptors for normal touch sensation in mouse and man. Nat. Neurosci. 15, 138–145. https://doi.org/10.1038/nn.2985

Hoshi, T., Zagotta, W.N., Aldrich, R.W., 1991. Two types of inactivation in Shaker K+ channels: effects of alterations in the carboxy-terminal region. Neuron 7, 547–556. https://doi.org/10.1016/0896-6273(91)90367-9

Howard, R.J., Clark, K.A., Holton, J.M., Minor, D.L., 2007. Structural Insight into KCNQ (Kv7) Channel Assembly and Channelopathy. Neuron 53, 663–675. https://doi.org/10.1016/j.neuron.2007.02.010

Islas, L.D., 2016. Functional diversity of potassium channel voltage-sensing domains. Channels 10, 202–213. https://doi.org/10.1080/19336950.2016.1141842

Jentsch, T.J., 2000. Neuronal KCNQ potassium channels: physiology and role in disease. Nat. Rev. Neurosci. 1, 21–30. https://doi.org/10.1038/35036198

Kanaumi, T., Takashima, S., Iwasaki, H., Itoh, M., Mitsudome, A., Hirose, S., 2008. Developmental changes in KCNQ2 and KCNQ3 expression in human brain: Possible contribution to the age-dependent etiology of benign familial neonatal convulsions. Brain Dev. 30, 362–369. https://doi.org/10.1016/j.braindev.2007.11.003

Kharkovets, T., Hardelin, J.P., Safieddine, S., Schweizer, M., El-Amraoui, A., Petit, C., Jentsch, T.J., 2000. KCNQ4, a K+ channel mutated in a form of dominant deafness, is expressed in the inner ear and the central auditory pathway. Proc. Natl. Acad. Sci. U. S. A. 97, 4333–4338. https://doi.org/10.1073/pnas.97.8.4333

Kim, D.M., Nimigean, C.M., 2016. Voltage-Gated Potassium Channels: A Structural Examination of Selectivity and Gating. Cold Spring Harb. Perspect. Biol. 8. https://doi.org/10.1101/cshperspect.a029231

Kim, R.Y., Pless, S.A., Kurata, H.T., 2017. PIP2 mediates functional coupling and pharmacology of neuronal KCNQ channels. Proc. Natl. Acad. Sci. U. S. A. 114, E9702–E9711. https://doi.org/10.1073/pnas.1705802114

Kim, R.Y., Yau, M.C., Galpin, J.D., Seebohm, G., Ahern, C.A., Pless, S.A., Kurata, H.T., 2015. Atomic basis for therapeutic activation of neuronal potassium channels. Nat. Commun. 6, 8116. https://doi.org/10.1038/ncomms9116

Kosenko, A., Hoshi, N., 2013. A Change in Configuration of the Calmodulin-KCNQ Channel Complex Underlies Ca2+-Dependent Modulation of KCNQ Channel Activity. PLOS ONE 8, e82290. https://doi.org/10.1371/journal.pone.0082290

Kreusch, A., Pfaffinger, P.J., Stevens, C.F., Choe, S., 1998. Crystal structure of the tetramerization domain of the Shaker potassium channel. Nature 392, 945–948. https://doi.org/10.1038/31978

Kuang, Q., Purhonen, P., Hebert, H., 2015. Structure of potassium channels. Cell. Mol. Life Sci. 72, 3677–3693. https://doi.org/10.1007/s00018-015-1948-5

Kubisch, C., Schroeder, B.C., Friedrich, T., Lütjohann, B., El-Amraoui, A., Marlin, S., Petit, C., Jentsch, T.J., 1999. KCNQ4, a Novel Potassium Channel Expressed in Sensory Outer Hair Cells, Is Mutated in Dominant Deafness. Cell 96, 437–446. https://doi.org/10.1016/S0092-8674(00)80556-5

Kurata, H.T., Fedida, D., 2006. A structural interpretation of voltage-gated potassium channel inactivation. Prog. Biophys. Mol. Biol. 92, 185–208. https://doi.org/10.1016/j.pbiomolbio.2005.10.001

Labro, A.J., Snyders, D.J., 2012. Being Flexible: The Voltage-Controllable Activation Gate of Kv Channels. Front. Pharmacol. 3. https://doi.org/10.3389/fphar.2012.00168

Lange, W., Geissendörfer, J., Schenzer, A., Grötzinger, J., Seebohm, G., Friedrich, T., Schwake, M., 2009. Refinement of the binding site and mode of action of the anticonvulsant Retigabine on KCNQ K+ channels. Mol. Pharmacol. 75, 272–280. https://doi.org/10.1124/mol.108.052282

Lauritano, A., Moutton, S., Longobardi, E., Mau-Them, F.T., Laudati, G., Nappi, P., Soldovieri, M.V., Ambrosino, P., Cataldi, M., Jouan, T., Lehalle, D., Maurey, H., Philippe, C., Miceli, F., Vitobello, A., Taglialatela, M., 2019. A novel homozygous KCNQ3 loss-of-function variant causes non-syndromic intellectual disability and neonatal-onset pharmacodependent epilepsy. Epilepsia Open 4, 464–475. https://doi.org/10.1002/epi4.12353

Lehman, A., Thouta, S., Mancini, G.M.S., Naidu, S., van Slegtenhorst, M., McWalter, K., Person, R., Mwenifumbo, J., Salvarinova, R., Guella, I., McKenzie, M.B., Datta, A., Connolly, M.B., Kalkhoran, S.M., Poburko, D., Friedman, J.M., Farrer, M.J., Demos, M., Desai, S., Claydon, T., 2017. Loss-of-Function and Gain-of-Function Mutations in KCNQ5 Cause Intellectual Disability or Epileptic Encephalopathy. Am. J. Hum. Genet. 101, 65–74. https://doi.org/10.1016/j.ajhg.2017.05.016

Leppert, M., Anderson, V.E., Quattlebaum, T., Stauffer, D., O'Connell, P., Nakamura, Y., Lalouel, J.M., White, R., 1989. Benign familial neonatal convulsions linked to genetic markers on chromosome 20. Nature 337, 647–648. https://doi.org/10.1038/337647a0

Lerche, H., Shah, M., Beck, H., Noebels, J., Johnston, D., Vincent, A., 2013. Ion channels in genetic and acquired forms of epilepsy. J. Physiol. 591, 753–764. https://doi.org/10.1113/jphysiol.2012.240606

Lewis, T.B., Leach, R.J., Ward, K., O'Connell, P., Ryan, S.G., 1993. Genetic heterogeneity in benign familial neonatal convulsions: identification of a new locus on chromosome 8q. Am. J. Hum. Genet. 53, 670–675.

Li, M., Jan, Y.N., Jan, L.Y., 1992. Specification of subunit assembly by the hydrophilic amino-terminal domain of the Shaker potassium channel. Science 257, 1225–1230. https://doi.org/10.1126/science.1519059

Li, Y., Gamper, N., Hilgemann, D.W., Shapiro, M.S., 2005. Regulation of Kv7 (KCNQ) K+ Channel Open Probability by Phosphatidylinositol 4,5-Bisphosphate. J. Neurosci. 25, 9825–9835. https://doi.org/10.1523/JNEUROSCI.2597-05.2005

Liu, Y., Holmgren, M., Jurman, M.E., Yellen, G., 1997. Gated Access to the Pore of a Voltage-Dependent K+ Channel. Neuron 19, 175–184. https://doi.org/10.1016/S0896-6273(00)80357-8

Lu, Z., Klem, A.M., Ramu, Y., 2002. Coupling between Voltage Sensors and Activation Gate in Voltage-gated K+ Channels. J. Gen. Physiol. 120, 663–676. https://doi.org/10.1085/jgp.20028696

Lu, Z., Klem, A.M., Ramu, Y., 2001. Ion conduction pore is conserved among potassium channels. Nature 413, 809–813. https://doi.org/10.1038/35101535

MacKinnon, R., 2003. Potassium channels. FEBS Lett. 555, 62–65. https://doi.org/10.1016/s0014-5793(03)01104-9

MacKinnon, R., 1991. Determination of the subunit stoichiometry of a voltage-activated potassium channel. Nature 350, 232–235. https://doi.org/10.1038/350232a0

MacKinnon, R., Yellen, G., 1990. Mutations affecting TEA blockade and ion permeation in voltage-activated K+ channels. Science 250, 276–279. https://doi.org/10.1126/science.2218530

Maljevic, S., Lerche, C., Seebohm, G., Alekov, A.K., Busch, A.E., Lerche, H., 2003. C-terminal interaction of KCNQ2 and KCNQ3 K+ channels. J. Physiol. 548, 353–360. https://doi.org/10.1113/jphysiol.2003.040980

Maljevic, S., Lerche, H., 2014. Potassium channel genes and benign familial neonatal epilepsy. Prog. Brain Res. 213, 17–53. https://doi.org/10.1016/B978-0-444-63326-2.00002-8

Maljevic, S., Wuttke, T.V., Seebohm, G., Lerche, H., 2010. KV7 channelopathies. Pflugers Arch. 460, 277–288. https://doi.org/10.1007/s00424-010-0831-3

Mannuzzu, L.M., Moronne, M.M., Isacoff, E.Y., 1996. Direct physical measure of conformational rearrangement underlying potassium channel gating. Science 271, 213–216. https://doi.org/10.1126/science.271.5246.213

McLaughlin, S., Wang, J., Gambhir, A., Murray, D., 2002. PIP2 and Proteins: Interactions, Organization, and Information Flow. Annu. Rev. Biophys. Biomol. Struct. 31, 151–175. https://doi.org/10.1146/annurev.biophys.31.082901.134259

Miceli, F., Soldovieri, M.V., Joshi, N., Weckhuysen, S., Cooper, E.C., Taglialatela, M., 1993. KCNQ3-Related Disorders, in: Adam, M.P., Ardinger, H.H., Pagon, R.A., Wallace, S.E., Bean, L.J., Stephens, K., Amemiya, A. (Eds.), GeneReviews®. University of Washington, Seattle, Seattle (WA).

Milh, M., Boutry-Kryza, N., Sutera-Sardo, J., Mignot, C., Auvin, S., Lacoste, C., Villeneuve, N., Roubertie, A., Heron, B., Carneiro, M., Kaminska, A., Altuzarra, C., Blanchard, G., Ville, D., Barthez, M.A., Heron, D., Gras, D., Afenjar, A., Dorison, N., Doummar, D., Billette de Villemeur, T., An, I., Jacquette, A., Charles, P., Perrier, J., Isidor, B., Vercueil, L., Chabrol, B., Badens, C., Lesca, G., Villard, L., 2013. Similar early characteristics but variable neurological outcome of patients with a de novo mutation of KCNQ2. Orphanet J. Rare Dis. 8, 80. https://doi.org/10.1186/1750-1172-8-80

Milh, M., Lacoste, C., Cacciagli, P., Abidi, A., Sutera-Sardo, J., Tzelepis, I., Colin, E., Badens, C., Afenjar, A., Coeslier, A.D., Dailland, T., Lesca, G., Philip, N., Villard, L., 2015. Variable clinical expression in patients with mosaicism for KCNQ2 mutations. Am. J. Med. Genet. A. 167A, 2314–2318. https://doi.org/10.1002/ajmg.a.37152

Miller, C., 2000. An overview of the potassium channel family. Genome Biol. 1, reviews0004.1. https://doi.org/10.1186/gb-2000-1-4-reviews0004

Millichap, J.J., Park, K.L., Tsuchida, T., Ben-Zeev, B., Carmant, L., Flamini, R., Joshi, N., Levisohn, P.M., Marsh, E., Nangia, S., Narayanan, V., Ortiz-Gonzalez, X.R., Patterson, M.C., Pearl, P.L., Porter, B., Ramsey, K., McGinnis, E.L., Taglialatela, M., Tracy, M., Tran, B., Venkatesan, C., Weckhuysen, S., Cooper, E.C., 2016. KCNQ2 encephalopathy: Features, mutational hot spots, and ezogabine treatment of 11 patients. Neurol. Genet. 2, e96. https://doi.org/10.1212/NXG.0000000000000096

Mizuno, N., Itoh, H., 2009. Functions and regulatory mechanisms of Gq-signaling pathways. Neurosignals 17, 42–54. https://doi.org/10.1159/000186689

Nakajo, K., Kubo, Y., 2015. KCNQ1 channel modulation by KCNE proteins via the voltage-sensing domain. J. Physiol. 593, 2617–2625. https://doi.org/10.1113/jphysiol.2014.287672

Nakajo, K., Kubo, Y., 2008. Second coiled-coil domain of KCNQ channel controls current expression and subfamily specific heteromultimerization by salt bridge networks. J. Physiol. 586, 2827–2840. https://doi.org/10.1113/jphysiol.2007.148601

Neyroud, N., Tesson, F., Denjoy, I., Leibovici, M., Donger, C., Barhanin, J., Fauré, S., Gary, F., Coumel, P., Petit, C., Schwartz, K., Guicheney, P., 1997. A novel mutation in the potassium channel gene KVLQT1 causes the Jervell and Lange-Nielsen cardioauditory syndrome. Nat. Genet. 15, 186–189. https://doi.org/10.1038/ng0297-186

Orhan, G., Bock, M., Schepers, D., Ilina, E.I., Reichel, S.N., Löffler, H., Jezutkovic, N., Weckhuysen, S., Mandelstam, S., Suls, A., Danker, T., Guenther, E., Scheffer, I.E., De Jonghe, P., Lerche, H., Maljevic, S., 2014. Dominant-negative effects of KCNQ2 mutations are associated with epileptic encephalopathy. Ann. Neurol. 75, 382–394. https://doi.org/10.1002/ana.24080

Padilla, K., Wickenden, A.D., Gerlach, A.C., McCormack, K., 2009. The KCNQ2/3 selective channel opener ICA-27243 binds to a novel voltage-sensor domain site. Neurosci. Lett. 465, 138–142. https://doi.org/10.1016/j.neulet.2009.08.071

Pan, Z., Kao, T., Horvath, Z., Lemos, J., Sul, J.-Y., Cranstoun, S.D., Bennett, V., Scherer, S.S., Cooper, E.C., 2006. A Common Ankyrin-G-Based Mechanism Retains KCNQ and NaV Channels at Electrically Active Domains of the Axon. J. Neurosci. 26, 2599–2613. https://doi.org/10.1523/JNEUROSCI.4314-05.2006

Panaghie, G., Abbott, G.W., 2007. The role of S4 charges in voltage-dependent and voltage-independent KCNQ1 potassium channel complexes. J. Gen. Physiol. 129, 121–133. https://doi.org/10.1085/jgp.200609612

Papazian, D.M., 1999. Potassium channels: some assembly required. Neuron 23, 7–10. https://doi.org/10.1016/s0896-6273(00)80746-1

Perozo, E., Santacruz-Toloza, L., Stefani, E., Bezanilla, F., Papazian, D.M., 1994. S4 mutations alter gating currents of Shaker K channels. Biophys. J. 66, 345–354.

Pless, S.A., Niciforovic, A.P., Galpin, J.D., Nunez, J.-J., Kurata, H.T., Ahern, C.A., 2013. A novel mechanism for fine-tuning open-state stability in a voltage-gated potassium channel. Nat. Commun. 4, 1784. https://doi.org/10.1038/ncomms2761

Rasmussen, H.B., Trimmer, J.S., 2018. The Voltage-Dependent K+ Channel Family. Oxf. Handb. Neuronal Ion Channels. https://doi.org/10.1093/oxfordhb/9780190669164.013.1

Robbins, J., 2001. KCNQ potassium channels: physiology, pathophysiology, and pharmacology. Pharmacol. Ther. 90, 1–19. https://doi.org/10.1016/s0163-7258(01)00116-4

Robbins, J., Marsh, S.J., Brown, D.A., 1993. On the mechanism of M-current inhibition by muscarinic m1 receptors in DNA-transfected rodent neuroblastoma x glioma cells. J. Physiol. 469, 153–178.

Robbins, J., Passmore, G.M., Abogadie, F.C., Reilly, J.M., Brown, D.A., 2013. Effects of KCNQ2 gene truncation on M-type Kv7 potassium currents. PloS One 8, e71809. https://doi.org/10.1371/journal.pone.0071809

Rogawski, M.A., 2013. AMPA Receptors as a Molecular Target in Epilepsy Therapy. Acta Neurol. Scand. Suppl. 9–18. https://doi.org/10.1111/ane.12099

Rogawski, M.A., 2000. KCNQ2/KCNQ3 K+ channels and the molecular pathogenesis of epilepsy: implications for therapy. Trends Neurosci. 23, 393–398. https://doi.org/10.1016/s0166-2236(00)01629-5

Rothenberg, I., Piccini, I., Wrobel, E., Stallmeyer, B., Müller, J., Greber, B., Strutz-Seebohm, N., Schulze-Bahr, E., Schmitt, N., Seebohm, G., 2016. Structural interplay of KV7.1 and KCNE1 is essential for normal repolarization and is compromised in short QT syndrome 2 (KV7.1-A287T). Hear. Case Rep. 2, 521–529. https://doi.org/10.1016/j.hrcr.2016.08.015

Rusten, T.E., Stenmark, H., 2006. Analyzing phosphoinositides and their interacting proteins. Nat. Methods 3, 251–258. https://doi.org/10.1038/nmeth867

Sanguinetti, M.C., Curran, M.E., Zou, A., Shen, J., Spector, P.S., Atkinson, D.L., Keating, M.T., 1996. Coassembly of K(V)LQT1 and minK (IsK) proteins to form cardiac I(Ks) potassium channel. Nature 384, 80–83. https://doi.org/10.1038/384080a0

Schenzer, A., Friedrich, T., Pusch, M., Saftig, P., Jentsch, T.J., Grötzinger, J., Schwake, M., 2005. Molecular determinants of KCNQ (Kv7) K+ channel sensitivity to the anticonvulsant retigabine. J. Neurosci. Off. J. Soc. Neurosci. 25, 5051–5060. https://doi.org/10.1523/JNEUROSCI.0128-05.2005

Schmitt, N., Schwarz, M., Peretz, A., Abitbol, I., Attali, B., Pongs, O., 2000. A recessive C-terminal Jervell and Lange-Nielsen mutation of the KCNQ1 channel impairs subunit assembly. EMBO J. 19, 332–340. https://doi.org/10.1093/emboj/19.3.332

Schroeder, B.C., Hechenberger, M., Weinreich, F., Kubisch, C., Jentsch, T.J., 2000. KCNQ5, a novel potassium channel broadly expressed in brain, mediates M-type currents. J. Biol. Chem. 275, 24089–24095. https://doi.org/10.1074/jbc.M003245200

Schroeder, B.C., Kubisch, C., Stein, V., Jentsch, T.J., 1998. Moderate loss of function of cyclic-AMP-modulated KCNQ2/KCNQ3 K+ channels causes epilepsy. Nature 396, 687–690. https://doi.org/10.1038/25367

Schwake, M., Athanasiadu, D., Beimgraben, C., Blanz, J., Beck, C., Jentsch, T.J., Saftig, P., Friedrich, T., 2006. Structural determinants of M-type KCNQ (Kv7) K+ channel assembly. J. Neurosci. Off. J. Soc. Neurosci. 26, 3757–3766. https://doi.org/10.1523/JNEUROSCI.5017-05.2006

Schwake, M., Jentsch, T.J., Friedrich, T., 2003. A carboxy-terminal domain determines the subunit specificity of KCNQ K+ channel assembly. EMBO Rep. 4, 76–81. https://doi.org/10.1038/sj.embor.embor715

Selyanko, A.A., Hadley, J.K., Wood, I.C., Abogadie, F.C., Jentsch, T.J., Brown, D.A., 2000. Inhibition of KCNQ1-4 potassium channels expressed in mammalian cells via M1 muscarinic acetylcholine receptors. J. Physiol. 522 Pt 3, 349–355. https://doi.org/10.1111/j.1469-7793.2000.t01-2-00349.x

Sesti, F., Goldstein, S.A., 1998. Single-channel characteristics of wild-type IKs channels and channels formed with two minK mutants that cause long QT syndrome. J. Gen. Physiol. 112, 651–663. https://doi.org/10.1085/jgp.112.6.651

Shah, V.N., Chagot, B., Chazin, W.J., 2006. Calcium-Dependent Regulation of Ion Channels. Calcium Bind. Proteins 1, 203–212.

Shamgar, L., Ma, L., Schmitt, N., Haitin, Y., Peretz, A., Wiener, R., Hirsch, J., Pongs, O., Attali, B., 2006. Calmodulin is essential for cardiac IKS channel gating and assembly: impaired function in long-QT mutations. Circ. Res. 98, 1055–1063. https://doi.org/10.1161/01.RES.0000218979.40770.69

Shapiro, M.S., Roche, J.P., Kaftan, E.J., Cruzblanca, H., Mackie, K., Hille, B., 2000. Reconstitution of muscarinic modulation of the KCNQ2/KCNQ3 K(+) channels that underlie the neuronal M current. J. Neurosci. Off. J. Soc. Neurosci. 20, 1710–1721.

Shorvon, S., Perucca, E., Jr, J.E., 2015. The Treatment of Epilepsy. John Wiley & Sons.

Singh, N.A., Charlier, C., Stauffer, D., DuPont, B.R., Leach, R.J., Melis, R., Ronen, G.M., Bjerre, I., Quattlebaum, T., Murphy, J.V., McHarg, M.L., Gagnon, D., Rosales, T.O., Peiffer, A., Anderson, V.E., Leppert, M., 1998. A novel potassium channel gene, KCNQ2, is mutated in an inherited epilepsy of newborns. Nat. Genet. 18, 25–29. https://doi.org/10.1038/ng0198-25

Singh, N.A., Westenskow, P., Charlier, C., Pappas, C., Leslie, J., Dillon, J., Anderson, V.E., Sanguinetti, M.C., Leppert, M.F., BFNC Physician Consortium, 2003. KCNQ2 and KCNQ3 potassium channel genes in benign familial neonatal convulsions: expansion of the functional and mutation spectrum. Brain J. Neurol. 126, 2726–2737. https://doi.org/10.1093/brain/awg286

Soh, H., Pant, R., LoTurco, J.J., Tzingounis, A.V., 2014. Conditional deletions of epilepsy-associated KCNQ2 and KCNQ3 channels from cerebral cortex cause differential effects on neuronal excitability. J. Neurosci. Off. J. Soc. Neurosci. 34, 5311–5321. https://doi.org/10.1523/JNEUROSCI.3919-13.2014

Soldovieri, M.V., Miceli, F., Taglialatela, M., 2011. Driving with no brakes: molecular pathophysiology of Kv7 potassium channels. Physiol. Bethesda Md 26, 365–376. https://doi.org/10.1152/physiol.00009.2011

Stafstrom, C.E., Carmant, L., 2015. Seizures and Epilepsy: An Overview for Neuroscientists. Cold Spring Harb. Perspect. Med. 5. https://doi.org/10.1101/cshperspect.a022426

Stewart, A.P., Gómez-Posada, J.C., McGeorge, J., Rouhani, M.J., Villarroel, A., Murrell-Lagnado, R.D., Edwardson, J.M., 2012. The Kv7.2/Kv7.3 heterotetramer assembles with a random subunit arrangement. J. Biol. Chem. 287, 11870–11877. https://doi.org/10.1074/jbc.M111.336511

Strutz-Seebohm, N., Pusch, M., Wolf, S., Stoll, R., Tapken, D., Gerwert, K., Attali, B., Seebohm, G., 2011. Structural basis of slow activation gating in the cardiac I Ks channel complex. Cell. Physiol. Biochem. Int. J. Exp. Cell. Physiol. Biochem. Pharmacol. 27, 443–452. https://doi.org/10.1159/000329965

Suh, B.-C., Hille, B., 2007. Regulation of KCNQ channels by manipulation of phosphoinositides. J. Physiol. 582, 911–916. https://doi.org/10.1113/jphysiol.2007.132647

Sun, J., MacKinnon, R., 2017. Cryo-EM Structure of a KCNQ1/CaM Complex Reveals Insights into Congenital Long QT Syndrome. Cell 169, 1042-1050.e9. https://doi.org/10.1016/j.cell.2017.05.019

Tatulian, L., Brown, D.A., 2003. Effect of the KCNQ potassium channel opener retigabine on single KCNQ2/3 channels expressed in CHO cells. J. Physiol. 549, 57–63. https://doi.org/10.1113/jphysiol.2003.039842

Tatulian, L., Delmas, P., Abogadie, F.C., Brown, D.A., 2001. Activation of expressed KCNQ potassium currents and native neuronal M-type potassium currents by the anti-convulsant drug retigabine. J. Neurosci. Off. J. Soc. Neurosci. 21, 5535–5545.

Tristani-Firouzi, M., Chen, J., Mitcheson, J.S., Sanguinetti, M.C., 2001. Molecular biology of K(+) channels and their role in cardiac arrhythmias. Am. J. Med. 110, 50–59. https://doi.org/10.1016/s0002-9343(00)00623-9

Tristani-Firouzi, M., Sanguinetti, M.C., 1998. Voltage-dependent inactivation of the human K+ channel KvLQT1 is eliminated by association with minimal K+ channel (minK) subunits. J. Physiol. 510, 37–45. https://doi.org/10.1111/j.1469-7793.1998.037bz.x

Wang, A.W., Yang, R., Kurata, H.T., 2017. Sequence determinants of subtype-specific actions of KCNQ channel openers. J. Physiol. 595, 663–676. https://doi.org/10.1113/JP272762

Wang, A.W., Yau, M.C., Wang, C.K., Sharmin, N., Yang, R.Y., Pless, S.A., Kurata, H.T., 2018. Four drug-sensitive subunits are required for maximal effect of a voltage sensor–targeted KCNQ opener. J. Gen. Physiol. 150, 1432–1443. https://doi.org/10.1085/jgp.201812014

Wang, C.K., Lamothe, S.M., Wang, A.W., Yang, R.Y., Kurata, H.T., 2018. Pore- and voltage sensor–targeted KCNQ openers have distinct state-dependent actions. J. Gen. Physiol. 150, 1722–1734. https://doi.org/10.1085/jgp.201812070

Wang, H.S., Pan, Z., Shi, W., Brown, B.S., Wymore, R.S., Cohen, I.S., Dixon, J.E., McKinnon, D., 1998. KCNQ2 and KCNQ3 potassium channel subunits: molecular correlates of the M-channel. Science 282, 1890–1893. https://doi.org/10.1126/science.282.5395.1890

Wang, Q., Curran, M.E., Splawski, I., Burn, T.C., Millholland, J.M., VanRaay, T.J., Shen, J., Timothy, K.W., Vincent, G.M., de Jager, T., Schwartz, P.J., Toubin, J.A., Moss, A.J., Atkinson, D.L., Landes, G.M., Connors, T.D., Keating, M.T., 1996. Positional cloning of a novel potassium channel gene: KVLQT1 mutations cause cardiac arrhythmias. Nat. Genet. 12, 17–23. https://doi.org/10.1038/ng0196-17

Waterhouse, A., Bertoni, M., Bienert, S., Studer, G., Tauriello, G., Gumienny, R., Heer, F.T., de Beer, T.A.P., Rempfer, C., Bordoli, L., Lepore, R., Schwede, T., 2018. SWISS-MODEL: homology modelling of protein structures and complexes. Nucleic Acids Res. 46, W296–W303. https://doi.org/10.1093/nar/gky427

Weckhuysen, S., Ivanovic, V., Hendrickx, R., Van Coster, R., Hjalgrim, H., Møller, R.S., Grønborg, S., Schoonjans, A.-S., Ceulemans, B., Heavin, S.B., Eltze, C., Horvath, R., Casara, G., Pisano, T., Giordano, L., Rostasy, K., Haberlandt, E., Albrecht, B., Bevot, A., Benkel, I., Syrbe, S., Sheidley, B., Guerrini, R., Poduri, A., Lemke, J.R., Mandelstam, S., Scheffer, I., Angriman, M., Striano, P., Marini, C., Suls, A., De Jonghe, P., 2013. Extending the KCNQ2 encephalopathy spectrum. Neurology 81, 1697–1703. https://doi.org/10.1212/01.wnl.0000435296.72400.a1

Weckhuysen, S., Mandelstam, S., Suls, A., Audenaert, D., Deconinck, T., Claes, L.R.F., Deprez, L., Smets, K., Hristova, D., Yordanova, I., Jordanova, A., Ceulemans, B., Jansen, A., Hasaerts, D., Roelens, F., Lagae, L., Yendle, S., Stanley, T., Heron, S.E., Mulley, J.C., Berkovic, S.F., Scheffer, I.E., de Jonghe, P., 2012. KCNQ2 encephalopathy: emerging phenotype of a neonatal epileptic encephalopathy. Ann. Neurol. 71, 15–25. https://doi.org/10.1002/ana.22644

Wen, H., Levitan, I.B., 2002. Calmodulin is an auxiliary subunit of KCNQ2/3 potassium channels. J. Neurosci. Off. J. Soc. Neurosci. 22, 7991–8001.

Whittaker, D.G., Colman, M.A., Ni, H., Hancox, J.C., Zhang, H., 2018. Human Atrial Arrhythmogenesis and Sinus Bradycardia in KCNQ1-Linked Short QT Syndrome: Insights From Computational Modelling. Front. Physiol. 9. https://doi.org/10.3389/fphys.2018.01402

Wu, D., Pan, H., Delaloye, K., Cui, J., 2010. KCNE1 Remodels the Voltage Sensor of Kv7.1 to Modulate Channel Function. Biophys. J. 99, 3599–3608. https://doi.org/10.1016/j.bpj.2010.10.018

Yang, W.-P., Levesque, P.C., Little, W.A., Conder, M.L., Shalaby, F.Y., Blanar, M.A., 1997. KvLQT1, a voltage-gated potassium channel responsible for human cardiac arrhythmias. Proc. Natl. Acad. Sci. 94, 4017–4021. https://doi.org/10.1073/pnas.94.8.4017

Yang, Y., Yan, Y., Sigworth, F.J., 1997. How does the W434F mutation block current in Shaker potassium channels? J. Gen. Physiol. 109, 779–789. https://doi.org/10.1085/jgp.109.6.779

Yau, M.C., Kim, R.Y., Wang, C.K., Li, J., Ammar, T., Yang, R.Y., Pless, S.A., Kurata, H.T., 2018. One drug-sensitive subunit is sufficient for a near-maximal retigabine effect in KCNQ channels. J. Gen. Physiol. 150, 1421–1431. https://doi.org/10.1085/jgp.201812013

Yellen, G., 2002. The voltage-gated potassium channels and their relatives. Nature 419, 35–42. https://doi.org/10.1038/nature00978

Yue, C., Yaari, Y., 2004. KCNQ/M channels control spike afterdepolarization and burst generation in hippocampal neurons. J. Neurosci. Off. J. Soc. Neurosci. 24, 4614–4624. https://doi.org/10.1523/JNEUROSCI.0765-04.2004

Yus-Najera, E., Santana-Castro, I., Villarroel, A., 2002. The identification and characterization of a noncontinuous calmodulin-binding site in noninactivating voltage-dependent KCNQ potassium channels. J. Biol. Chem. 277, 28545–28553. https://doi.org/10.1074/jbc.M204130200

Zaydman, M.A., Cui, J., 2014a. PIP2 regulation of KCNQ channels: biophysical and molecular mechanisms for lipid modulation of voltage-dependent gating. Front. Physiol. 5, 195. https://doi.org/10.3389/fphys.2014.00195

Zaydman, M.A., Silva, J.R., Delaloye, K., Li, Y., Liang, H., Larsson, H.P., Shi, J., Cui, J., 2013. Kv7.1 ion channels require a lipid to couple voltage sensing to pore opening. Proc. Natl. Acad. Sci. 110, 13180–13185. https://doi.org/10.1073/pnas.1305167110

Zhang, H., Craciun, L.C., Mirshahi, T., Rohács, T., Lopes, C.M.B., Jin, T., Logothetis, D.E., 2003. PIP2 Activates KCNQ Channels, and Its Hydrolysis Underlies Receptor-Mediated Inhibition of M Currents. Neuron 37, 963–975. https://doi.org/10.1016/S0896-6273(03)00125-9

Zhou, Y., Morais-Cabral, J.H., Kaufman, A., MacKinnon, R., 2001. Chemistry of ion coordination and hydration revealed by a K+ channel-Fab complex at 2.0 A resolution. Nature 414, 43–48. https://doi.org/10.1038/35102009